National Library of Canada
Bibliothèque nationale du Canada

Canadian Theses Service
Service des thèses canadiennes

Ottawa, Canada
K1A 0N4

NOTICE

The quality of this microform is heavily dependent upon the quality of the original thesis submitted for microfilming. Every effort has been made to ensure the highest quality of reproduction possible.

If pages are missing, contact the university which granted the degree.

Some pages may have indistinct print especially if the original pages were typed with a poor typewriter ribbon or if the university sent us an inferior photocopy.

Previously copyrighted materials (journal articles, published tests, etc.) are not filmed.

Reproduction in full or in part of this microform is governed by the Canadian Copyright Act, R.S.C. 1970, c. C-30.

AVIS

La qualité de cette microforme dépend grandement de la qualité de la thèse soumise au microfilmage. Nous avons tout fait pour assurer une qualité supérieure de reproduction.

S'il manque des pages, veuillez communiquer avec l'université qui a conféré le grade.

La qualité d'impression de certaines pages peut laisser à désirer, surtout si les pages originales ont été dactylographiées à l'aide d'un ruban usé ou si l'université nous a fait parvenir une photocopie de qualité inférieure.

Les documents qui font déjà l'objet d'un droit d'auteur (articles de revue, tests publiés, etc.) ne sont pas microfilmés.

La reproduction, même partielle, de cette microforme est soumise à la Loi canadienne sur le droit d'auteur, SRC 1970, c. C-30.

NL-339 (r. 88/04)

Canada

THE UNIVERSITY OF ALBERTA

ASPECTS OF MASS SPECTROMETRIC ANALYSIS OF NONVOLATILE COMPOUNDS: FAST ATOM BOMBARDMENT, THERMOSPRAY AND LIQUID CHROMATOGRAPHY-TANDEM MASS SPECTROMETRY

BY

ANTHONY JOHN ALEXANDER

A THESIS SUBMITTED TO
THE FACULTY OF GRADUATE STUDIES AND RESEARCH
IN PARTIAL FULFILMENT OF THE REQUIREMENTS FOR THE
DEGREE OF DOCTOR OF PHILOSOPHY

DEPARTMENT OF CHEMISTRY

EDMONTON, ALBERTA

FALL 1987

Permission has been granted to the National Library of Canada to microfilm this thesis and to lend or sell copies of the film.

The author (copyright owner) has reserved other publication rights, and neither the thesis nor extensive extracts from it may be printed or otherwise reproduced without his/her written permission.

L'autorisation a été accordée à la Bibliothèque nationale du Canada de microfilmer cette thèse et de prêter ou de vendre des exemplaires du film.

L'auteur (titulaire du droit d'auteur) se réserve les autres droits de publication; ni la thèse ni de longs extraits de celle-ci ne doivent être imprimés ou autrement reproduits sans son autorisation écrite.

ISBN 0-315-41050-7

University of Alberta
Edmonton
Canada T6G 2G2

Department of Chemistry
Faculty of Science
E3-43 Chemistry Building East, Telephone (403) 432-3254

July 6, 1987.

Mr. A. J. Alexander,
Chemistry Department,
University of Alberta,
Edmonton, Alberta.

Dear Alex:

Re: Manuscript on Thermospray-MS

I am pleased to extend permission to you to submit the contents of our joint manuscript entitled "Thermospray Mass Spectrometry. Use of Gas-Phase Ion/molecule Reactions to Explain Features of Thermospray Mass Spectra" as part of your Ph.D. thesis.

Sincerely,

P. Kebarle

P. Kebarle
Professor of Chemistry

mw/

University of Alberta
Edmonton
Canada T6G 2G2

Department of Chemistry
Faculty of Science
E3-43 Chemistry Building East, Telephone (403) 432-3254

July 6, 1987.

Mr. A. J. Alexander,
Chemistry Department,
University of Alberta
Edmonton, AB T6G 2G2

Dear Alex:

Re: Manuscript on FABMS

I am pleased to extend permission to you to submit the contents of our joint manuscript entitled "Characterization of a Saddle-field Discharge Gun for FABMS using Different Discharge Vapors" as part of your Ph.D. thesis.

Sincerely,

A. M. Hogg
Faculty Service Officer

mw

ALBERTA CANCER BOARD

CROSS CANCER INSTITUTE
NORTHERN ALBERTA CANCER PROGRAM

June 30, 1987

Mr. A.J. Alexander
Chemistry Department
Chemistry Building
University of Alberta
Edmonton, ~~Alberta~~

Dear Alex:

RE: MANUSCRIPT ON THE LC-MS OF POLY A

I am pleased to extend permission to you to submit the contents of our joint manuscript entitled "Characterization of Radiation-Induced Damage to Polyadenylic Acid Using High Performance Liquid Chromatography - Tandem Mass Spectrometry" as part of your Ph.D. thesis. This work is very much a demonstration of the potential of LC-MS in resolving problems in molecular radiobiology. It would not have been done without your enthusiasm and expertise.

Sincerely,

Jim Raleigh

J.A. Raleigh, Ph.D.
Radiobiology
Cross Cancer Institute

JAR/glk

11560 UNIVERSITY AVENUE, EDMONTON, ALBERTA, CANADA T6G 1Z2 • (403) 432-8771

July 2, 1987

Faculty of Graduate Studies
University of Alberta
Edmonton, AB, Canada

Dear Sir/Madam,

I hereby give my permission for A. J. Alexander to use the manuscript entitled "Characterization of Radiation-Induced Damage to Polyadenylic Acid Using High-Performance Liquid Chromatography-Tandem Mass Spectrometry" by A. J. Alexander, P. Kebarle, A. F. Fuciarelli and J. A. Raleigh, in his Ph.D. thesis.

Sincerely,

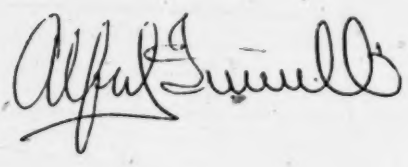

Alfred F. Fuciarelli, Ph.D.

National Bureau of Standards
Bldg. 222, Rm B348
Gaithersburg, MD
20899 U.S.A.

(301) 975-2585

THE UNIVERSITY OF ALBERTA

RELEASE FORM

NAME OF AUTHOR: ANTHONY JOHN ALEXANDER

TITLE OF THESIS: ASPECTS OF MASS SPECTROMETRIC ANALYSIS OF NONVOLATILE COMPOUNDS: FAST ATOM BOMBARDMENT, THERMOSPRAY AND LIQUID CHROMATOGRAPHY-TANDEM MASS SPECTROMETRY.

DEGREE FOR WHICH THESIS WAS PRESENTED: Ph.D.

YEAR THIS DEGREE GRANTED: 1987.

Permission is hereby granted to the UNIVERSITY OF ALBERTA LIBRARY to reproduce single copies of this thesis and to lend or sell such copies for private, scholarly or scientific research purposes only.

The author reserves other publication rights, and neither the thesis nor extensive extracts from it may be printed or otherwise reproduced with the author's written permission.

Signed: A.J. Alexander

Permanant address: Atlantic Research Lab.
NRC of Canada,
1411, Oxford St, Halifax,
Nova Scotia, B3H 3Z1.

Dated: July 16, 1987.

THE UNIVERSITY OF ALBERTA

FACULTY OF GRADUATE STUDIES AND RESEARCH

The undersigned certify that they have read, and recommended to the Faculty of Graduate Studies and Research, for acceptance, a thesis entitled **Aspects of Mass Spectrometric Analysis of Nonvolatile Compounds: Fast Atom Bombardment, Thermospray and Liquid Chromatography-Tandem Mass Spectrometry** submitted by **Anthony John Alexander** in partial fulfilment of the requirements for the degree of **Doctor of Philosophy.**

Supervisor .....

.....

.....

.....

.....

External Examiner .....

Date: July 3, 1987

TO ISLA

whose love and support made

this work possible

ABSTRACT

A fast atom bombardment (FAB) gun which can be operated at elevated temperatures was constructed. This permitted mercury and polyatomic vapors to be evaluated relative to argon and xenon. The composition of the particle beams, their ion/neutral species ratios and their energies were examined under various operating conditions to determine what factors are important in obtaining the best "molecular" ion yield from a sample in a liquid matrix. Mercury vapor was shown to be suitable for routine use but is not significantly superior to xenon. Heavy polyatomic particles (MW>200) are not produced efficiently by the saddle-field discharge and hence their usefulness is still unknown.

A thermospray (TSP) ion source was constructed and interfaced to a quadrupole mass filter. TSP mass spectra for a range of organic bases, were obtained by pumping solutions of known analyte and buffer compositions to the interface. The relative ion intensities were found to be strongly dependent on gas phase ion/molecule reactions. With volatile and moderately volatile analytes (B) in ammonium acetate buffer, the BH^+ ions are formed by gas phase protonation of gaseous B by the ammonium reagent ions.

Several inorganic cations could also be detected by TSP mass spectrometry. Alkali metal cluster ions of the form $X^+(H_2O)_n$ were observed, where X^+ was the alkali ion in solution. The relative distribution of water clusters for a

given ion were close to the predicted gas phase equilibrium values.

The existing TSP source was modified for operation with pulsed electron beam ionisation. This allowed the flow velocity through the TSP source and the reaction time under normal TSP conditions to be estimated.

A triple quadrupole mass spectrometer, with a heated nebulizer APCI source, was employed to analyse a mixture of radiolysis products by HPLC-MS/MS. A model nucleic acid, polyadenylic acid, was irradiated in aqueous solution at neutral pH and then enzymatically hydrolysed to the mononucleoside level prior to analysis. The radiation induced products: R- and S-8,5'-cycloadenosine, 8-hydroxyadenosine, α-adenosine and adenine were positively identified by comparison of retention times and MS/MS spectra with those of authentic standards. LC peaks corresponding to 8-hydroxyadenine and 4-amino-5-formylamino-6-(ribosyl)aminopyrimidine were also identified by MS/MS.

ACKNOWLEDGEMENTS

I would like to thank my supervisor Professor Paul Kebarle for his advice and support throughout the course of this study.

My special thanks also go to Dr. Alan Hogg whose help and advice have been greatly appreciated.

I would also like to thank members of the mass spectrometry group, in particular Dr. Jan Sunner, Gordon Nicol and Michael Ikonomou for their assistance and for many helpful discussions over the last four and a half years. In addition I wish to thank Dr. Jan Sunner for the HPMS ion distribution P(t) shown in Figure 2.5 and the numerical integrations involved in the evaluation of equation 18 Chapter 2.

The work presented in Chapter 4 was carried out in collaboration with Alfred Fuciarelli, a fellow graduate student, whose expertise in the field of radiation chemistry is acknowledged.

During the course of this work technical assistance was obtained from many people within the Chemistry department. In this respect I wish to express my gratitude to members of the Machine, Electronics and Glassblowing workshops and to the staff of the Analytical Mass Spectrometry laboratory. In particular I wish to thank Hubert Hoffmann, who machined the parts for the thermospray source, Eric Schartner, who constructed the parts for the fast atom bombardment gun,

Ed Feschuk and Henry Stolk for their skill in construction and repair of numerous items of electronic equipment and Don Morgan for help with the operation of the MS-9 data system.

The financial assistance provided by the Chemistry Department, University of Alberta and the National Research Council of Canada is acknowledged

TABLE OF CONTENTS

CHAPTER PAGE

GENERAL INTRODUCTION.....1

REFERENCES.....7

1 CHARACTERIZATION OF A SADDLE-FIELD GUN FOR FABMS USING DIFFERENT DISCHARGE VAPORS

INTRODUCTION

Background.....9

Sputtering of atoms and molecules.....12

Sputtering of "molecular" ions.....15

Influence of primary particle mass and energy.....18

EXPERIMENTAL.....21

RESULTS AND DISCUSSION

MH^+ ion yields as a function of discharge vapor.....27

Characterization of particle beams.....30

Mechanism of neutralization to give fast atoms.....41

Energy distribution of ions.....43

MH^+ yield as a function of discharge parameters.....46

CONCLUSIONS.....52

REFERENCES.....54

2 THERMOSPRAY MASS SPECTROMETRY: USE OF GAS PHASE ION-MOLECULE REACTIONS TO EXPLAIN FEATURES OF THERMOSPRAY MASS SPECTRA

INTRODUCTION

Background.....58

CHAPTER PAGE

2 Mechanism of thermospray ionization.....60
Ion molecule reactions in ammonia CI.....62
Nature of present investigation.....63
EXPERIMENTAL
Construction of thermospray source.....64
Operation of thermospray interface.....69
Mass calibration and quadrupole discrimination.....74
RESULTS AND DISCUSSION
TSP mass spectrum of ammonium acetate.....75
Formation of MH^+ ions.....83
Application of cluster stability rules to TSP.....101
CONCLUSIONS.....105
Postscript.....106
APPENDIX
TSP evaporation of inorganic ions.....108
Relative ion evaporation efficiencies.....111
REFERENCES.....114

3 THERMOSPRAY PULSED ELECTRON IONISATION EXPERIMENTS
INTRODUCTION.....118
EXPERIMENTAL
Modifications to existing TSP source.....119
Mounting and alignment of electron gun.....121
Pulsing of the electron beam.....125
Detection system.....125

CHAPTER PAGE

3 Typical operating conditions.....128
Measurement of time dependence & data treatment....128
RESULTS AND DISCUSSION
Time dependence of ions at normal flow rate.....134
Time dependence of ions as reduced flow rates.....141
CONCLUSIONS.....145
REFERENCES.....147
4 CHARACTERIZATION OF RADIATION INDUCED DAMAGE TO POLYADENYLIC ACID USING HIGH PERFORMANCE LIQUID CHROMATOGRAPHY TANDEM-MASS SPECTROMERTY
INTRODUCTION
Radiation damage to living cells.....148
Detection of molecular damage.....150
Tandem mass spectrometry.....151
EXPERIMENTAL
Reagents.....152
Irradiation and hydrolysis of Poly A.....153
Chromatography.....154
Mass spectrometry/description of APCI interface....155
Sample ionization.....159
Operation/optimization of interface.....161
Operation of triple quadrupole MS.....164
RESULTS AND DISCUSSION
APCI and CID mass spectrum of adenosine.....166
APCI and CID mass spectra of radiolysis products...171

CHAPTER PAGE

4 Detection of damage at low radiation doses.....188

Yield of MH^+ under APCI conditions.....190

CONCLUSIONS.....192

REFERENCES.....194

CONCLUDING SUMMARY.....198

REFERENCES.....207

LIST OF TABLES

Page

Table 1.1 Relative secondary ion yields for 0.05 M beta-cyclodextrin in neutral glycerol using different bombarding vapors.....29

Table 1.2 Summary of results showing the ratio of ions to neutrals in various beams generated from monoatomic and polyatomic vapors in a saddle-field discharge.....38

Table 2.1 Relative intensities of BH^+ ions of bases B in TSP mass spectra.....95

Table 3.1 Typical operating voltages for pulsed-EI TSP electron gun.....124

Table 4.1 APCI mass spectra of radiolysis products from polyadenylic acid irradiated in N_2O saturated aqueous solution at neutral pH.....173

LIST OF FIGURES

Page

Figure 1.1 Schematic diagram of heated FAB gun showing internal components.....22

Figure 1.2 Cross-section of the FAB ion source showing relationship to gun and sample probe.....26

Figure 1.3 Schematic diagram showing the apparatus used to characterize the beams generated from monoatomic and polyatomic vapors.....26

Figure 1.4 Time exposure photographs of beams generated with argon, xenon, mercury, DC 705 and Santovac-5.....33

Figure 1.5 Mass spectra of ionic components present in a beam generated from mercury, Santovac-5 and DC 705 vapors.....35

Figure 1.6 Kinetic energy distributions of Xe^+ and Hg^+ ions produced by a saddle-field discharge.....45

Figure 1.7 Relationship of secondary ion yield to applied anode potential at constant discharge current for xenon.....48

Figure 1.8 Relationships of secondary ion yield to discharge current at constant anode potentials for xenon and mercury.....50

Figure 2.1 Mounting of TSP ion source relative to quadrupole mass analyzer and pumping system.....65

Figure 2.2 Detail of TSP ion source.....66

Figure 2.3 Total TSP ion current from 0.1 M aqueous ammonium acetate as a function of vaporizer temperature for different source temperatures.....72

Figure 2.4 TSP mass spectrum of 0.1 M aqueous ammonium acetate, jet temperature 180°C.....76

Figure 2.5 Ion residence time distributions in pulsed high pressure ion source mass spectrometer at 2 and 1 torr total pressure.....81

Figure 2.6 TSP mass spectra observed for 4-MePy (B) in 0.1 M aqueous ammonium acetate.....85

Figure 2.7 Observed TSP ion intensities in percent of total ion intensity for 4-MePy in 0.1 M aqueous ammonium acetate.....86

Figure 2.8 Plot of $\ln[I(AH^+)]$ versus $[B]_{aq}$ for B = 4-MePy and 4-Me_2NPy.....90

Figure 2.9 Same as Figure 2.7, except in this case B = 4-Me_2NPy.....92

Figure 2.10 TSP mass spectra for mixture of pyridines in 0.1 M aqueous ammonium acetate.....94

Figure 2.11 Stability of hydrogen bonded adducts $B_2H^+ \cdot OH_2$ 103

Figure 2.12 TSP cluster ions generated from 10^{-3} M aqueous solutions of alkali metal salts.....109

Figure 2.13 TSP mass spectrum of an aqueous mixture of Li, Na, K, Rb and Cs salts each at 10^{-4} M.....112

Figure 3.1 Top and cross-sectional views of TSP source modified for pulsed-EI operation.....120

Figure 3.2 Schematic diagram of electron gun used for pulsed-EI TSP operation.....122

Figure 3.3 Schematic diagram showing electrical circuitry employed for pulsed-EI TSP operation.....126

Figure 3.4 Time dependence for $H_3O^+(H_2O)_n$ intensities where n=3,4,5 under "static" operation.....130

Figure 3.5 Time dependence for $NH_4^+(H_2O)_n$ intensities where n=2,3,4 under "static" operation.....131

Figure 3.6 Time dependence for $H_3O^+(H_2O)_n$ and PyH^+ intensities generated from pulsed-EI ionization of TSP flow.....135

Figure 3.7 Time dependence for $H_3O^+(H_2O)_2$ cluster ion intensity as a function of increasing electron beam pulse width.....138

Figure 3.8 Time dependence of PyH^+ generated from pulsed-EI ionization of TSP flow as a function of liquid flow rate.....142

Figure 3.9 Time dependence of $H_3O^+(H_2O)_2$ and PyH^+ generated from pulsed-EI ionization of TSP vapor under conditions of reduced flow.....143

Figure 4.1 Schematic diagram showing internal construction of the Sciex HPLC/MS nebulizer.....156

Figure 4.2 Schematic diagram showing Sciex TAGA 6000E APCI interface.....158

Figure 4.3 APCI spectrum of nebulized HPLC eluent (10% methanol/0.02 M aqueous ammonium formate).....160

Figure 4.4a APCI spectrum of adenosine (about 10^{-7} moles) after background subtraction.....167

Figure 4.4b CID spectrum of the MH^+, m/z 268 ion of adenosine.....167

Figure 4.4c CID spectrum of the $(BH+H)^+$, m/z 136 ion of adenosine.....169

Figure 4.4d CID spectrum of the MNH_4^+ adduct ion from D-ribose.....169

Figure 4.5 HPLC chromatogram of a nitrous oxide saturated, enzyme hydrolysed, solution of poly A irradiated to 1000 Gy at neutral pH.....172

Figure 4.6 Reconstructed ion chromatograms for m/z 136, m/z 266, m/z 268 and m/z 284.....174

Figure 4.7 CID spectrum corresponding to peak 18, identified as 8-hydroxyadenosine (MH^+, m/z 284).....176

Figure 4.8 CID spectrum corresponding to peak 13, identified as S-8,5'-cycloadenosine.....176

Figure 4.9 Reconstructed ion chromatograms for m/z 286, m/z 152, m/z 268 and m/z 250.....179

Figure 4.10a CID spectrum corresponding to peak 1, identified as 4-amino-5-formylamino -6-(ribosyl)aminopyrimidine (MH^+,m/z 286).....181

Figure 4.10b CID spectrum of $(BH+H)^+$ corresponding to peak 1.....181

Figure 4.11 CID spectrum corresponding to peak 7, identified as 8-hydroxyadenine (MH^+,m/z 152).....183

Figure 4.12 CID spectrum corresponding to peak 8, identified as α-adenosine (MH^+,m/z 268).....183

Figure 4.13 CID spectrum corresponding to peak 16.. ...185

Figure 4.14 CID spectrum of MH^+,m/z 250, corresponding to a major product from the irradiation of S-8,5′-cycloadenosine-5′-monophosphate under reducing conditions.....185

Figure 4.15 Ion chromatograms obtained for m/z 266 and m/z 152 from a sample of Poly A irradiated to a dose of 10 Gy.....189

GENERAL INTRODUCTION

The work presented in this thesis is concerned with two important areas of analytical mass spectrometry: that of fast atom bombardment (FAB) and high performance liquid chromatography/mass spectrometry (HPLC-MS).

FAB is a method of ionization in which secondary ions are generated by bombarding an analyte, dissolved in a liquid matrix, with fast atoms. It is directly related to a much older technique (1),secondary ion mass spectrometry (SIMS), which traditionally employed fast ions as the primary species. Since its introduction in 1981 by Barber and colleagues (2) FAB has virtually revolutionised biomedical mass spectrometry, in that it has made possible the direct determination of high mass involatile or thermolabile compounds (3). Previously, field desorption (FD) was the only method of ionization which could be used with such molecules (4). However, FD spectra were often difficult to reproduce. Conventional ionization techniques, such as electron ionization (EI) or chemical ionization (CI) both require prior thermal vaporization of the sample (5). In cases where a more volatile derivative could be made, this approach has proved to be very successful. However, it is limited to those samples that can be efficiently volatilized. Also, for large molecules, with many derivatizable groups, conversion to the TMS or similar derivative makes

the molecule much heavier. As the transmission loss in most mass spectrometers is greater at higher mass, this often results in a loss in sensitivity for the "molecular" ion.

At first glance it is striking that biomolecules can be ionized by bombardment with keV atoms/ions without destroying them in the process. Abundant molecular ions ($[M+H]^+$, $[M-H]^-$) are the rule, with generally moderate fragmentation. The "soft" ionization mechanism(s) involved in this process have been studied extensively and are still the subject of speculation (6).

In most laboratories a saddle-field cold cathode discharge gun is used to generate the beam of fast atoms (7). Due to its availability and low cost, argon (40 amu) was initially used as the primary beam gas. However increased "molecular" ion yields were obtained with Xenon (131 amu) and this gas is now predominantly used. At the time this work was begun, only a few publications had appeared addressing optimization of the FAB experiment (8,9). A considerable volume of SIMS literature was available; however this dealt mainly with the formation of atomic species from the bombardment of metal surfaces (10). In particular, two short publications dealing with the influence of primary particle mass on the resulting FAB mass spectrum came to our attention. One reported a 10-fold increase in "molecular" ion yield by bombardment with mercury compared to that obtained with argon (11). The other reported the use of a high molecular weight vapor

(DC705 diffusion pump oil) in a commercial saddle field gun (12). The "molecular" ion yield obtained for stachyose was an order of magnitude higher with fast molecular ion than with fast mercury atom bombardment. The general implication of this work was that higher mass particles give superior secondary ion yields. However, closer examination of these papers revealed that mercury was not compared to xenon and DC 705 was not examined at high enough saddle field current to be of value. It was decided therefore to mount a systematic investigation in order to gain a better understanding of the instrumental parameters which are important when saddle-field sources are used to generate bombarding particles. In the process it was hoped that some of the uncertainties concerning the nature and relative merits of the emitted particles derived from various vapors could be clarified. The results obtained are described and discussed in Chapter 1.

During the past decade rapid progress has been made in overcoming the substantial technical problems associated with the coupling of HPLC and MS (13,14). Several commercial interfaces are now available and the number of reported applications has rapidly increased (14). One such interface is the Thermospray (TSP) source, pioneered by Vestal, which has evolved through various stages of development since the late 1970s (15).

In this design vaporization of the HPLC effluent is achieved by heating the end of a capillary tube used to

connect the liquid chromatograph to the mass spectrometer source. Other HPLC/MS interfaces have also been based on heated capillary vaporizers (13); however, the TSP source differs in one important aspect. By careful selection of capillary i.d. and control of liquid flow rate and temperature, complete vaporization of the effluent is avoided. Instead the liquid front disintegrates inside the capillary to produce a fine mist of droplets (16). Under these conditions, with an ammonium acetate buffer present in the mobile phase, ions are generated without any external source of ionisation. This ionization process is very "soft" and yields primarily "molecular" ions for a large number of nonvolatile, polar compounds. This mode of operation has subsequently become known as TSP ionization or "filament-off" TSP ionization. It is, however, by no means universally applicable and "filament-on" TSP, that is with ionization achieved by use of an electron-emitting filament, is required for the detection of many less polar samples.

Two possible mechanisms of ion formation have been advanced to account for the ions observed in TSP mass spectra: direct evaporation of ions in solution from charged droplets (17) and chemical ionization by reagent ions in the gas phase (18). In both cases ion evaporation occurs, either of analyte ions (MH^+) in solution or of NH_4^+ ions from the buffer (for negative ions the corresponding species would be $(M-H)^-$ and CH_3COO^-, however the discussion here will be limited to positive ions). The distinction

lies in which is the primary process: direct evaporation of MH^+ or small $MH^+(H_2O)_n$ clusters, or evaporation of NH_4^+ reagent ions which thenionize the neutral analyte via ion/molecule proton transfer reactions in the gas phase. The work described in Chapters 2 and 3 is a systematic study of the consequence of the ion/molecule stage in TSP ionization.

The sucessful coupling of HPLC and MS has opened up an alternative route of analysis for many mixtures of biochemical origin. This is the case for complex mixtures of nucleosides, as has been demonstrated recently by studies using both thermospray (19) and direct liquid introduction (20) HPLC-MS interfaces. The majority of HPLC-MS interfaces and other "soft" ionization methods, such as FAB, produce abundant "molecular" ions, but few fragment ions. Thus, in most cases only limited structural information is obtained. This inherent lack of information can be overcome by the use of tandem mass spectrometry (MS/MS) to generate structurally significant daughter ions (21). In instruments employing triple quadrupole geometry ($Q_1Q_2Q_3$), such as the Sciex Taga 6000E, this is achieved by mass selecting the desired parent ion with Q_1 and collisionally dissociating it with argon in Q_2. The ionic products of decomposition (daughter ions) are then mass analysed by Q_3.

The characterization of radiolysis products resulting from the exposure of nucleic acids to ionizing radiation is an important area of cancer research (22). It is also a

challenging analytical problem as the products are numerous, present in low yields and exhibit considerable structural variety. The study described in Chapter 4, that is the characterization by HPLC-MS/MS of products resulting from radiation damage to a model nucleic acid, was undertaken as a collaborative project with Dr. J.A. Raleigh*. The irradiations and subsequent enzymatic hydrolysis of the polymer, polyadenylic acid, was performed by A.F. Fuciarelli, a graduate student working under the guidance of Dr. Raleigh. He was also responsible for establishing the optimum HPLC conditions for the separation of radiolysis products.

Such MS/MS instrumentation, by its very nature, is complex and expensive. Consequently it has generally been concentrated in large academic or industrial laboratories. However, there are indications that a new generation of less expensive MS/MS instruments will soon be available (23). This will undoubtedly encourage wider utilization of the technique.

* Department of Radiobiology, Cross Cancer Institute, 11560 University Avenue, Edmonton, Alberta, T6G 1Z2, CANADA.

REFERENCES

1. Honig, R.E.; "The development of Secondary Ion Mass Spectrometry (SIMS)", 32nd. Annual Conference on Mass Spectrometry and Allied Topics, Retrospective Lectures, San Antonio, Texas, 1984.
2 Barber, M.; Bordoli, R.S.; Sedgewick, R.D.; Tyler, A.N.; J.C.S Chem. Comm.,1981, 325-327.
3. Fenselau, C.; in "Ion Formation from Organic Solids", Burlingame, A. (Ed.), Springer-Verlag, N.Y. 1983, pp. 90-100.
4. Rollgen, F.W.; ibid, pp.2-13.
5. Rose, M.E.; Johnstone, R.A.W.; "Mass Spectrometry for Chemists and Biochemists", Cambridge University Press, Cambridge, 1982, Chapter 2.
6. Pachuta, S.J.; Cooks, R.G.; in "Desorption Mass Spectrometry are SIMS and FAB the same ?", Lyon, P.A. (Ed), ACS Symposium Series Vol. 291, ACS 1985, pp.1-42.
7 Franks, J.; Int.J. Mass Spectrom. Ion Phys., 1983, 46, 343-346.
8. Martin, S.A.; Costello, C.E.; Biemann, K.; Anal. Chem., 1982, 54, 2362-2368.
9. Morris, H.R.; Panico, M.; Haskins, N.J.; Int. J. Mass Spectrom. Ion Phys., 1983, 46, 363-366.
10. McHugh, J.A.; in "Methods of Surface Analysis", Czanderna, A.W. (Ed), Elsevier, N.Y. 1975, pp.223-278.

11. Stoll, R.; Schade,U.; Rollgen, F.W.; Int. J. Mass Spectrom. Ion. Phys., 1982, 43, 227-229.

12. Wong, S.S.; Stoll, R.; Rollgen, F.W.; Z. Naturforsch 1982, 37a, 718-719.

13. Bruins, A.P.; J.Chromatog. 1985, 323, 99-111.

14. Arpino, P.J.; J.Chromatog. 1985, 323, 3-11.

15. Vestal, M.L.; Science (Washington, D.C), 1984, 226, 275-281.

16. Blakley, C.R.; Vestal, M.L.; Anal. Chem. 1983, 55, 740-754.

17. Vestal, M.L.; in "Ion Formation from Organic Solids", Benninghoven, A. (Ed), Springer-Verlag, N.Y. 1983, pp. 246-263.

18. Voyksner, R.D.; Haney, C.A.; Anal. Chem. 1985, 57, 991-996.

19. Edmonds, C.G.; Vestal, M.L.; McCloskey, J.A.; Nucleic acids Res. 1985, 13, 8197-8206.

20. Esmans, E.L.; Geboes, P.; Luyten, Y.; Alderweireldt, F.C.; Biomed. Mass. Spectrom. 1985, 12, 241-245.

21. McLafferty, F.W.; (Ed), "Tandem Mass Spectrometry", Wiley, N.Y. 1983.

22. Huttermann, J.; Kohnlein, W.; Teoule, R.; (Eds), "Effects of Ionizing Radiation on DNA", Springer-Verlag, Berlin, 1978.

23. Focus MS/MS Instrumentation, Anal. Chem. 1986, 58, 406A-412A.

CHAPTER 1

CHARACTERISATION OF A SADDLE-FIELD GUN FOR FABMS USING DIFFERENT DISCHARGE VAPORS.

INTRODUCTION

Background

The use of fast atoms to generate secondary ions by bombardment of analytes dissolved in a liquid matrix, such as glycerol, is known as fast atom bombardment mass spectrometry (FABMS). Although this technique was only introduced in 1981, it is in fact a variation on a much older analytical method, that of secondary ion mass spectrometry (SIMS), whose roots go back to the 1930's (1).

Bombardment of a surface with low energy (KeV) ions results in secondary emission of ions, neutrals, electrons and photons (2). The total sputter yield, that is the yield of ions and neutrals per incident ion, is dependent on the mass and energy of the incident ion, on the angle of the ion beam to the surface, and on the nature of the surface itself (3). Compared to the total sputter yield the yield of secondary ions, both positive and negative, is very small, typically between 0.001 and 1% (2). It is the mass analysis

1. A version of this chapter has already been published: Alexander, A.J.; Hogg, A.M.; Int. J. Mass Spectrom. Ion Processes, 1986, 69, 297-311.

of these secondary ions, generally with a quadrupole mass filter, that forms the basis of SIMS. Historically the evolution of SIMS can be traced along two distinct lines (1).

The first and original use was as an analytical tool for depth profiling and surface analysis (4). This SIMS method, referred to as "dynamic SIMS" uses a focussed primary ion beam of high flux ($> 10^{-6}$ A/cm^2) to generate high specimen sputtering rates. The second SIMS method, pioneered by Benninghoven and coworkers in the early 1970's (5), allows surface monolayers of organic samples to be analysed. This is achieved by reducing the primary ion intensity to a level (typically $< 10^{-9}$ A/cm^2) such that there is a negligible chance of more than one impact event occurring on any given area over the time of the experiment. This avoids further damage to the immediate vicinity of the impact site, and allows the ejection of intact secondary ions. In order to compensate for the inherently low signal intensity the analysis area was increased by either defocussing or rastering the primary beam (6). This "static", low damage or molecular SIMS allowed long-lived (minutes to hours) ion signals ($[M+H]^+$, $[M-H]^-$) to be obtained from involatile and thermolabile organic molecules (7). Sample preparation involved depositing the analyte as a thin film on a metal surface. Since 1976 Benninghoven and coworkers (8), as well as many other groups (9), have published a considerable volume of work on molecular SIMS.

Despite impressive results the molecular SIMS method did suffer from several drawbacks. At all but the lowest practical primary ion intensity, bombardment induced damage (fragmentation) often resulted in low intensity short-lived "molecular" ion signals (10). In many cases sample charging is not completely eliminated by compensating techniques such as electron flooding (11). The inherently low ion signal coupled with problems of focussing the primary ion beam made the technique generally inaccessible to those using magnetic sector mass spectrometers. These problems were overcome by Barber and colleages in 1981 (12) who initiated an era of explosive growth in the area of molecular secondary ion mass spectrometry.

Instead of depositing the sample as a dry surface film, it was dissolved in a glycerol or related viscous fluid matrix and bombarded with a fast (2-10 keV) neutral atom beam. This technique (FABMS) was capable of producing more intense and stable secondary ion signals than molecular SIMS and because a neutral beam was employed was readily adaptable to high mass, high resolution sector instruments. In the two initial publications by Barber et al (12,13), it was emphasised that the primary beam was neutral rather than ionic, in order to avoid charging of the sample. However neutral beams had been used before to investigate both organic and inorganic insulators (14). The important feature of FAB, which was responsible for the far more intense and stable secondary ion signals, was the use of a

liquid matrix to contain the sample. This aspect of the technique came to light only in a latter publication (15). During particle bombardment this allows the analyte molecules at the surface to be constantly replenished by diffusion from the bulk liquid, thereby circumventing the main limitation of "static" SIMS. Although there has been considerable debate on how closely FAB is related to molecular SIMS, it is now recognised that they are both based on the same sputtering phenomenon (16). Several groups have demonstrated that ion beams (Cs^+) can be used effectively with liquid matrix targets and yield virtually identical spectra to those obtained with Xe^o FAB (17,18) Benninghoven has suggested that liquid-SIMS be adopted as the correct term for this process, but so far FABMS seems to be well rooted. The large volume of recent FABMS papers have been reviewed by Fenselau (19), Colton and colleagues (9) and by Burlingame et al (20,21).

Sputtering of atoms and molecules

The sputtering of neutral atoms from solid surfaces has been studied extensively (3,22). A particle with energy in the keV range will either be back-scattered from a surface atom (a low probability event) or it will penetrate the surface to some depth - possibly up to 100 angstroms - and dissipate its energy to the lattice atoms. A surface atom will be sputtered if the energy transfered to it has a component normal to the surface which is larger than the

surface binding energy. Three quantitatively different situations can be distinguished, the single knock-on regime; the linear cascade regime and the spike regime (23). In the single knock-on regime, the bombarding particle transfers energy to a target atom which, possibly after having undergone a small number of collisions, is ejected from the surface. In the other cases, recoil atoms are energetic enough to generate secondary recoil cascades, some of which may intersect the surface with enough energy to eject a surface atom. The linear cascade differs from the spike regime in that in the former knock-on collisions dominate and collisions between moving atoms are rare, whereas in the latter the density of recoil atoms is so high that the majority of atoms within the spike volume are in motion. The sputtering of organic molecules has been considered by Magee (24) and Garrison and Winograd (25) in terms of the nature of the momentum transfer process just described. Magee concludes that:

(a) Ejection of material from the surface occurs by two principal mechanisms, direct knock-on sputtering and linear cascade sputtering. Within several angstroms of the point of impact, direct knock-on sputtering will dominate and highly energetic (10-100eV) single atoms or small clusters will be produced. As far away as 30-40 angstroms from the point of original impact extended linear cascade sputtering will eject intact molecules with low energy (<1eV), assuming that such entities exist on the surface prior to bombardment.

(b) The sputtering process is not influenced by the charge state of the primary bombarding particle.

(c) Particle bombardment of a liquid is identical to that of a solid on the time scale of a collision cascade. The time which elapses from initial impact of the bombarding particle until all atomic motion ceases is about 10^{-13} to 10^{-12} sec. During this period, the molecules of a typical liquid, with a diffusion coefficient of 10^5 cm^2 sec^{-1}, are essentially stationary, and thermal vibrations may be ignored.

(d) Low bombarding particle energy will favour direct knock-on sputtering events due to insufficient energy necessary to initiate large extended collisions.

(e) Low mass bombarding particles will likewise favour direct knock-on sputtering if the target is of low atomic weight due to the more favourable energy transfer incurred between atoms of similar mass.

(f) The degree of fragmentation can be affected by changing the angle of incidence of the beam. Beams at large angles of incidence result in higher yields of sputtered particles with a lower degree of fragmentation than those normal to the surface.

According to Röllgen and Giessmann (26) sputtering of intact molecules and molecular ions must be related to non-linear collision cascade effects such as the formation of spikes. Spike formation is, they say, favoured by high mass primary particles of "lower" energies. However, the energy range that this corresponds to is not specified. Direct evidence

in favour of spike formation stems from bombardment with molecular species (23,27). In the case of bombardment with diatomic molecular ions each atom will generate a collision cascade so that twice the amount of energy is deposited in roughly the same volume as that for atomic ion bombardment (23)

Sputtering of "molecular" ions

Pachuta and Cooks (16) have recently reviewed the state of molecular SIMS with particular emphasis on the mechanism of ion formation. The mechanism by which organic "molecular" ions are sputtered from a surface or liquid matrix is still not clearly understood, although the theory concerning the sputtering of neutral atoms and clusters from surfaces is well advanced. There is considerable debate about the events that occur between the initial energy deposition and the final appearance of an intact "molecular" species. Several theories have been proposed, and these will be briefly outlined.

Benninghoven, from his work with molecular and liquid SIMS, has advocated a precusor model for secondary ion formation and emission (8). The main points of this theory can be summarised as:

(a) precursor formation,

(b) fast transfer of kinetic energy from the projectile to an area near the point of impact,

(c) transformation of precursor into secondary ion,

(d) fragmentation.

According to Benninhoven prior to any bombardment a precursor of the finally emitted secondary ion exists at the target surface. The low energy tail of the collision cascade is responsible for the fast evaporation (10^{-12} sec.) of the unfragmented precursor. The charge sign of the emitted secondary ion is determined by the charge state of the precursor. That is, a positively charged precursor such as a protonated base-counter ion pair, will be emitted with a high probability as the protonated positive ion. The high energy region of the collision cascade is responsible for fragments of the surface precursor, as well as atomic species. In addition fragmentation of excited "molecular" ions may occur after their separation from the surface.

Busch and Cooks (28) have developed a desorption ionisation model of secondary ion formation in molecular SIMS and FABMS,which they believe is also applicable to other ionisation methods such as field-desorption, Californium-252 plasma desorption and laser desorption. The chief features of this are:

(a) isomerisation (loss of identity) of the input energy,

(b) desorption of preformed ions or intact molecules directly from the condensed phase,

(c) ion/molecule reactions such as cationization, $[M+C]^+$ where $C^+=H^+$, Na^+, Ag^+ etc, occuring in the near surface region (selvedge),

(d) dissociation of energetic ions well removed from the

surface to give fragments.

Michl (29), after studying the secondary ion spectra of low temperature solids such as Ar, Kr, Xe, and CO_2, proposed a model with three principal mechanistic features:
(a) primary damage formation during the collision cascade regime (e.g. fragmentation of molecules, ejection of fragments, ionisation and excitation of molecules and their fragments and local charging in the impact region),
(b) secondary damage formation during the thermal spike regime (e.g. chemical reactions in the damage track) and,
(c) ejection (e.g. explosive expansion of high pressure gas into the vacuum).

Vestal has presented a unified model for the generation of ions from nonvolatile molecules (30).. He speculates that the intermediate stage between energy deposition and "molecular" ion formation is a cluster or droplet which is separated from the bulk sample by a rapid non-equilibrium processes. The important steps in the overall process are:
(a) energy deposition,
(b) explosive disruption of the surface,
(c) formation of clusters and droplets,
(d) producion of molecular ions from droplets by field assisted ion evaporation.

Influence of primary particle mass and energy in FABMS

FABMS is now a routine tool in a large number of laboratories and the majority of these use a saddle-field cold-cathode discharge gun as the source of bombarding particles. When the technique was first introduced, argon was the first gas used in the discharge but it was found in many laboratories that xenon (the highest atomic weight non-radioactive rare gas) gave a useful increase in secondary ion yield. Depending on the nature of the sample, this has been variously estimated at between 4 and 10 times that of argon (31,32). The consumption of gas is so low in these devices that the high cost of xenon is not a drawback to its use and most laboratories have now abandoned argon. Martin et al (32), as part of a systematic investigation, also compared the secondary ion yields of other permanent gases (N_2,Ne,CH_4,CO,CO_2 and SF_6) and found none to be as good as xenon. As a result of this it seems to be generally believed that the greater the mass of the bombarding particle the more efficient the production of secondary ions. Rudat and McEwen (18) used a miniture capillaritron gun and a cesium ion gun, both mounted directly on a mass spectrometer ion source, to compare the secondary ion yields with argon, xenon and Cs^+, respectively. In general, they found that the same ions were present in spectra obtained when using xenon or Cs^+ in place of argon, but that the intensities of the higher mass ions were increased relative to the lower mass ions when using the heavier particles.

The only atom with an atomic weight greater than xenon which has a vapor pressure compatible with that required for a saddle-field discharge is mercury and Stoll et al (33) have described its use in a commercial Ion Tech gun (34). They reported that it gave secondary ion yields 10 times greater than argon but did not compare it directly with xenon and gave few experimental details. Campana (35) has commented on this study, pointing out that it is well known from SIMS/surface science research that the energy, mass and angle of incidence of the primary particle controls the sputter yield and also, at least to a first approximation, controls the absolute secondary ion yield which is directly proportional to the sputter yield. He concludes that it remains to be seen whether mercury provides any advantage over xenon or cesium, all of which have similar masses. Röllgen and Giessmann (26) replied saying that, while a correlation between overall sputter yield and molecular ion yield formed the working hypothesis, no experiments had yet been done to correlate the absolute secondary ion yield with the molecular ion yield, which is of primary importance for the analytical use of SIMS. They also maintained that the SIMS literature, relating mostly to the sputtering of metals and metal oxides, was of limited value when trying to understand the ionisation phenomena in molecular SIMS or FABMS.

The only reported use of a high molecular weight vapor is that of Wong et al (36) who introduced trimethylpentaphenyl

trisiloxane (DC 705 diffusion pump oil) into a commercial Ion Tech gun. Again, few experimental details were given and they obtained only a weak "beam current" of 10 μA. They did, however, conclude that if the sensitivities were quoted in terms of flux of secondary ions produced per μA of "beam current" DC 705 was "an order of magnitude" better than mercury. However data quoted show that the mercury discharge was operated at a much lower anode potential than that used with DC 705. The base peak in the electron ionization (EI) mass spectrum of DC 705 is $[M - CH_3]^+$ at m/z 531 and in their view it was probable that this fragment was also the main component of the fast ion beam.

In a saddle-field discharge one has only limited control over the energy of the emitted particles. Using xenon gas and adjusting the pressure in the gun it is possible, for example, to maintain a discharge current of 1 mA while varing the anode potential over a range of about 4 to 12 kV. Many workers, including ourselves, have found that better yields of secondary ions can be obtained by operating at higher anode potentials; however, the only reports that have appeared which attempt to quantify this (37,38) involved the use of capillaritron rather than saddle-field guns.

The work reported here was therefore undertaken in order to gain a better understanding of the instrumental parameters which are important in the application of saddle-field cold cathode discharges as sources of

bombarding particles in FABMS and to clarify some of the uncertainties concerning the nature and relative merits of the emitted particles derived from various vapors.

EXPERIMENTAL

In this laboratory Dr.Alan Hogg has used FABMS for several years with bombarding particles produced by a simple saddle-field gun (39), see Figure 1.1 The major components of this gun are:

- 2 aluminium cathodes which are identically shaped, except that one has a single central exit channel, whilst the other has several channels, one for the insulated high voltage connection to the anode and the others to permit gas flow to the discharge cavity.
- a circular stainless steel anode with a central hole and 6 semi-circular notches on its periphery.
- 6 insulating ruby balls, each set of 3 located symmetrically above and below the anode.

A 0-10kV, 6mA power supply (Spellman RHR-10P60/CR), which can be operated in either a voltage or current regulated mode, is used to supply the anode potential. In a saddle-field source electrons oscillate under the influence of a constant electrostatic field applied between the positive anode and grounded cathodes. Electrons originating in the cathode region are accelerated toward the anode and pass through the central hole. Once past the anode they decelerate as they approach the other cathode and ultimately

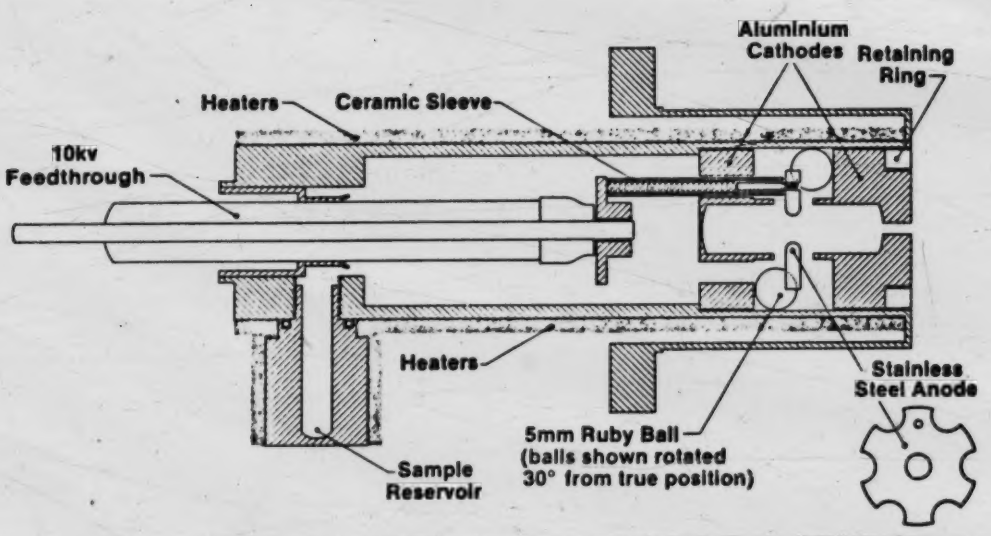

Figure 1.1 Schematic diagram of heated FAB gun showing internal components.

return toward the anode again to repeat the reverse path. These electrons form ions by impact upon the gas or vapor introduced into the gun cavity and generate a self sustaining plasma. Depending on where the positive ions are formed within the cavity they are accelerated towards either the front or back cathodes. Only those moving towards the front cathode will pass through the exit channel to form an ion beam. In or just outside the exit channel appreciable neutralisation of the ion beam occurs with little or no loss of kinetic energy to give a fast atom/ion beam (see later discussion). The discharge current, that is the current flowing between anode and cathode as measured by the total drain on the high voltage power supply, is controlled by varing the high voltage and /or gas flow.

If vapors other than permanent gases are to be used with adequate control of the pressure in the gun it is necessary to provide a heating jacket and thermostats so that the gun can be operated stably at temperatures up to 250^{o}C (Figure 1.1). The gun heater was constructed by fitting Hotwatt 8609 (1/8" x 2") 35W cartridge heaters into slots cut in a cylindrical metal sleeve which could be slid over the outside of the gun casing. A removable reservoir was filled with a charge of the liquid whose vapor was being used and thermostatted separately from the gun heater jacket. The reservoir heater was hand-wound nichrome wire. The gun was operated by initially heating the casing to approximately 175^{o}C with the high voltage switched on and

set to the required value. At this stage the discharge current meter should read close to zero unless the gun insulation is faulty. The reservoir temperature was then slowly raised until a stable discharge was maintained at the required current. To "shut the gun down" the reverse procedure was employed.

In the original design (39) the gas flow to the gun was regulated by means of a fixed leak backed up by a needle valve. Although this arrangement gives the constant gas flow necessary for routine operation, the time lag between adjustment of the valve and the establishment of new stable discharge conditions is relatively long. For this study the fixed leak and backup valve on the conventional gun was replaced by a high quality needle valve (Negretti and Zambra model 1.V.Vac). This was connected directly to the hollow 10KV feedthrough by means of a short length of rubber tubing. Using this valve, discharge conditions (i.e. new discharge current at a fixed voltage , or a new voltage at a fixed current) could be quickly and reproducibly set by accurate control of the gun pressure.

In order to compare the effect of bombarding a sample with particles from the heated gun and xenon atoms/ions from a conventional gun, an AEI MS9 double focussing mass spectrometer was fitted with both the heated and original (39) guns symmetrically mounted on the source housing. This allowed the sample probe in a simple FAB source (Figure 1.2) to be rotated to intercept the beam from either gun

without the necessity for its removal or reloading with sample. In this way the two guns could be switched on and off in sequence while rotating the probe and a series of intensity measurements made on the secondary ions produced from the sample. This compensated for the normally observed change in ion yield with time which is a feature of any FABMS analysis using a liquid matrix.

In a different series of experiments the heated gun was mounted on a flange which replaced the normal source flange on the MS9. In this configuration the beam emerging from the gun is directed down the ion optical axis of the mass spectrometer and by adjusting the voltages on the electric sector to match the energy of the ionic component of the particle beam, a mass spectrum of these ions was obtained. Also, using this configuration and with a Faraday cup replacing the magnet flight tube, the energy distribution of the ionic component was determined by stepping through the electric sector voltages while recording the current at the Faraday cup. For these experiments the normal electric sector power supply was disconnected and positive and negative voltages supplied by 2 variable DC power supplies (Hewlett Packard model 6110A). The ion current was measured with a Keithley 610C electrometer held at ground potential.

An auxillary vacuum chamber on which both types of saddle-field gun could be mounted was also used in this study (Figure 1.3). This was pumped by a 2" diffusion pump (Edwards E02) and the pressure was monitored by an ion gauge

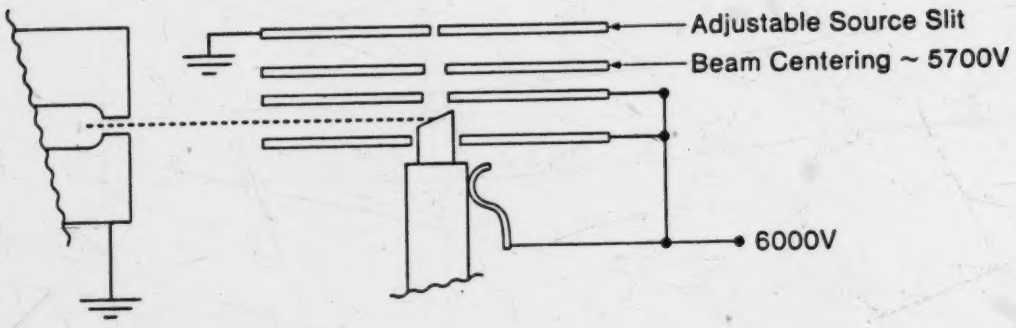

Figure 1.2 Cross-section of FAB ion source showing relationship to the FAB gun and sample probe.

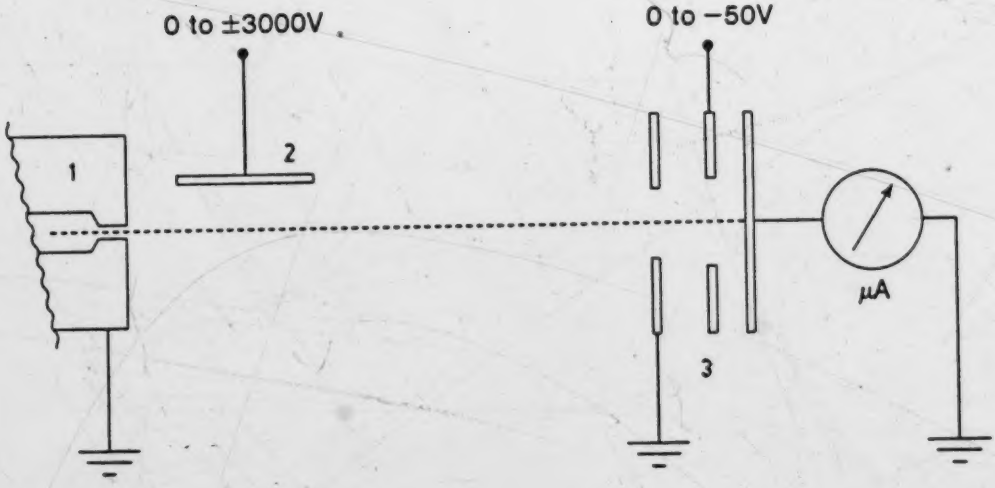

Figure 1.3 Schematic diagram showing the apparatus used to characterize the beams generated from monoatomic and polyatomic vapors. 1: FAB gun, 2: Deflection plate, 3: Faraday cup detector with suppressor plate.

(Metrovac Type VC-9) located just above the cooling baffle. With a gun operating on xenon (1mA discharge current at 8kV) the pressure measured was typically 5×10^{-6} torr. Inside the chamber a copper Faraday cup and secondary electron suppressor plate assembly was mounted such that the particle beam was normally intercepted by the cup. A deflection plate mounted between the gun and the cup allowed the ionic part of the beam to be deflected past the cup by applying either a positive or negative high voltage to the plate. The top of the vacuum chamber was sealed with a glass window which allowed the beams to be observed and recorded by time exposure photography. Both the ionic and neutral components of the beams are luminous and could be easily viewed in a darkened room. A 3 minute exposure at f4 on ASA 1000 colour film was sufficient for a permanant record.

RESULTS AND DISCUSSION

"Molecular" ion yields as a function of discharge vapor

The five vapors, argon, xenon, mercury, trimethyl-pentaphenyl trisiloxane (DC 705) and 5-ring polyphenyl ether (Santovac -5) were selected for detailed study as sources of bombarding particles for the heated saddle-field gun. Xenon was used as the reference gas in the conventional gun and was also periodically introduced into the heated gun to allow correction for any inherent differences in performance of the two guns. It was found that, depending on the condition of the electrodes in the guns, a change by as much

as a factor of two could be observed in the intensity of secondary ion produced from the same sample when alternatively bombarded by xenon particles from the two guns, both operating at the same voltage and current. Mercury has an atomic weight of approximately 200 (50% larger than xenon and only 18% smaller than uranium) and is the only monoatomic species that would be a practical higher mass alternative to xenon for FABMS. Of the potential sources of polyatomic particles with a molecular weight significantly greater than 200, DC 705 was selected because its use had been reported earlier (33) and Santovac-5 because, unlike DC 705, the base peak in its EI mass spectrum is the molecular ion (m/z 446) accounting for 60% of the total ion current. It also has remarkable thermal stability and hence would be more likely to survive the saddle-field discharge intact. Additionally it would not contribute a new source of contamination to the MS9 which already utilises Santovac-5 in its diffusion pumps.

Relative sensitivity measurements using the five vapors were made on glycyl tyrosine (MH^+=239), stachyose (MH^+=667), beta-cyclodextrin (MH^+=1135, $[M-H]^-$=1133) and cesium iodide clusters ($Cs^+[CsI]_n$), using standard 0.05 M solutions of the analytes in neutral glycerol. Despite the most careful control over the operating conditions there was a considerable variation in the values obtained from replicate experiments. Table 1.1 summarises the results obtained for beta-cyclodextrin where the secondary ion yields are reported relative to xenon having a

"Molecular" Ion	Bombarding Species				
	Argon	Xenon	Mercury	DC 705	Santovac 5
$[MH]^+$ 1135	11-14	100	75-150	1-2	2-5
$[M-H]^-$ 1133	11-14	100	75-150	7-17	4-13
Gun Temperature (°C)	N/A	N/A	150	160	180
Reservoir Temperature (°C)	N/A	N/A	85	100	140

Table 1.1 Relative secondary ion yields for 0.05 M beta-cyclodextrin in neutral glycerol using different bombarding species. Gun conditions: applied potential 9 kV, discharge current 1 mA.

value of 100. Similar trends in sensitivity were obtained for the other analytes studied. In all experiments the saddle-field gun was operated at a discharge current (the current flowing between anode and cathodes (as measured by the total drain on the high voltage power supply) of 1 mA and an anode potential of 9 kV. While the discharge current cannot be directly related to the intensity of the beam of particles emerging from the gun, as will be discussed later, it is at least an easily measureable quantity. In earlier work the terms "equivalent ion current of the neutral beam" (Martin), "discharge current" (Stoll) and "beam current" (Wong) have been used without definition and without explanation of how they were measured.

Characterisation of particle beams

Before any conclusions could be drawn from these relative sensitivities it was necessary to characterise the particle beam emerging from the heated gun. This was done by recording the currents collected by the Faraday cup in the test chamber (Figure 1.3) with and without beam deflection and with and without secondary ion suppression. If the assumption is made that the emission of secondary electrons from the surface of the Faraday cup is the same for neutral and ionic particles of the same mass, then the relative proportions of neutrals and ions in the beam can be determined according to the following rationale.

No deflection,	no suppression:	Total current [I_T]
2.6kV deflection,	no suppression:	Secondary electron emission from neutrals [I_{EN}]
2.6kV deflection,	suppression:	Meter set to zero by adjusting suppression voltage [-30 to -60 v]
No deflection,	suppression:	Primary ion current of beam [I_I]

I_T = Primary ion current [I_I] + Secondary electron emission from neutrals [I_{EN}] + Secondary electron emission from ions [I_{EI}].

Hence $I_{EI} = I_T - I_I - I_{EN}$.

If the ion beam, of intensity I_I, produces I_{EI} secondary electrons then the current equivalent of the neutral beam [I_N] can be calculated from: $I_N = (I_I \times I_{EN}) / I_{EI}$

The results of a series of measurements made with a discharge current of 1 mA and an anode potential of 7 kV are summarised in Table 1.2.

In the photographs taken with the deflector plate at high voltage (see Figure 1.4), the relative proportions of neutrals and ions can be semi-quantitatively estimated from the density of the photographic images of the straight and curved beams respectively. These obsevations are in close agreement with the Faraday cup results. Other features of the photographs are as follows:

(a) Argon and xenon look almost identical except for a slight difference in colour of the light.

(b) Mercury has a much higher proportion of neutrals compared to argon and xenon and the luminosity of both the neutral and ionic beams decrease markedly as they cross the chamber (with all other vapors the beams are of apparently constant luminosity until they collide with the Faraday cup or the chamber wall). Even allowing for the lower velocity of the mercury particles as compared with xenon it appears that the lifetimes of the radiating excited states is shorter for mercury.

(c) The ion beams from both DC 705 and Santovac-5 contain an appreciable component which shows a much smaller radius of deflection (and therefore much lower energy)

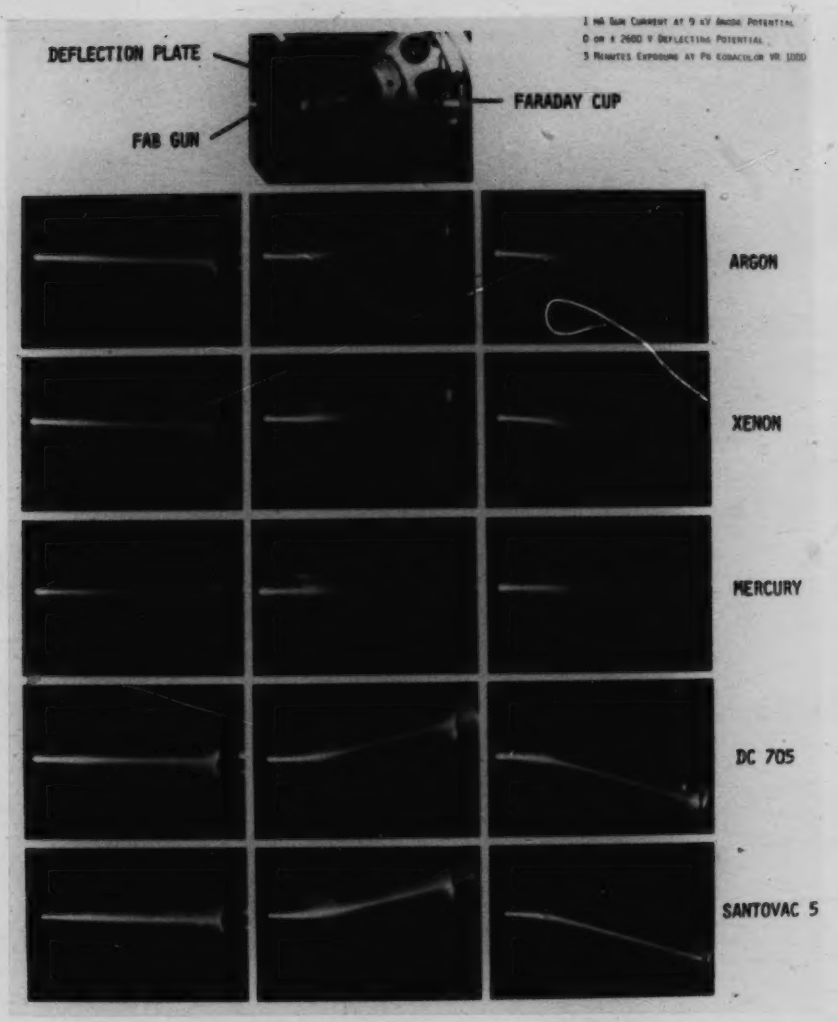

Figure 1.4 Time exposure photographs of beams generated with argon, xenon, mercury, DC 705 and Santovac-5 vapors. Gun conditions: applied voltage 9kV, discharge current 1 mA. 0 or +/- 2600 V deflection potential, 3 mins exposure at F4 Kodacolor VR 1000.

than the major component of the beam, whereas the atomic vapors appear to be largely monoenergetic.

(d) The centre line of the deflected ion beam from argon, xenon, mercury, DC 705 and Santovac-5 all pass by the rim of the Faraday cup on apparently very similar trajectories, indicating that the major components of the different ion beams are similar in energy.

The beams were further characterised by examining the mass spectra of their ionic components. This was achieved by directing the beam down the ion optical axis of the MS9 and adjusting the electric sector voltages to transmit the ions while operating the gun in the voltage regulated mode. Although the ions do not all have the same energy, as will be discussed later, with all the vapors studied the large majority of the ions do occur within a narrow band of energies corresponding to somewhat less than the appied anode potential. This is the energy for which the MS9 was set to transmit. Furthermore, by calibrating the instrument with a reference compound (perfluorokerosene) in a conventional EI source while using the same electric sector voltages the data system could be used to record the mass spectra. Figure 1.5 illustrates typical results for mercury, Santovac-5 and DC 705.

Xenon produces mostly singly charged ions (70%) with a smaller amount of doubly (23.4%) and triply (6.4%) charged

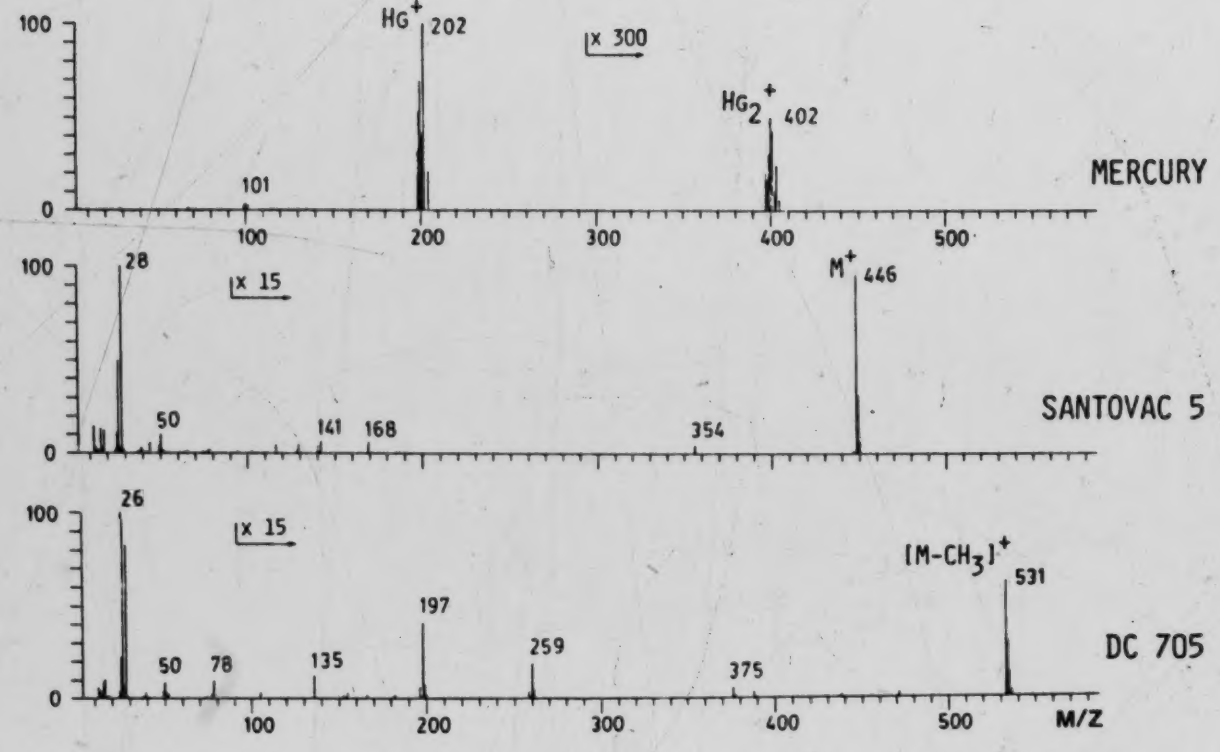

Figure 1.5 Mass spectra of the ionic components present in a beam generated from a saddle-field discharge using mercury, Santovav-5 and DC 705 vapors.
Gun conditions: applied voltage 9 kV, discharge current 1 mA.

ions and the values for argon are closely similar. Mercury produces mostly singly charged ions (92%) with a small amount of doubly charged ions (4.6%) and traces of triply charged ions (1.7%) and Hg_2^+ (0.2%).

In the mass spectra of DC 705 and Santovac-5 the most intense ions above m/z 12 are m/z 26 and m/z 28 accounting for 32% and 26% of the total ion current in DC 705 and 21% and 38% in Santovac-5 respectively. At a resolution of 1,400 the m/z 26 peak was a symmetrical singlet, while the m/z 28 peak was a doublet with the higher mass component A being less than 1% of the lower mass component B. The possible structures for m/z 28 are $C_2H_4^+$ (m/z=28.03130), N_2^+ (m/z=28.00615) or CO^+ (m/z=27.99491). At this resolution, if both N_2^+ and CO^+ were present, N_2^+ would appear as a shoulder on the high-mass side of the CO^+ peak. As N_2^+ is unlikely to be present as neither DC 705 or Santovav-5 contain nitrogen, and no shoulder was observed, peak B is probably CO^+, while peak A is $C_2H_4^+$. For the peak at m/z 26 the corresponding structures are $C_2H_2^+$ (m/z=26.01565) or CN^+ (m/z=26.00307), again with the presence of the nitogen containing species being unlikely. Using high resolution peak matching the following mass ratios were obtained for the these peaks:

28A/28B = 1.001290, 28B/26 = 1.07613, 28A/26 = 1.07720

Assuming the presence of $C_2H_4^+$, CO^+ and $C_2H_2^+$ the theoretical ratios are:

C_2H_4/CO = 1.001300, CO/C_2H_2 = 1.07608, C_2H_4/C_2H_2 = 1.07748

Normal peak matching circuitry has the accelerating voltage slaved to the electric sector voltages and consequently it automatically tracks the electric sector voltages when they are switched. However, if the ratios are small and the energy spread of the ions relatively large one can still peak match with reasonable accuracy by only switching the electric sector voltages. This was the case in this experiment, and as a consequence the error in the 28/26 ratios was larger than in the 28A/28B ratio. However, the results were accurate enough to confirm that m/z 26 is C_2H_2 and m/z 28 is almost exclusively CO^+. There is also an appreciable amount of H_2 produced in each case but this intensity was not quantitatively measured relative to that of the ions above m/z 12. Above about m/z 100 the spectra for the two compounds look very similar to their conventional 70 eV EI spectra but the ions in this range constitute only a very small proportion of the total ion current (2% in the case of DC 705 and 3% for Santovac-5). This is contrary to the assumption made by Wong et al. (36) that m/z 531 would be the main component of the fast ion beam generated from DC 705. It seems unlikely that the neutral component of these beams contains an appreciable amount of fast molecules of the original compounds, but to determine this directly would require time of flight measurements such as those described by Fitch et al. (40).

If we now examine Table 1.2 we can see that argon and xenon behave very similarly giving a neutral current

	Argon	Xenon	Mercury	DC 705	Santovac 5
Total Beam Current $[I_T]$ μA	14.5	10.5	3.2	27.2	30.0
Secondary Electron Emission From Neutrals $[I_{EN}]$ μA	4.0	1.7	1.1	2.8	5.5
Secondary Electron Emission From Ions $[I_{EI}]$ μA	4.0 ± 0.3	1.8 ± 0.2	0.3 ± 0.2	7.9 ± 0.3	9.0 ± 0.3
Neutral Current Equivalent $[I_N]$ μA	6.5 ± 0.5	6.6 ± 1.3	6.6 ± 4.6	5.8 ± 0.3	9.5 ± 0.4
Primary Ion Current $[I_I]$ μA	6.5	7.0	1.8	16.5	15.5

Table 1.2 Summary of results showing the ratio of ions to neutrals in various beams generated from monoatomic and polyatomic vapors in a saddle-field discharge using the apparatus shown in Figure 1.3.

Gun conditions: applied voltage 7 kV, discharge current 1 mA.

Estimated errors: Measured currents 0 -10 μA range ± 0.1 μA.

Measured currents 10-30 μA range ± 0.2 μA.

equivalent of 6.5 μA and a primary ion current of 6.6-7.0 μA. The lower emission of secondary electrons for xenon is consistant with literature values for rare gases in this energy range (41). It is therefore reasonable to conclude that for argon and xenon the difference between the observed secondary ion yields (Table 1.1) must be a direct consequence of their different atomic masses.

In the cases of DC 705 and Santovac-5, the particle beams have quite different characteristics from those of the rare gases. While the neutral components are of comparable intensity, the ionic components are more than twice as great. In the MS9 source configuration used, it was observed that most of the ionic component of the beam is deflected away from the probe tip even when its energy is substantially above that needed to penetrate the field generated by the source potential of 6 kV. Thus for positive ions only the neutral component of the beam is principally responsible for the observed secondary ion yield. This calls into question whether a comparison of FAB source sensitivities at constant gun anode potential and constant discharge current is justified. A constant anode potential and constant neutral flux would seem more appropriate under these circumstances. For the measurement of negative ions the probe tip is in a potential well of -6kV and deflection of the ionic component of the beam is not a significant problem. However, even under these source conditions the secondary ion yields with the two polyatomic

beams were still very poor relative to that obtained with xenon. This does not of course mean that large polyatomics may not be advantageous in improving the performance of particle bombardment sources but only that they cannot be practically generated from a saddle-field discharge.

Mercury is also different in character from the rare gases generating a beam that is apparently about 80% neutralised as opposed to 50%. Thus on the basis of neutral beam intensity alone, that is discounting the mass difference, mercury would be expected to exhibit a sensitivity advantage over xenon of 1.6 times. Unfortunately, inherent variations in the FAB experiment itself make such a small increase difficult to confirm. Our results indicate that for comparable gun conditions the sensitivity for mercury is very similar to that of xenon within the accuracy limits of replicate measurements. Certainly within the mass range of our study mercury does not produce a significant increase in "molecular" ion yield over that obtained with xenon.

Mechanism of neutralisation to give fast atoms

It appears widely accepted (15) that the mechanism for the production of fast atoms from a saddle- field discharge is resonant charge transfer, which can occur efficiently when a fast ion collides with a thermal atom of the same mass resulting in neutralisation of the charge with little or no loss of kinetic energy. An alternative mechanism is electron capture where this term is taken to mean the capture by a fast ion of a gas phase electron or one near or on the surface of a conductor.

Franks (42) has proposed that neutralisation in an argon saddle-field discharge occurs mainly by electron capture, possibly both of the secondary electrons produced by ion bombardment and of slow electrons near reversal of their trajectories, at which their velocities match those of the ions. Ross et al. (43) have discussed and investigated the possible mechanisms for electron capture that occur when an ion beam is partially neutralised by passage through a narrow metal aperture. Potential and kinetic emission of electrons (by ions) from the metal were found to govern the ion neutralisation efficiency, presumably by providing a "sea" of low-energy electrons in the vicinity of the surface for the ions to capture.

Potential emission processes generally occur if the condition $W<I$ is fulfilled, where W is the work function of the metal surface and I is the ionization energy of the incident ion (7). As the ion approaches the surface, within

a distance of the order of angstroms, the probability of neutralization by an Auger process becomes appreciable. That is, a conduction band electron from a level with an energy, say α, below the vacuum level neutralizes the ion to the ground state. An excess of energy $I-\alpha$ is created in this process which can be transfered in a radiationless transition to another conduction band electron (say at level β). When $I-\alpha > \beta$, emission of this electron into the vacuum is energetically possible.

Kinetic emission of electrons occurs when the ion velocity is larger than about 10^5 m sec^{-1} (7). In this case the ion has enough kinetic energy to penetrate into the metal and generate inner-shell vacancies. This results in electrons being created via an Auger process by the target atoms. The contribution of electron yield from kinetic emission increases with the velocity and the angle of incidence of the primary ion.

Of the metals studied, aluminium was found to be the most efficient, giving about a 7-fold enhancement in the neutral component of the primary beam. The beams obtained from both DC 705 and Santovac-5 contain an appreciable and similar proportion of neutrals and in both cases the predominant ions are $C_2H_2^+$ and CO^+. Experiments where the vapor from the heated gun, running on either DC 705 or Santovac-5, was passed through an EI source and the mass spectra of the molecules obtained show that, when the discharge is switched on, there is about a 25% decrease in

the intensity of the molecular ions. This indicates that most of the vapor survives the plasma intact and that ion collisions with neutral species in the gun will normally involve DC 705 or Santovac-5 molecules and not, for instance, acetylene or carbon monoxide. Resonant charge transfer is thus not likely to be a significant mechanism for neutralisation of these polyatomic ions leaving some form of electron capture as the likely alternative. There is no reason to believe that this is not also the case with the monatomic gases.

Energy distribution of ions from a saddle-field source

The energy distribution of the Xe^+ ions produced by an Ion Tech saddle-field source has been examined by Ligon (44). In this study the gun was mounted behind a EI/FI/FD conventional ion source such that the beam was directed down the optical axis of a double-focussing mass spectrometer after passage through the main ion source. He found that the energy spectrum for Xe^+ exhibited distinct maxima, corresponding to multiples (2 to 6 times) of 3 kV (75% of the applied anode potential). Of interest was the fact that the largest maximum occurred at 6 keV, with very few ions having energies at or below the anode potential. These maxima, with higher energies than that corresponding to the anode voltage, were attributed to initial acceleration of multiply charged ions in the saddle-field discharge with subsequent neutralisation to give singly charged ions. Thus

the maximum at 6 keV, arose from the acceleration of Xe^{2+} and likewise the maximum at 9 keV from Xe^{3+}. On the lack of Xe^{+} ions with a kinetic energy of 3 keV, Ligon speculated that " it is not unreasonable to consider that singly charged ions might be formed in the greatest abundance and also neutralised most efficiently, so they would not be observed in this experiment".

Hogg (39), however, pointed out that the cross sections for electron capture for the processes Xe^{+} to Xe^{0}, Xe^{2+} to Xe^{0} and Xe^{2+} to Xe^{+} had been measured and that while the results showed that Xe^{+} should be neutralised faster than Xe^{2+} this was only by a factor of 2. He concluded therefore that "if it(Xe^{+}) were produced as the most abundant species in the initial ionisation it should still be prominent in the residual ionic component of the beam".

Figure 1.6 shows the results obtained for xenon and mercury in the experiments where the magnet flight tube of the MS9 was replaced with a Faraday cup detector and the electric sector voltages stepped through a range corresponding to that required for transmission of ions having energies between 4 and 18 keV. The gun was voltage regulated at an anode potential of 7 kV with a discharge current of 1mA. Replicate experiments showed some variation in the intensities of the minor maxima but in all cases the beams had their principal maximum at 5.7-5.9 keV. These results are consistent with the photographic recording of the luminous beams and are in agreement with Franks and Ghander (45) who reported that the energies of Ar^{+} ions from an Ion

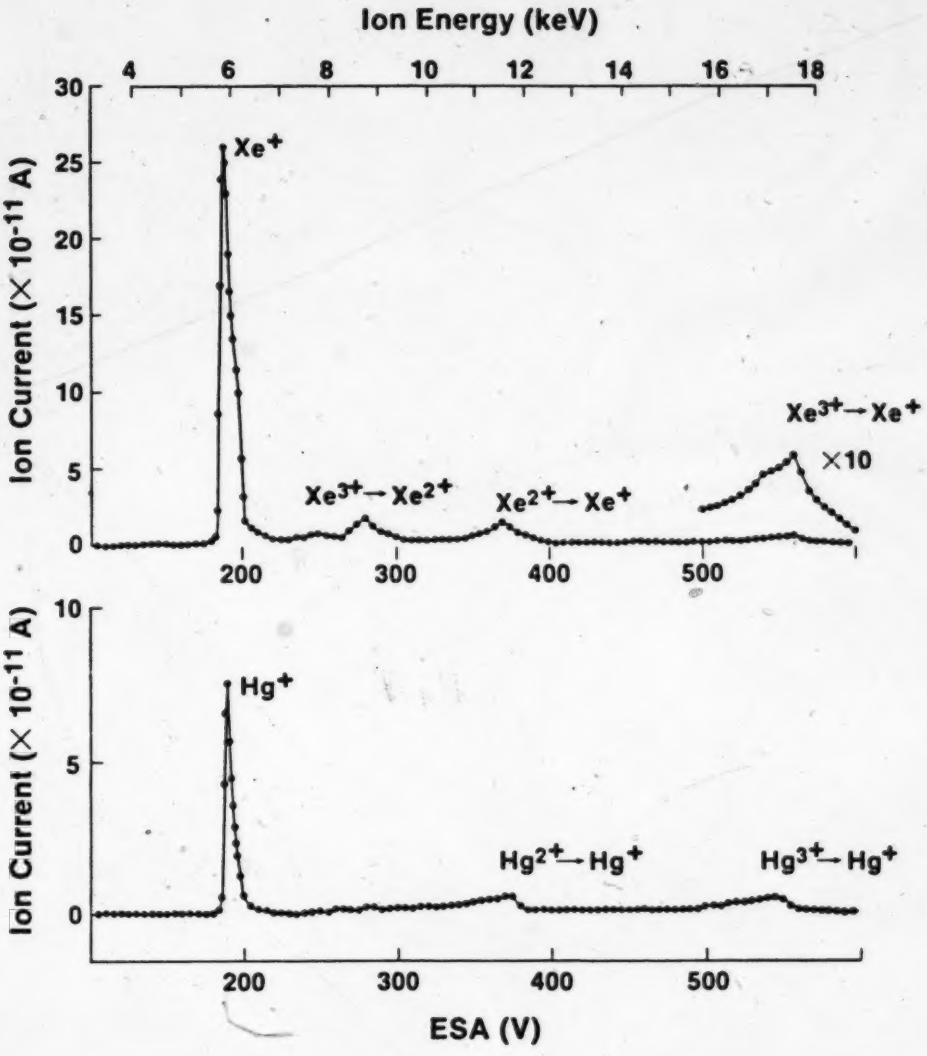

Figure 1.6 Kinetic energy distribution of Xe^+ and Hg^+ ions produced by a saddle field discharge.
Gun conditions: applied voltage 7 kV, discharge current 1 mA.

Tech saddle-field gun were "about 0.85 of the anode potential". [note: as ions accelerated by a constant potential difference follow the same path through an electric sector irrespective of their charge number, Xe^{2+} (23.4%) and Xe^{3+} (6.4%) will also contribute to the ion current measured for the principal maximum].

It is now apparent that in Ligon's study the field of the electron beam collimating magnets prevented the initially formed Xe^{+} ions from being detected, and in a more recent experiment with these magnets removed (46) he finds an additional maximum at an energy corresponding to 79% of the anode potential. It is 8.5x as intense as the $Xe^{2+} \rightarrow Xe^{+}$ maximum which he had previously reported as being the most intense. Franks and Ghander also found multiple maxima at energies <u>below</u> the anode potential. Under certain conditions we have observed an additional maximum corresponding to between 0.72 and 0.77 of the applied potential. The energy and intensity of this peak was found to vary significantly with the pressure in the gun whilst the principal maximum showed only a slight pressure dependence. Similar observations have been discussed by Pomathoid et al (47) in a different context.

"Molecular" ion yield as a function of discharge parameters

The relationship of secondary ion yield to applied anode potential at constant discharge current was explored for xenon using the m/z 1125 MH^{+} ion of beta-cyclodextrin.

Each measurement was made with a fresh sample and only the maximum ion current after switching on the gun was recorded. No attempt was made to obtain an integrated ion current as the signal decayed. The results are plotted in Figure 1.7 and confirm that increasing the anode potential increases the ion yield with no maximum up to the 15 kV limit imposed by our power supply and the gun's insulators. For positive ions only the neutral component of the beam is principally responsible for the observed secondary ion yield (see preceding discussion) and at a constant discharge current the neutral component of the beam decreases with increasing applied voltage. Thus the results obtained would indicate that in the generation of secondary ions the increasing energy of the bombarding atom more than compensates for the decreasing neutral content of the beam. The discontinuities in the curve were found to be reproducible and are possibly artifacts of the particular gun. This could be caused, for instance, by a secondary gas discharge contributing to the 1 mA constant discharge current. They may also be related to changes in discharge "modes" of the saddle-field gun as postulated by Rushton et al. (48) and expanded on by Pomathoid et al. (47). Three such modes of operation of a saddle-field discharge are apparent if the discharge voltage is plotted against the pressure inside the source for several values of the discharge current (47). They are a glow discharge mode characterized by high pressure and low voltage (<2kV), an

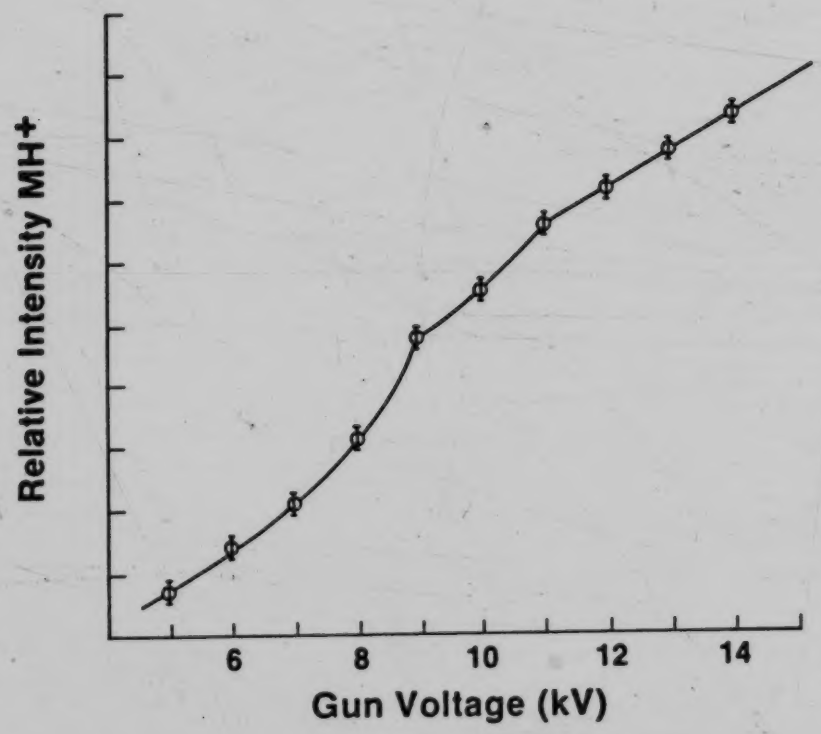

Figure 1.7 Relationship of secondary ion yield to applied anode potential at constant discharge current (1mA) for xenon. Sample: 0.05 M Beta-cyclodextrin in neutral glycerol. Ion monitored: MH^+, m/z 1135.

oscillating mode for which the conditions are a low pressure and a relatively high voltage (>6kV), and a transition mode being an intermediate state for the system.

Figure 1.8 shows for xenon and mercury the effect of increasing discharge current at constant anode potential and in this case a maximum in the secondary ion yield is obtained in the region of 2 mA. It is clear that the secondary ion yield is greatest when the gun is operated at the highest tolerable anode potential and at a discharge current high enough to reach the maximum on the corresponding intensity/discharge current curve. If 10 kV is taken as the practical limit for the anode insulators then 2 mA is the highest useful discharge current and the gun will be dissipating 20 watts. While this is acceptable for intermittent operation, the lifetime of the cathodes is reduced and experience has shown that the secondary ion signals are short-lived and there is a rapid development of a continuum of ions at virtually all masses resulting from collision-induced damage to the sample/matrix at the site of impact.

The measurements in Table 1.2 were obtained using a current regulated power supply set to 1 mA, and adjusting the gun pressure to give the required anode voltage of 7 kV for each discharge vapor (a lower pressure corresponding to a higher anode potential and vice versa). Additional measurements, again at a constant discharge current of 1 mA, indicated that the monoatomic beams had a progressively

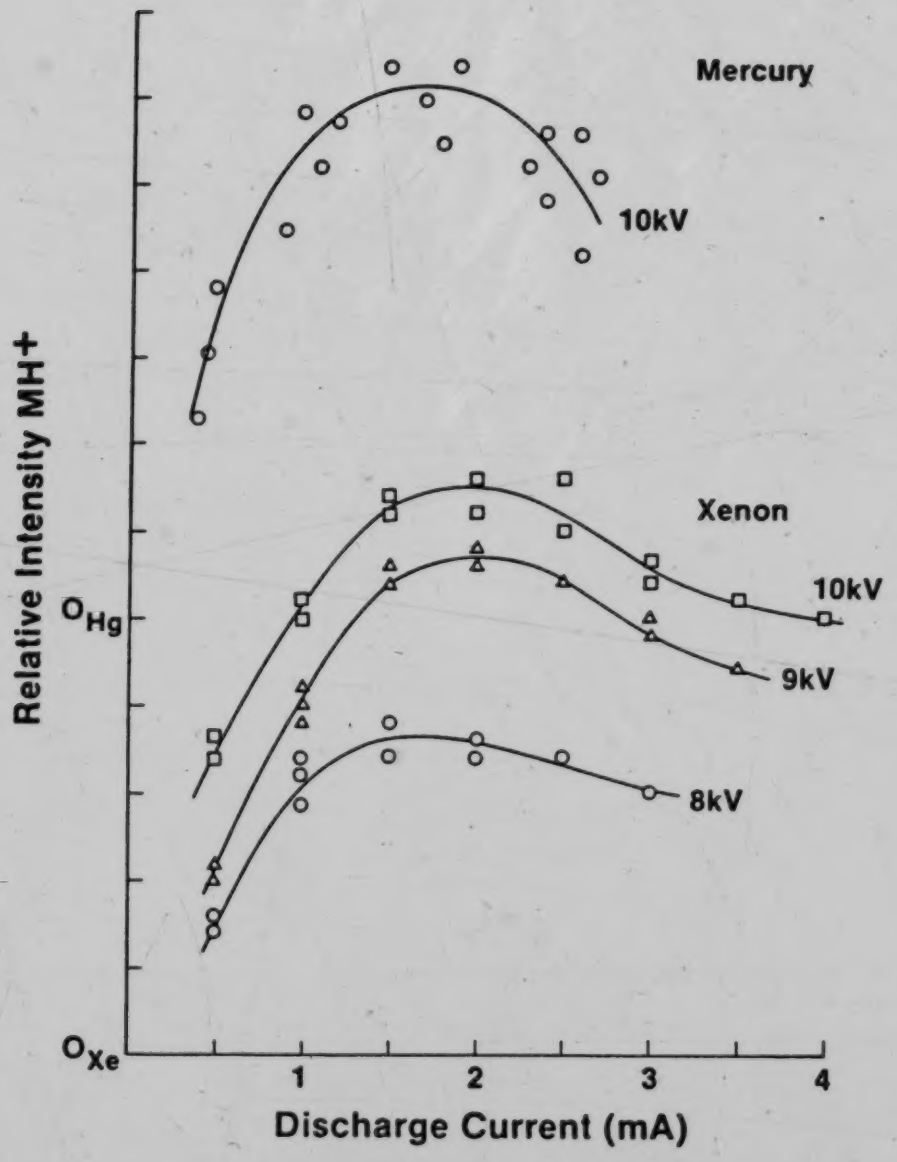

Figure 1.8 Relationship of secondary ion yield to discharge current at constant anode potentials for xenon and mercury. Sample: 0.05 M Beta-cyclodextrin in neutral glycerol. Ion monitored: MH^+, m/z 1135. Note: the zero on the intensity scale for mercury (0_{Hg}) has been displaced for clarity.

larger ionic component as the applied voltage was increased (pressure decreased). For example, the intensity of the ion beam from an argon discharge varies from 6.5 μA at 5 kV to 12.5 μA at 9 kV whilst the neutral current equivalent of the atom beam decreases from 4.8 μA to 2.9 μA for the same range of applied potential. That is, at lower pressure the neutralisation process is less efficient. Conversely, for a given applied voltage and discharge current, it was found that the degree of neutralisation within the beam could be increased by increasing the length of the beam exit channel. For an exit channel approximately 4 times longer than that used in the original cathode design (39) the intensity of an argon atom beam (neutral current equivalent) was found to increase from 4.8 μA to 12.5 μA at 5 kV and from 2.9 μA to 4.4 μA at 9 kV.

We have also found that just by returning the gun to a particular applied potential and discharge current does not necessarily result in the same intensity fast atom beam being generated. The condition of the cathode surfaces is, we believe, the major variable contributing to this phenomenon. For a given incident ion the surface condition of the cathodes determines the secondary electron yield within the saddle-field discharge. A greater electron yield means that for a given current the discharge can be maintained at a lower pressure. The process of neutralisation to give fast atoms will undoubtedly be pressure dependent whatever the mechanism. Consequently the ion/neutral ratio

in the generated beam will be different. As the pressure inside the gun is not monitored directly, and most of the ionic part of the beam is deflected by the source high voltage, it would be possible for a change in secondary ion yield to be observed for apparently identical gun conditions.

CONCLUSIONS

A wide range of monoatomic and polyatomic vapors can be used to produce a discharge in a saddle-field FABMS gun provided it can be operated at elevated temperatures. Within the mass range of this study the "molecular" ion yields obtained with mercury vapor are equal to that of xenon but not appreciably superior.

Heavy polyatomic particles (MW >200) cannot be produced efficiently by simply using organic vapors in a saddle field gun. DC 705 and Santovac-5 were found to produce only intense H_2^+, $C_2H_2^+$, and CO^+ ions and presumably the corresponding molecules comprise the neutral component of the beam. It appears unlikely that any other organic vapor would be significantly more successful, nor is it likely that high-mass ions could be produced in any type of gun utilising a plasma discharge. Thus, if the value of using high mass polyatomic particles in FABMS is to be determined, another type of gun, for instance one using electron ionization followed by acceleration will have to be employed.

The energy of the great majority of the ions in the beam correspond to between 81% and 84% of the applied anode

potential irrespective of the vapor being used and not multiples of this value as originally reported by Ligon (44).

The particle beams generated from both Santovac-5 and DC 705 show an appreciable neutral component. In neither case can resonant charge transfer be a significant process leading to neutralisation, whereas some form of electron capture is a more likely mechanism. There is, therfore, reason to believe that this might also be the predominant process for the monoatomic species which show similar degrees of neutralisation.

The reproducibility of many of these measurements in this study was found to be poor. In part this is due to the nature of the sputtering experiment itself. However, our experience has shown that variations within the saddle-field discharge are significant particularly if the gun has been current or voltage cycled during a series of measurements.

If a study comparing the secondary ion yields of different bombarding particles is to have any value it is important that the comparison be made under controlled conditions. The total particle flux of the beam, the ion/neutral ratio, the particle energies and the trajectories of the ions and neutrals in the ion source field must all be known. Furthermore, a distinction must be made between instantaneous ion current measured for "molecular" and other diagnostic ions and the total integrated flux of all secondary ions produced. Our experience shows that this is very difficult to accomplish.

REFERENCES

1. Honig, R.E. "The development of Secondary Ion Mass Spectrometry (SIMS)", 32nd Annual Conference on Mass Spectrometry and Allied Topics, Retrospective Lectures, San Antonio, Texas, 1984.
2. Mc.Hugh, J.A.; in "Methods of Surface Analysis", A.W. Czanderna (Ed), Elsevier, N.Y. 1975, pp. 223-278.
3. Wehner, G.K. ibid pp. 5-37
4. Morrison, G.H.; Slodzian, Anal. Chem., 1975, 47, 932A-943A.
5. Benninghoven, A.; Sichtermann, W.K.; Anal. Chem., 1978, 50, 1180-1184.
6. Campana, J.E.; DeCorpo, J.J; Wyatt, J.R.; Rev. Sci. Instrum., 1981, 52, 1517.
7. Benninghoven, A; Rudenauer, F.G.; Werner, H.W.; "Secondary Ion Mass Spectrometry", Chemical Analysis Vol. 86, Wiley-Interscience, N.Y. 1987.
8. Benninghoven, A.; in "Ion Formation from Organic Solids", A. Benninghoven (Ed), Springer-Verlag, N.Y, 1983, pp. 64-87.
9. Turner, N.H.; Dunlap, B.I.; Colton, R.J.; Anal. Chem., 1984, 56, 373R-416R.
10. Turner, N.H.; Colton, R.J.; Anal. Chem., 1982, 54, 293R-322R. also Day, R.J.; Unger. S.E.; Cooks, R.G.; Anal. Chem., 1980, 52, 557A-572A.

11. Colton, R.J.; Campana, J.E.; Barlak, T.M.; DeCorpo, J.J.; Wyatt, J.R.; Rev. Sci. Instrum., 1980, 51, 1685-1689

12. Barber, M.; Bordoli, R.S.; Sedgewick, R.D.; Tyler, A.N.; J.C.S Chem. Comm., 1981, 325-327.

13. Barber, M.; Bordoli, R.S.; Sedgewick, R.D.; Tyler, A.N.; Nature, 1981, 293, 270-275.

14. Devienne, F.M.; Roustan, J.C.; Org. Mass. Spectrom., 1982, 17, 173-176.

15. Barber, M.; Bordoli, R.S.; Elliott, G.J.; Sedgewick, R.D.; Tyler, A.N.; Anal. Chem., 1982, 54, 645A-657A.

16. Pachuta, S.J.; Cooks, R.G.; in "Desorption Mass Spectrometry are SIMS and FAB the same ?", P.A. Lyon (Ed), ACS Symposium Series Vol. 291, ACS 1985, pp 1-42.

17. Aberth, W.; Straub, K.M.; Burlingame, A.L.; Anal. Chem., 1982, 54, 2029-2034.

18 Rudat, M.A.; McEwen, C.N.; Int, J. Mass Spectrom. Ion Phys., 1983, 46, 351-354.

19 Fenselau, C.; in "Ion Formation from Inorganic Solids", A.Burlingame (Ed), Springer-Verlag, N.Y. 1983, pp.90-100.

20 Burlingame, A.L.; Whitney, J.O.; Russell, D.H.; Anal. Chem., 1984, 56, 417R-467R.

21. Burlingame, A.L.; Baille, T.A.; Derrick, P.J.; Anal. Chem., 1986, 58, 165R-211R.

22. Oechsner, H.; Appl. Phys., 1975, 8, 185-198.

23. Sigmund, P.; in "Sputtering by Particle Bombardment I",

Topics in Applied Physics Vol. 47, R. Behrich (Ed), Springer-Verlag, N.Y. 1981, pp.9-71.

24. Magee, C.W.; Int. J. Mass Spectrom. Ion Phys., 1983, 49, 211-221.

25. Garrison, B.J.; Winograd, N.; Science (Washington DC), 1982, 216, 805-812.

26. Rollgen, F.W.; Giessmann, U.; Int. J. Mass Spectrom. Ion Proc. 1984, 56, 229-231.

27. Thompson, D.A.; Johar, S.S.; Appl. Phys. Lett., 1979, 34, 342-344 and references therein.

28. Cooks, R.G.; Busch, K.L.; Science (Washington DC), 1982, 218, 247-254. also Int.J. Mass Spectrom. Ion Proc. 1983, 53, 111-124.

29. Michl, J,; Int. J. Mass Spectrom. Ion Phys. 1983, 53, 255-272.

30. Vestal,M.L.; Mass Spectrom. Rev. 1983, 2, 447-480.

31. Morris, H.R.; Panico, M.; Haskins, N.J.; Int. J. Mass Spectrom. Ion Phys., 1983, 46, 363-366.

32. Martin, S.A.; Costello, C.E.; Biemann, K.; Anal. Chem. 1982, 54, 2362-2368.

33. Stoll, R.; Schade, U.; Rollgen, F.W.; Int. J. Mass Spectrom. Ion Phys., 1982, 43, 227-229.

34. Ion Tech Ltd, 2 Park Street, Teddington, Middlesex, TW11 OLT, Great Britain.

35. Campana, J.E.; Int. J. Mass Spectrom. Ion Phys., 1983, 51, 133-134.

36. Wong, S.S.; Stoll, R.; Rollgen, F.W.; Z. Naturforsch 1982, 37a, 718-719.

37. Rudat, M.A.; Anal. Chem., 1982,54, 1917-1919.

38. Faull, K.F.; Tyler, A.N.; Sim, H.; Barchas, J.D.; Massey, I.J.; Kenyon, C.N.; Goodley, P.C.; Mahoney, J.F.; Perel, J.; Anal. Chem., 1984, 56, 308-311.

39. Hogg, A.M.; Int. J. Mass Spectrom. Ion Phys., 1983, 49, 25-34.

40. Fitch, R.K.; Ali, K.S.; Inman, M.; J. Phys. E: Sci. Instrum., 1984, 17, 939-941.

41. Healea, M.; Houtermans, C.; Phys. Rev., 1940, 608-610.

42. Franks, J.; Int. J. Mass Spectrom. Ion Phys., 1983, 46, 343-346.

43. Ross, M.M.; Wyatt, J.R.; Colton, R.J.; Campana, J.E.; Int. J. Mass Spectrom. Ion Proc., 1983, 54, 237-247.

44. Ligon , W.V.; Int. J. Mass Spectrom. Ion Phys., 1982, 41, 205-208.

45. Franks, J.; Ghander, A.M.; Vacuum, 1974, 24, 489-491.

46. Ligon, W.V.; Dorn, S.B.; private communication 1985, subsequently published Int. J. Mass Spectrom. Ion Proc., 1986, 72, 317-319.

47. Pomathoid, L.; Henry, D.; Arnal, Y.; Boswell, R.; in "Low Energy Ion Beams", Institute of Physics, Bristol 1980, pp. 309-315.

48. Rushton, G.J.; O'Shea, K.R.; Fitch, R.K.; J. Phys. D: Appl. Phys. 1973, 6, 1167-1172.

CHAPTER 2

THERMOSPRAY MASS SPECTROMETRY. USE OF GAS PHASE ION ION-MOLECULE REACTIONS TO EXPLAIN FEATURES OF THERMOSPRAY MASS SPECTRA.

INTRODUCTION

Background

Compared to GC-MS the technical difficulties encountered in combining high performance liquid chromatography and mass spectrometry (HPLC-MS) are formidable (1). Firstly, mass spectrometry is a gas phase technique that requires relatively low pressures, that is approximately 10^{-4} torr for electron ionisation (EI), or between 0.5 and 1.0 torr for chemical ionisation (CI). Conversely, HPLC operates at atmospheric pressure with liquid flow rates in the range of 0.5 to 2.0 mL/min. Only about 1% of this mass flow, that is between 5 and 20 µL/min., can be tolerated by a conventional CI mass spectrometer (2). Additionally, nonvolatile salts are often used to adjust the pH of the mobile phase and, if gradient elution is employed, the composition of the solvent is also changed during the analysis (3). Therefore, in order to couple the two systems, the LC effuent must be vaporized

1. A version of this chapter has already been published: Alexander, A.J.; Kebarle, P.; Anal. Chem.,1986, 58, 471-478.

and either the HPLC or MS conditions modified such that these basic incompatibilities are minimised. Secondly, as there is little point in analysing relatively volatile compounds which are amenable to GC/MS, the mass spectrometer should ideally employ an ionisation technique which does not necessarily rely on prior thermal vaporization (4).

During the past decade rapid progress has been made on overcoming these problems (4-7). The success of this research effort can be judged by the fact that several commercial interfaces are now available (5,8). One such interface is the Thermospray (TSP) source which has been under continuous development by Vestal and coworkers since the late 1970's (4,9).

In the present design (10,11) the total chromatographic eluent is passed through a short length of stainless steel capillary tubing maintained at up to 300°C. The tip of this protrudes into a region of reduced pressure (1 to 10 torr), which is pumped by a 150 L/sec mechanical rotary pump. This generates a supersonic jet of vapor containing a mist of fine particles and solvent droplets. As the droplets traverse the heated ion source they continue to vaporize due to heat transfer from the surrounding vapor. Under the right conditions, that is, polar analyte and polar mobile phase containing 0.1 M of a salt such as ammonium acetate, ions of the analyte are formed in the spray without any external source of ionisation. A cone placed in the path of the vapor jet is used to sample these ions into the

mass spectrometer. Factors which determine the number of ions sampled include the source temperature and pressure, diameter of the sampling hole, location of the sampling cone and source geometry (10). This method of ionisation yields "molecular" ions with very little fragmentation, and even thermally labile samples suffer little decomposition, presumably because the vaporization of the mobile phase shields the analyte from an excessive rise in temperature during its rapid transit through the vaporizer.

Ion intensities generated by thermospray ionisation are highly dependent on the control of the different temperature regions within the interface (10). The temperature of the vaporizer tip, the ion source and the vapor are all critical to optimum performance (12,13). In particular, the combination of eluent flow rate, eluent composition, nature of sample and the diameter of the capillary strongly influence the operation of the vaporizer,[data published by Vestal (14) which appeared after the work described in this chapter had been completed].

Mechanism of Thermospray ionisation

Two distinct stages are involved in the formation of TSP mass spectra ultimately observed with the mass spectrometer. The first stage is the formation of gaseous ions out of the microdroplets produced by the vaporizer. The ions produced in this process will be called the primary TSP ions. The second stage involves the primary TSP ions

in gas phase ion-molecule reactions. The mechanism for the formation of the primary TSP ions has received considerable attention (9,10,15). The following processes are believed to be involved:

(a) In the presence of an electrolyte at least part of the microdroplet population is electrically charged, with equal numbers of positive and negative droplets being formed. In the absence of any applied field this appears to result from statistical fluctuations in the distribution of the positive and negative ions retained in the droplet as it is sheared off from the bulk liquid, a charging mechanism known from earier work (16).

(b) The initial droplet sizes are on the order of 1 μm or less and if they are charged the mean field strength at the surface is about 10^7 V/m and increases rapidly as the microdroplet evaporates (4). When the surface field is high enough, the evaporation of molecular ions or small clusters containing the molecular ion becomes thermodynamically competitive with the evaporation of neutrals (17,18). Consequently, according to this model, any analyte that is present as either a positive or negative ion in aqueous solution will undergo direct ion evaporation into the gas phase. Primary ions produced from ammonium acetate are apparently identical to those present in solution, namely NH_4^+, CH_3COO^-, and clusters of these ions with water, ammonia and acetic acid (9).

The second stage, in which gas-phase ion molecule

reactions may remove the primary TSP ions and produce new product ions, has been recognised as of possible importance (9,10,19), but has received less attention. Vestal (10) has reported that thermospray ionisation does not produce molecular ions from large involatile analytes which are neutral in solution. However, molecules which are slightly volatile and thermally stable can be ionised by either ion-molecule reactions with reagent ions produced from thermospray ionisation of the buffer or by gas-phase processes initiated by electron ionisation [filament-on thermospray]. Several other thermospray practitioners have also remarked on the similarity between TSP and ammonia CI spectra (13,20).

Ion-molecule reactions in ammonia CI

Under CI conditions, with ammonia as the reagent gas, the primary ions formed by electron impact are NH_2^+ and NH_3^+ which subsequently undergo ion-molecule reactions with ammonia to form NH_4^+ (21). This ion then undergoes further clustering reactions according to equations (1) and (2).

$$NH_4^+ + NH_3 = NH_4^+NH_3 \quad (1)$$

$$NH_4^+[NH_3]_{n-1} + NH_3 = NH_4^+[NH_3]_n \quad (2)$$

where the value of n is dependent on the source pressure and temperature. Analytes (M) are ionised by both the ammonium ion (NH_4^+) and cluster ions, with the overall exothermicity

of the reaction governing the degree of fragmentation. Two types of reactions can occur:

(a) protonation of M to yield MH^+

(b) adduct ion formation with M to give $[M + NH_4]^+$.

Which reaction predominates is determined by the proton affinity (PA) of M, that is - $\triangle H^o$ for reaction (3).

$$M + H^+ = MH^+ \qquad (3)$$

In general if $PA(M) > PA(NH_3)$ where $PA(NH_3)$ = 204 kcal/mol (22), then protonated species are observed in the mass spectrum, whereas if $PA(M) < PA(NH_3)$ hydrogen bonded adduct ions are more likely to be formed. However, if PA(M) is less than about 188 kcal/mol then analytically useful $[M + NH_4]^+$ ion intensities are not observed (23). Furthermore, it also appears that a lone pair of electrons at the basic site is a necessary prerequisite for formation of the adduct ion.

Nature of present investigation

The present work is a systematic study of the possible consequences of the ion-molecule stage in TSP ionisation. In order to obtain TSP spectra which are typical of the apparatus generally used, a TSP ion source was constructed closely following the design of Vestal, [see experimental section]. TSP spectra were obtained without the use of a liquid chromatograph, but by pumping prepared solutions of accurately known analyte concentration and solvent composition through the interface.

Investigations of gas phase ion molecule reactions,

kinetics and equilibria have been the central area of previous research from this laboratory (24). It so happens that much of the gas-phase ion chemistry of possible importance in the second TSP stage, namely ion-molecule reactions, ion-solvent molecule equilibria, and ion-solvent molecule cluster stabilities have been investigated in this laboratory in connection with their importance to the correlation of ionic reactions and ionic solvation in the gas phase and solution. Furthermore, some of the conditions in the apparatus used in these investigations, a pulsed electron beam high pressure ion source mass spectrometer (HPMS), bear resemblence to the conditions in the TSP second stage. The present study was undertaken with the belief that the understanding of the conditions and data acquired in the HPMS work will be of help in the investigation of the much more complex conditions of the TSP second stage.

EXPERIMENTAL

Construction of thermospray source

The thermospray apparatus used is illustrated in Figures 2.1 and 2.2. The thermospray ion source, (Figure 2.2) was constructed according to details given by Vestal and co-workers. (10), and interfaced to a Granville Phillips quadrupole mass filter of range 2-500 amu.

The liquid flow was delivered by a 100 μm i.d. stainless steel capillary (Alltech Associates #30211) the exit end of which was silver brazed into an electrically

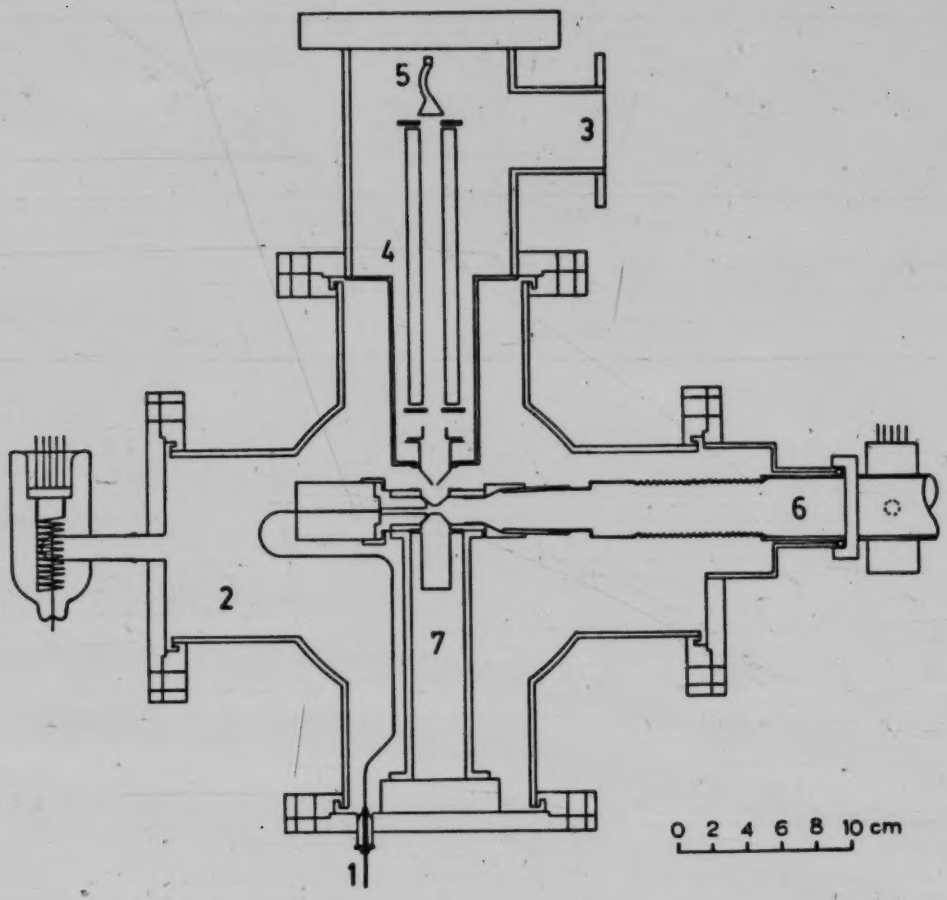

Figure 2.1 Mounting of TSP ion source relative to quadrupole mass analyzer and pumping system.

1. Liquid phase inlet capillary.
2. To 6" diffusion pump.
3. To 3" diffusion pump.
4. Quadrupole mass analyzer.
5. Channeltron electron multiplier.
6. Vapor pumping line.
7. TSP ion source.

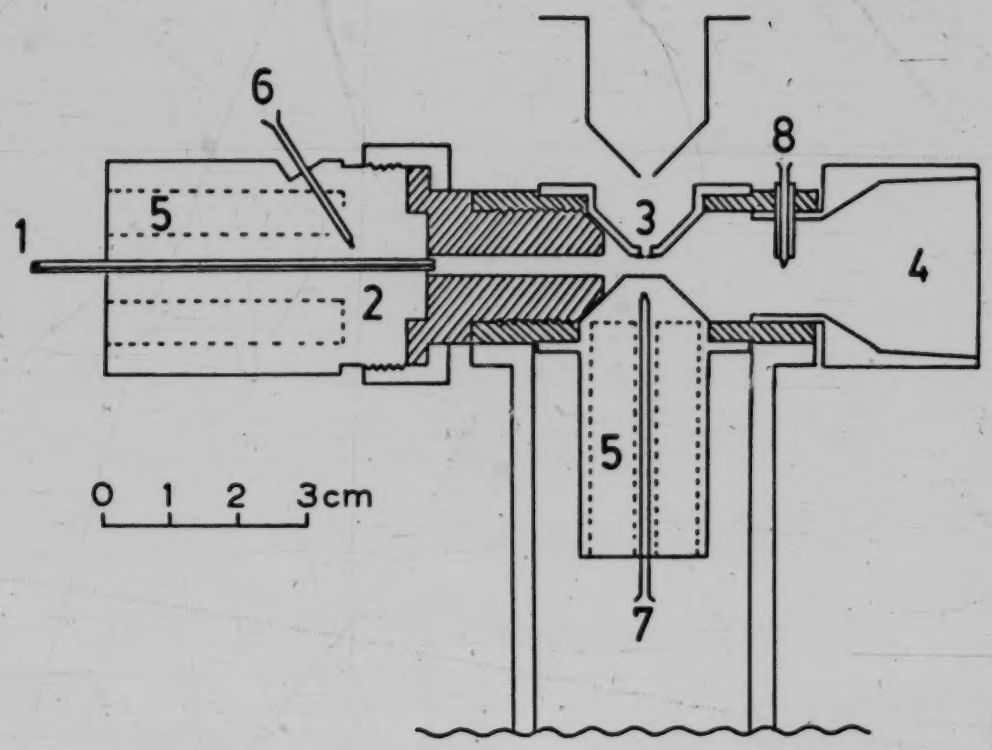

Figure 2.2 Detail of TSP ion source.

1. Liquid phase inlet capillary.
2. Vaporizer.
3. Ion exit orifice.
4. Joint to vapor pumpout line.
5. Cartridge heater.
6. Vaporizer temperature thermocouple.
7. Source temperature thermocouple.
8. Jet temperature thermocouple.

heated copper block (vaporizer). This in turn was connected to a limited expansion volume copper tube which was screwed into a stainless steel chamber (source). A conical exit aperture (450 μm) allows a proportion of the ions generated to pass from the source into the vacuum system containing the mass analyser (Figure 2.1).

The ion source was connected via a 1.5 in. valve to a dry ice/acetone-cooled trap and a 300 L/sec double-stage rotary pump. This total pumping line was about 1 m and of a minimum 1.0 in. diameter. The valve, although essential for isolating the ion source when changing traps, also allows the pressure in the ion source to be varied for a given vaporizer temperature and solvent flow rate. The ion source pressure was measured by a convectron gauge (Granville Philips #275) mounted as shown in Figure 2.1.

The quadrupole was differentially pumped by a 3 in. oil diffusion pump (Edwards #E02) and the main chamber was pumped through its bottom opening by a 6 in. oil diffusion pump (NRC #VHS-6). Typical thermospray operating pressures were about 1 torr ion source, 3×10^{-5} torr in main chamber, and 2×10^{-6} torr at the back of the quadrupole chamber.

The copper vaporizer was drilled to accommodate three 0.25 in. x 1.5 in. 75 W cartridge heaters (Superwatt # HS 2515, Danvers, Mass.) and a thermocouple. The heaters were wired in parallel and powered by a conventional variable output transformer. Eight 75 W cartridge heaters were used for the source, two of these being mounted as shown in

Figure 2.2, and the other six disposed around the perimeter of the ion source. These were also wired in parallel but powered from a separate variable output transformer. The location of thermocouples (iron constantan) in the source is shown in Figure 2.2. A digital pyrometer (Newport #267B-JC1) was used to measure the distribution of temperature. The thermocouple measuring the jet temperature was thermally isolated from the source by passing the wires through two longtitudinal channels in a short length of ceramic rod, the ceramic rod was then fitted through a hole drilled in the top of the ion source.

The section of pumpout line inside the vacuum system consisted of a metal bellows to which a male joint, machined from Vespel SP-1 resin (Du Pont Inc.), was fitted with epoxy resin. This was designed to be a push-fit into the ion source and provided both thermal as well as electrical isolation. The LC input capillary was also electrically isolated from the source flange by passing it through a hollow glass feedthrough and sealing the joint with epoxy resin. On the outside of the this flange the metal capillary was isolated from the HPLC pump by means of a short length of Teflon tubing (1/16 in. o.d. x 0.012 in. i.d.).

The ions were detected by a Channeltron electron multiplier (Galileo Electro-Optics Corp. #CEM 4830). This was operated in the analog mode and gave a gain of approximately 10^6 with an accelerating voltage of 2.5 kV. The output current from the CEM was measured with a high speed

picoammeter (Keithley #416 with #4160 input head).

Sample solutions were continuously pumped into the ion source at a flow rate of 1 mL/min with an Eldex Duplex HPLC pump (Eldex #AA-72-S). Pulsations in the flow were minimised by using a dampening system constructed according to details given by Nikelly (25). The buffer used throughout was 0.1 M ammonium acetate, either in water or as a 75:25 mixture with methanol.

It is not clear which of the measured temperatures most closely reflects the temperature at which the gas phase ion molecule reactions occur (see results and discussion). A fourth thermocouple attached to the metal diaphram containing the ion exit orifice would probably provide this temperature.

Operation of the Thermospray interface

The initial experiments to obtain thermospray ionization were carried out with 0.1 M ammonium acetate and operation of the quadrupole in the total-ion mode. The flow rate was held constant at 1 mL/min, while systematic adjustments were made to the vaporizer temperature, source temperature, source pressure, and ion extraction voltages. Initially, considerable difficulty was encountered and only a very weak fluctuating ion current was obtained. After a great deal of investigation it was realised that one of the crucial aspects of thermospray operation is the condition of the exit hole in the heated metal capillary. This has to be

re-opened after cutting the tubing, and if the jet is not directed co-axially through the source but instead hits the wall of the expansion volume region, then sensitivity is dramatically reduced.

The following method of capillary preparation was evolved to overcome this problem. Approximately 1 cm of capillary has to be left protruding from the face of the vaporizer so that it is not blocked during the brazing operation. This excess capillary is then broken off after first cutting around the circumference as close as possible to the hole, but without penetrating through the wall. This leaves a ragged but open hole of larger diameter than the tube was originally drawn to. The vaporizer is then mounted vertically in a V-block, with the tip pointing down, and the other end of the capillary connected to the HPLC pump. With distilled water flowing through the capillary at about 1 mL/min the end is then rubbed with a circular motion over 600 grit emery paper mounted on a flat surface. After the end of the capillary has been polished flat it is inspected under magnification. At this stage the hole is unlikely to be circular and any excess material is removed by carefully inserting a 100 μm o.d HSS twist drill (Sphinxwerke Muller A.G, Switzerland) into the hole. The polishing stage is then repeated until a hole of the correct i.d. is obtained. A "good" capillary was found to give a straight symmetrical water stream at a flow rate of 2 mL/min. with a back pressure no greater than 200 psi.

Having obtained efficient thermospray ionisation (see Figure 2.3) the ion source was operated at +5 volts, the skimmer cone at the entrance to the quadrupole at -30 volts and the quadrupole at 0 volts. For aqueous systems typical TSP ion source conditions were as follows: vaporizer temperature 240°C, source temperature 300°C, jet temperature 170°C and exit line pressure about 1 torr. When optimizing the TSP conditions to obtain a stable maximum ion intensity, it was observed that the total ion current increased up to a maximum as the vaporizer temperature increased, for a given source temperature and mobile phase composition. About 10°C above this maximum the total ion current often decreased drastically (see Figure 2.3). However, the maximum was reproducible within + or - 10°C for a given mobile phase and flow rate.This behaviour has been observed by other groups (10,12,13).

The experimental procedure for the routine operation of the TSP interface is as follows:

1. Increase TSP source temperature to about 250°C. At this stage the jet and vaporizer temperatures will also be close to 250°C.
2. Attach trap to pumpout line and fill Dewar with acetone/dry ice mixture. Switch on TSP rotary pump and after about 5 minutes open valve to TSP source. The pressure reading on the convectron gauge will rise to about 10 mtorr. Remove the vacuum seal from the capillary inlet to TSP source and attach connection from HPLC pump.

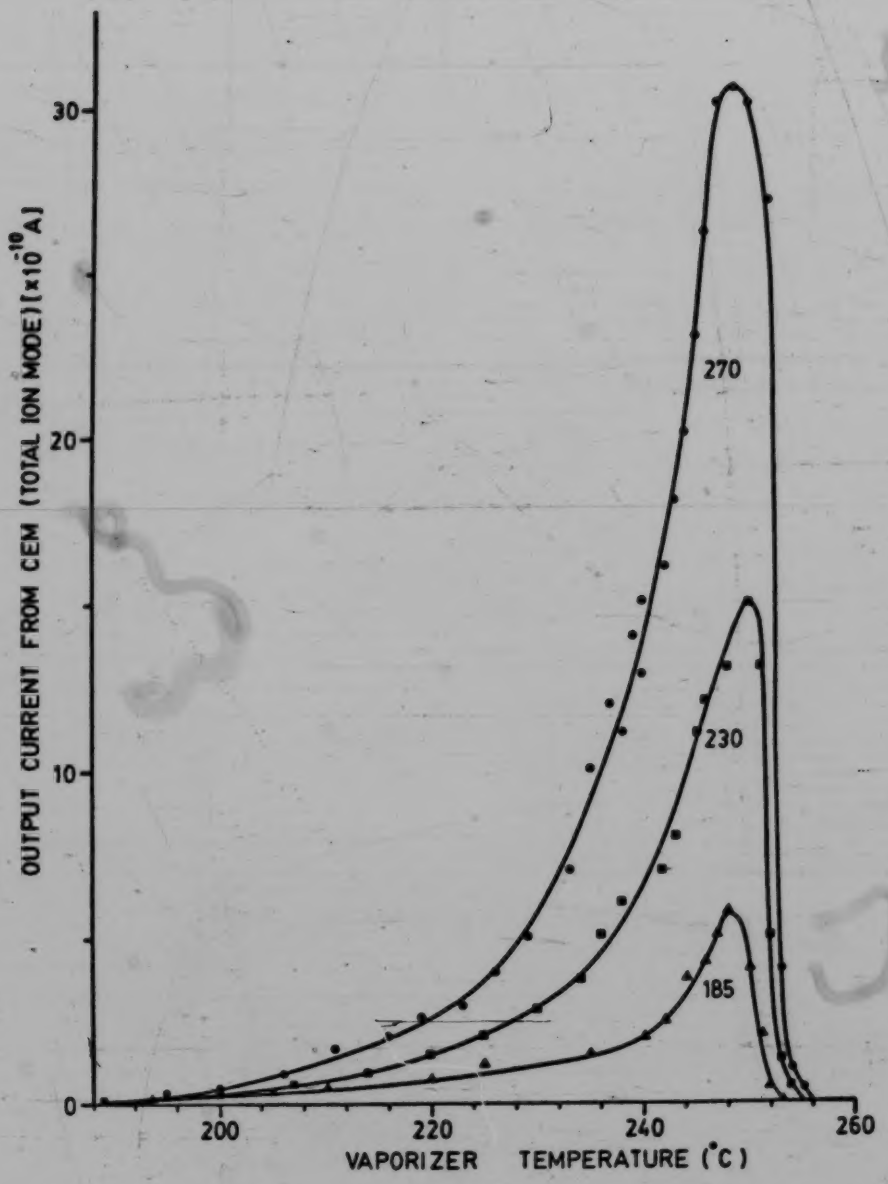

Figure 2.3 Total TSP ion current from 0.1 M aqueous ammonium acetate as a function of vaporizer temperature for different source temperatures.

3. Adjust HPLC pump flow to desired flow rate and switch on. The pressure in the pumpout line will rise rapidly to about 950 mtorr and the back pressure on the HPLC pump will oscillate about a reading of 250-300 psi. At this point the vaporizer and jet temperatures will start to decrease.
4. Increase the vaporizer and source heater voltages to compensate until the source temperature rises to about 300°C and the jet temperature is stable at around 180°C.
5. At the end of the experiment it is advisable to flush the system through with just mobile phase (50:50 methanol water mixture) for several minutes. During this operation the TSP temperatures were reduced so that the interface ran slightly "wetter" than during normal operation.
6. Switch off and disconnect HPLC pump, reduce TSP source and vaporizer temperatures to about 200°C.
7. Open exhaust valve on TSP rotary pump for about 5 minutes to expel any condensed vapor that has passed through the acetone/dry ice trap and collected in the pump oil.
8. During this time the TSP source should have "dried-out" sufficiently for the pumpout line valve to be closed. This can be checked by temporarily closing this valve and observing the pressure rise. If the convectron gauge reads a steady 20 mtorr, then leave the valve closed and switch off the TSP rotary pump. As the source pumps out overnight the pressure will drop to about 5 mtorr.

Mass calibration and measurement of quadrupole discrimination

The quadrupole was tuned using the DC bias and resolution controls, to give a constant peak width and 1 amu baseline resolution across the mass range 15 - 300 amu. The quadrupole discrimination against higher mass ions (26) was then determined by running a 70 eV spectrum of perfluoro-tert-butylamine, $[(CF_3)_3C]_3N$, with an auxillary low pressure ion source (27) mounted on the front of the quadrupole. The relative intensities (I_Q) were then compared with those obtained from an AEI MS-12 magnetic mass spectrometer (I_M) operated with the same energy. The quadrupole discrimination, Q.D., was then calculated as $QD = I_Q/I_M$ for different masses. For clarity these numbers are given at the top of each mass spectrum.

Perfluoro-tert-butylamine and p-bromophenetole [$p\text{-}BrC_6H_4OC_2H_5$] were also used for mass calibration [for mass spectra of these compounds see references (28) and (29) respectively]. The latter was particularly useful for checking resolution as the major ions in its EI mass spectrum are characteristic doublets of equal height at m/z 172,174 and m/z 200,202.

RESULTS AND DISCUSSION

(a) TSP mass spectrum of ammonium acetate. Gas phase thermodynamic control of NH_4^+ cluster intensities

Ammonium acetate is the most used additive to the aqueous or aqueous/methanol mobile phase. Therefore, the interpretation of the observed TSP mass spectrum of this additive in terms of available gas phase ion-molecule information is of special interest. The observed TSP spectrum of 0.1 M aqueous ammonium acetate is shown in Figure 2.4. The main features of the mass spectrum are similar to those reported by Vestal (9,10). The major peaks are due to $NH_4^+.NH_3$, $NH_4^+.H_2O$, $NH_4^+.NH_3.H_2O$, $NH_4^+(H_2O)_2$ and $NH_4^+.CH_3COOH$ cluster ions. The relative intensities of these peaks can be compared with intensities predicted on the basis of ion-molecule equilibrium measurements. The gas phase equilibria (4) and (5) in addition to

$$NH_4^+.H_2O + NH_3 = NH_4^+.NH_3 + H_2O \qquad (4)$$

$$NH_4^+(H_2O)_2 + NH_3 = NH_4^+.H_2O.NH_3 + H_2O \qquad (5)$$

many other equilibria involving $NH_4^+(H_2O)_w(NH_3)_n$ were studied (30) with the HPMS some time ago. These results provide equilibrium constants K_1 and K_2 for reactions (4) and (5) at different temperatures. The ligand switching equilibria (4) and (5) have relatively weak temperature dependence (30). Assuming that the TSP gas phase ion source

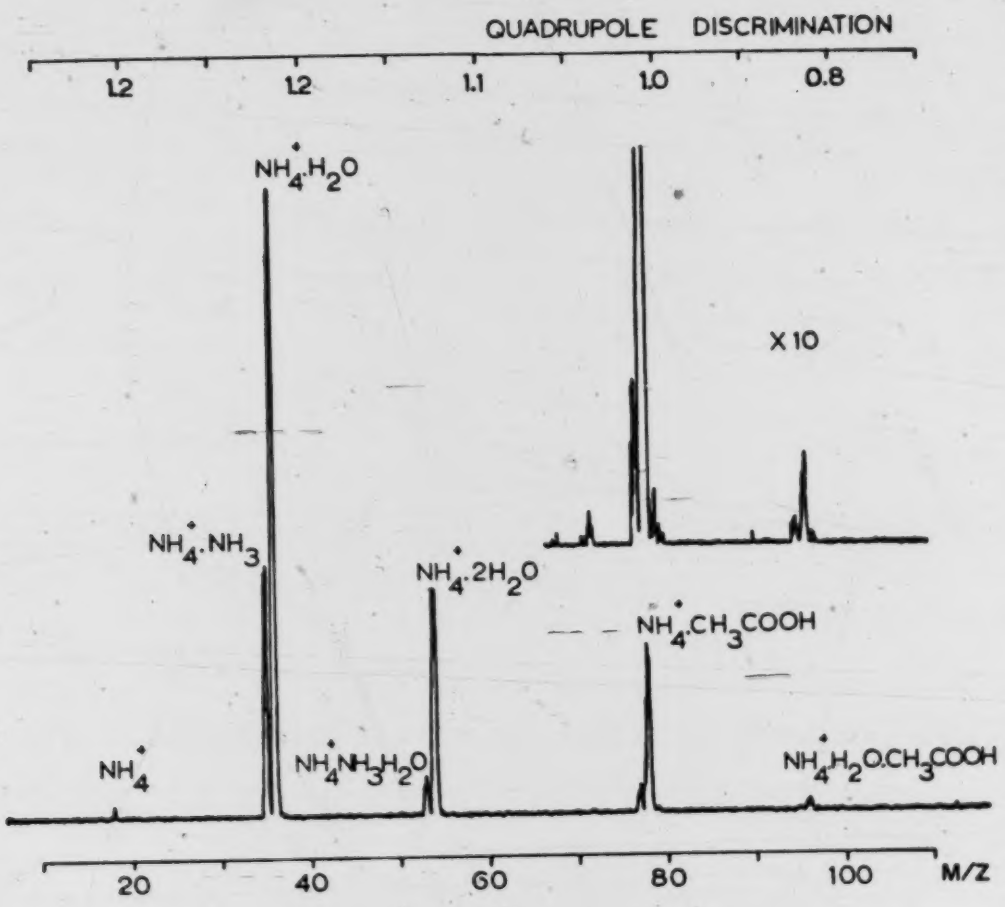

Figure 2.4 TSP mass spectrum of 0.1 M aqueous ammonium acetate, jet temperature 180°C.

has a prevailing temperature of 177°C[450°K], [see experimental], one can evaluate the expected equilibrium ion intensity ratios for $I[NH_4^+.OH_2]/I[NH_4^+.NH_3]$ and $I[NH_4^+(OH_2)_2]/I[NH_4^+.NH_3.OH_2]$ from K_1 and K_2 given in equations (6) and (8).

$$K_4 = \frac{I[NH_4^+.NH_3]}{I[NH_4^+.OH_2]} \cdot \frac{P_{H_2O}}{P_{NH_3}} = 190 \qquad (450K)^{30} \qquad (6)$$

$$\frac{I[NH_4^+OH_2]}{I[NH_4^+.NH_3]} = \frac{1}{K_1} \frac{P_{H_2O}}{P_{NH_3}} = \frac{1}{190} 555 = 2.9 \qquad (7)$$

The experimentally observed ratio (Figure 2.4) is about 3.

$$K_5 = \frac{I[NH_4^+.OH_2.NH_3]}{I[NH_4^+(OH_2)_2]} \frac{P_{H_2O}}{P_{NH_3}} = 70 \qquad (450K)^{30} \qquad (8)$$

$$\frac{I[(NH_4^+.(OH_2)_2]}{I[NH_3^+.NH_3.OH_2]} = \frac{1}{K_2} \frac{P_{H_2O}}{P_{NH_3}} = \frac{1}{70} 555 = 7.9$$

The experimentally observed ratio (Figure 2.4) is about 7.

$$P(NH_3)/P(H_2O) = [CH_3COO.NH_4]_{aq.}/55.5$$

For the partial pressure ratio of H_2O and NH_3 in the gas phase we have used the molar ratio (ammonium acetate)/(water) in solution. The agreement obtained between the ion ratios

observed in Figure 2.4 and those predicted by the equilibrium expressions leads to the following conclusions:

(a) The thermospray vaporization has converted nearly all the ammonium acetate into NH_3 and CH_3COOH molecules in the gas phase.

(b) The gas phase clustering equilibria (4) and (5) have been attained in the TSP ion source.

The presence of CH_3COOH in the gas phase is supported by the observation of the $NH_4^+.CH_3COOH$ cluster ion in Figure 2.4. Cluster stability rules [see section (c) of Results and Discussion] predict preferential take up of CH_3COOH compared to H_2O by the monosolvated NH_4^+ for equal partial pressures of H_2O and CH_3COOH gases. Therefore, the observed intensity ratio $NH_4^+.OH_2$ versus $NH_4^+.CH_3COOH$ is within the expected magnitude assuming that (nearly) all the ammonium acetate was vaporized to NH_3 and CH_3COOH.

The ion ratio $I[NH_4^+(OH_2)_2]/I[NH_4^+.OH_2]$ in the TSP spectrum Figure 2.4 can be compared with predictions (30) for the gas phase clustering equilibrium (9).

$$NH_4^+.OH_2 + OH_2 = NH_4^+(OH_2)_2 \qquad (9)$$

$$K_9 = \frac{I[NH_4^+(OH_2)_2]}{I[NH_4^+(OH_2)]\ P_{H_2O}} \approx 0.5\ (torr)^{-1} \qquad (450K)\ ^{30}$$

$$I[NH_4^+(OH_2)_2]/I[NH_4^+.OH_2] = 0.5 \text{ to } 0.25$$
$$\text{for } P(H_2O) = 1 \text{ to } 2 \text{ torr.}$$

The predicted equilibrium ratio for 1 to 2 torr H_2O pressure in the TSP ion source is close to the observed ratio of approximately 0.3, Figure 2.4. The exact pressure in the TSP ion source is not known since the measured pressure of 1 torr is a down-stream gauge pressure [see experimental section].

The agreement of the observed TSP ion intensities of Figure 2.4 with the predictions of the gas phase equilibrium data, [equations (6) to (9)], represents strong evidence that the $NH_4^+.OH_2$, $NH_4^+.NH_3$, $NH_4^+(OH_2)_2$, $NH_4^+(NH_3.OH_2)$ and $NH_4^+.CH_3COOH$ ion intensities are thermodynamically controlled. Can such a control be expected for the conditions of the TSP experiment? The temperature, pressure and flow conditions in the TSP ion source are not uniform but change in a complex and poorly defined manner. Nevertheless, the above results embolden us to suggest that the conditions in the region near the TSP ion exit orifice, which determine the observed gas phase ion chemistry, may be somewhat similar to those present in the HPMS ion source. In the HPMS apparatus, the ions are produced by a spreading electron beam whose centre is some 3 mm above the ion exit orifice. The ions reach the walls or the orifice by diffusion through the gas, a mode that may also be present in the electrically field free TSP ion source.

A measured HPMS ion residence time distribution at 2 torr and 1 torr at 450°K is shown in Figure 2.5. This was obtained by measuring the total ion flux exiting the ion source as a function of time after initial ionisation by a pulsed electron beam. The most probable ion residence time is 160 μsec, while the average residence time t_a = 480 μsec. The residence time distribution is essentially independent of ion mass so long as the ion mass is considerably larger than that of the major gas (31). This is a consequence of the diffusion rate of an ion through a gas being dependent on $(1/\mu)^{1/2}$ where μ is the reduced mass of the ion and neutral species (32). For major gases CH_4 or H_2O very similar distributions are expected (31).

The rates of exothermic gas phase ion-molecule reactions can be predicted from the Langevin-ADO orbiting capture rates (21). These depend on reduced mass, polarisability and dipole moment, and are close to the collision limit of about 10^{-9} molecules^{-1}.cm^3.sec^{-1} for most reactions. Assuming pseudo first order kinetics a halflife for reaction (4) or (5) in the forward direction at the expected TSP pressure: $P(NH_3)$ = 1/555 torr and temperature: T = 450°K can be calculated if the rate constant k_4 (or k_5) is assumed to be 2 x 10^{-9} molecules^{-1} cm^3 sec^{-1} [equation (10)].

$$t_{1/2} = (0.7)/(kn) = 10\ \mu sec \qquad (10)$$

$$n = 9.8 \times 10^{18}\ (T)^{-1}\ P(NH_3)\ (torr)$$

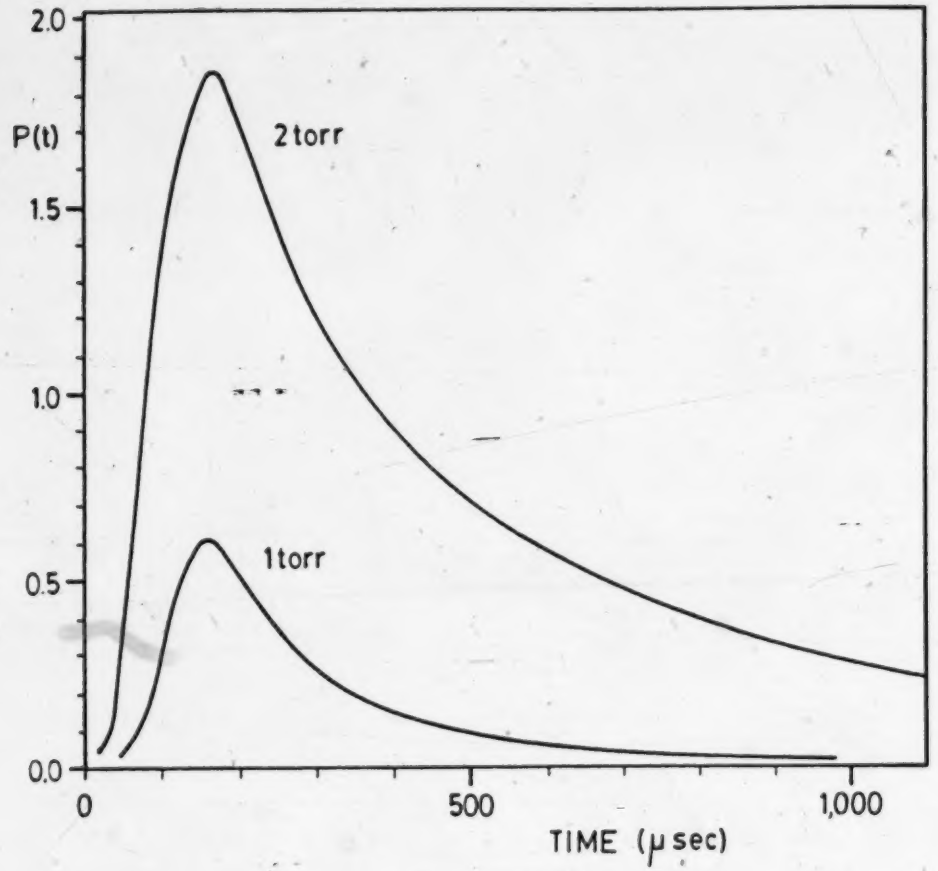

Figure 2.5 Ion residence time distribution in pulsed high pressure ion source mass spectrometer at 2 and 1 torr total pressure. Major gas CH_4, positive (and negative) ions present are in the m/e = 100 range. The ion intensity of the 2 torr curve has been normalized to give $\int_0^\infty (t)dt = 1$.

n is the number of ammonia molecules/cm^3 in the gas phase. The ligand switching reactions (4) and (5) are known to have rate constant values close to the collision limit used above (33).. Thus, there is ample time to establish equilibrium (4), if one assumes that the TSP t_a is not vastly different from t_a of HPMS. Similarly, it can be shown that hydration equilibria like (9) are also established within microseconds (33,34). In this case the high partial pressure of H_2O, about 1 torr, is especially beneficial. These considerations show that the establishment of clustering equilibria with clustering gases in the 2 mtorr (NH_3, CH_3COOH) to 1000 mtorr (H_2O) pressure range is to be expected under TSP conditions.

It should be noted that the ion residence times in conventional CI ion sources operated in the positive ion mode are much shorter than those shown for the HPMS in Figure 2.5. In the CI experiment secondary electrons are continuously produced. Their rapid diffusion to the wall produces a positive space charge which drives the positive ions to the wall much faster than is the case for the ambipolar positive ion-negative ion low charge density diffusion conditions prevailing in HPMS and probably also in TSP. This generally limits normal CI residence times to about 10 μsec (21).

Vestal has reported on the change of the relative intensities in TSP mass spectra observed at different ammonium acetate concentrations [Figure 9, Vestal (9)].

The positive ions are all ammonium ions. At low molarities, 10^{-3} to 10^{-2} M, the ions $NH_4^+.OH_2$ and $NH_4^+(OH_2)_2$ dominate and no $NH_4^+.NH_3$ and $NH_4^+.CH_3COOH$ ions are observed. At high molarity, 10^{-1} to 1 M, the dominant ions are $NH_4^+.NH_3$ and $NH_4^+.CH_3COOH$. These observations are readily explained in terms of the gas phase ion-molecule reactions and equilibria described above. At the low molarities there are correspondingly low partial pressures of NH_3 and CH_3COOH gas produced. Therfore the expected relative $NH_4^+.NH_3$ and $NH_4^+.CH_3COOH$ intensities at gas phase equilibrium will be very low. In addition to this, as will be shown in the next section, the gas phase ion-molecule kinetics involving the neutral NH_3 and CH_3COOH molecules are also slow at these low partial pressures. These effects combine and lead to dominance of the $NH_4^+(OH_2)_n$ cluster ions. At high molarities, the NH_3 and CH_3COOH partial pressures are high and the kinetics are fast. This leads to rapid approach to equilibrium and dominance of the $NH_4^+.NH_3$ and $NH_4^+.CH_3COOH$ ions. As mentioned earlier, both NH_3 and CH_3COOH form more strongly bonded clusters to NH_4^+ than H_2O, [see also part (c) in Results and discussion].

(b) Formation of MH^+ ions. Gas phase kinetic control of MH^+ intensities at low [M] and thermodynamic control at high [M]

The MH^+ peaks of analytes M are probably the most useful for the identification and quantitation of M. TSP

mass spectra obtained with aqueous 0.1 M ammonium acetate and two different concentrations of 4-methylpyridine (4-MePy) are shown in Figure 2.6. The ammonium acetate derived primary ions ($NH_4^+.OH_2$, $NH_4^+.NH_3$ etc.) = AH^+ have large intensities while the protonated 4-MePy (BH^+) is rather small, at the 4-MePy concentration of 10^{-4} M, Figure 2.6a. At the higher, 5×10^{-3} M, concentration, the AH^+ intensity is small and there is a corresponding increase in BH^+ intensity. The two spectra shown in Figure 2.6 are part of a series of experiments in which the ammonium acetate concentration of 0.1 M and all other conditions were kept constant, while the aqueous 4-MePy concentration = $[B]_{aq}$ was changed from run to run. The ion intensity changes observed in these experiments are shown in Figure 2.7, where the intensities of the ammonium ions: $I(AH^+) = I(NH_4^+.OH_2 + NH_4^+.NH_3 + NH_4^+(OH_2)_2 + \text{etc.})$ is about $2I(NH_4^+.OH_2)$ and the 4-MePy derived ions are plotted versus $[B]_{aq}$. The ion intensities I are given in percent of the total ion intensity (total ionisation). This was done in order to reduce the scatter due to changes in apparatus sensitivity or gradually changing TSP conditions from run to run. The total ionisation changed by no more than 10% from run to run and no systematic changes with increasing 4-MePy concentration were observed.

At low $[B]_{aq}$ one observes BH^+ as the only B derived ion, however at higher $[B]_{aq}$ the B_2H^+ ion appears, becoming dominant at the highest $[B]_{aq}$, Figure 2.7. The observed

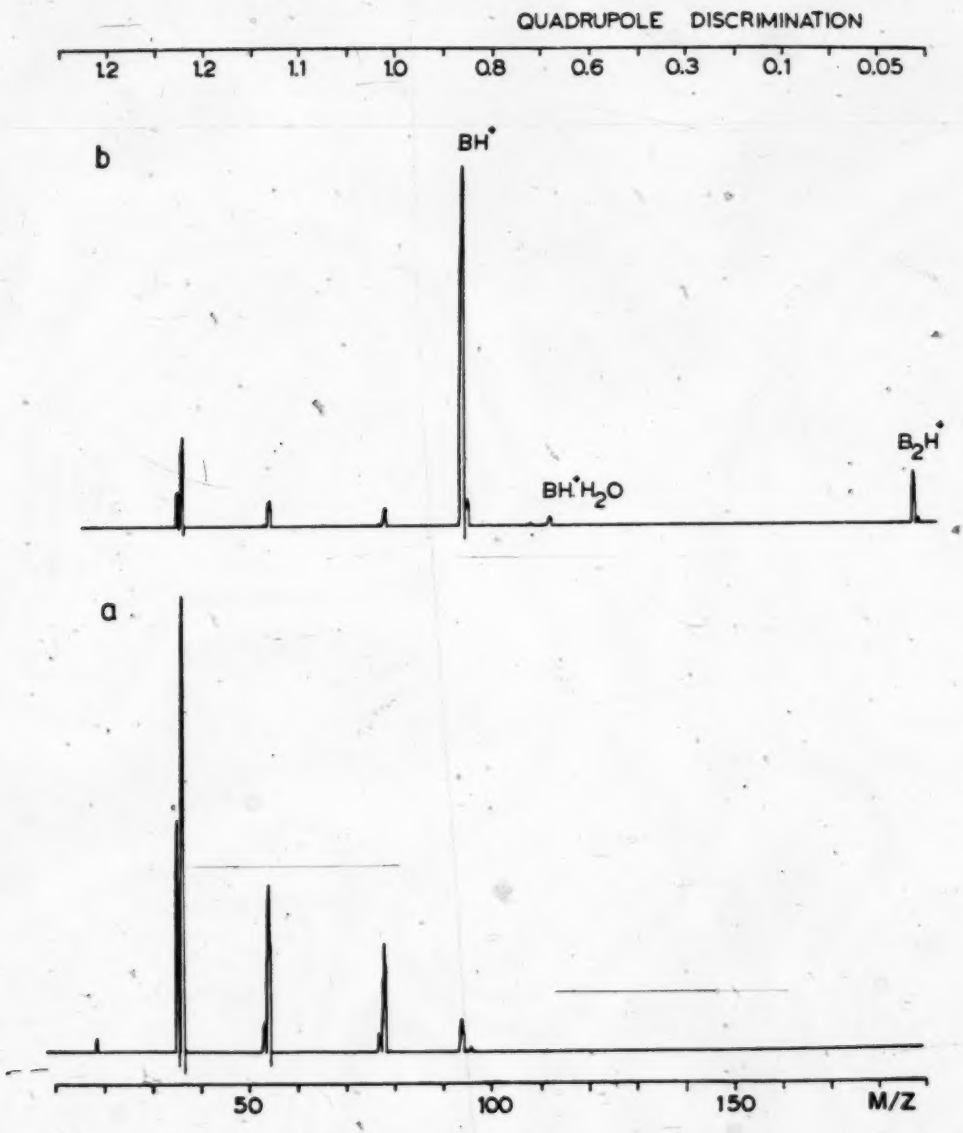

Figure 2.6 TSP mass spectra observed with 4-MePy (B) aqueous solutions containing 0.1 M ammonium acetate: (a) $[B]_{aq} = 10^{-4}$ M; (b) $[B]_{aq} = 5 \times 10^{-3}$ M.

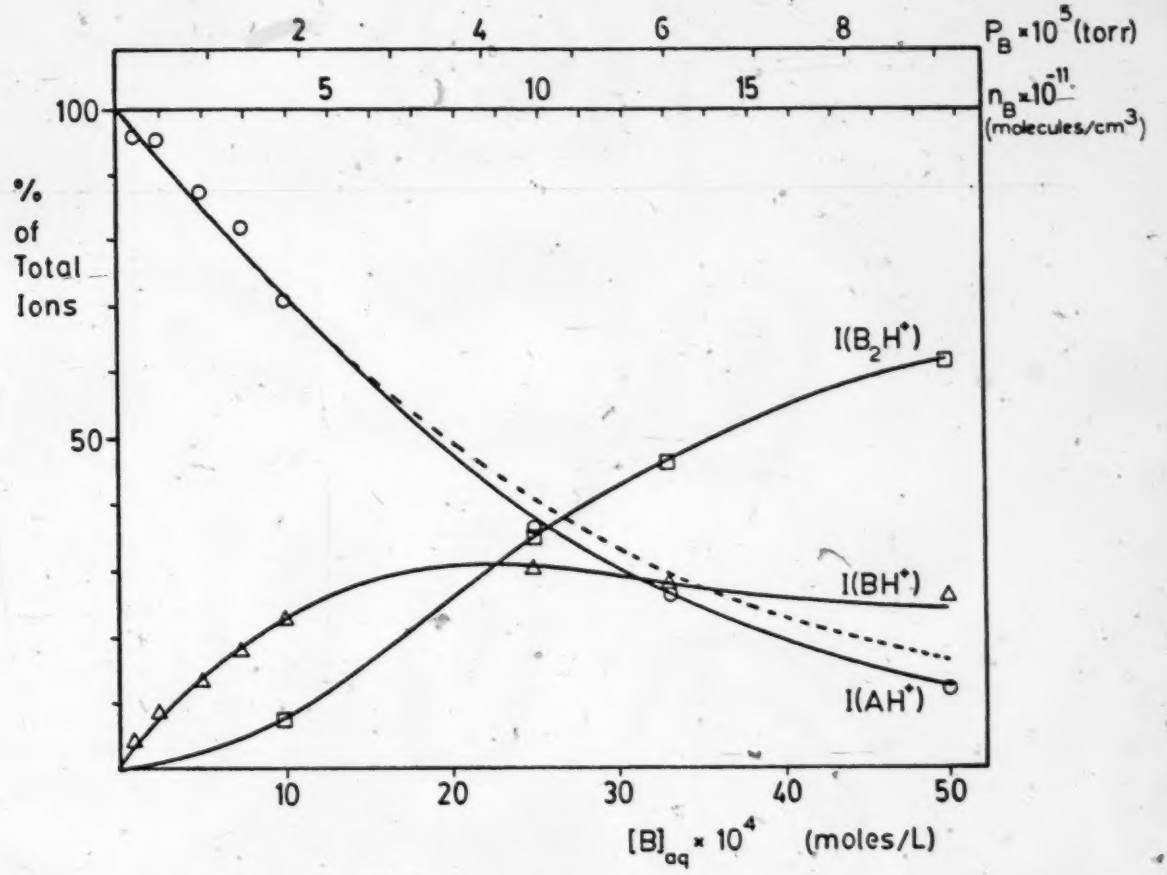

Figure 2.7 Observed TSP ion intensities in percent of total ion intensity; aqueous solutions 0.1 M ammonium acetate; B = 4-MePy. $I(AH^+)$ is the combined intensity of the ammonium ions. AH^+ is involved in the gas phase protonation of B. Dashed curve shown for $I(AH^+)$ is calculated with first order kinetics equation (13). n_B is concentration of B in gas phase calculated with equation (16).

$I(AH^+)$ change with $[B]_{aq}$ can be fitted by expression (11) as shown in Figure 2.7.

$$I(AH^+) = 100\ e^{-\alpha [B]_{aq}} \qquad (11)$$

$$\alpha = 3.567 \times 10^2 \text{ (litre/mol)} \qquad [B]_{aq} = [4\text{-MePy}]_{aq}$$

Relationship (11) can be derived on the basis of gas phase ion-molecule kinetics. We assume that the ammonia ions AH^+ are the only abundant ions produced by the TSP primary ionisation for $[B_{aq}]$ from 10^{-4} M up to 5×10^{-3} M. This assumption is justified by the observation that the total ionisation in the experiments used in Figure 2.7 did not increase noticeably with increase of $[B]_{aq}$. It is assumed that the BH^+ ion is formed by gas phase protonation of B molecules as shown in equation (12).

$$AH^+_{(g)} + B_{(g)} = A_{(g)} + BH^+_{(g)} \qquad (12)$$

The gas phase partial pressure of B is assumed proportional to $[B]_{aq}$ as shown in equations (15) and (16). The proportionality constant β is assumed equal to 55.5, which is the number of moles of H_2O in 1 litre of solution. This means that the molar ratio H_2O to B in solution is assumed to be (approximately) preserved also in the gas phase. Water being the only solvent leads to $P(tot) = P(H_2O)$.

The gas phase intensity of the AH^+ ions involved in

reaction (12) should obey first order kinetics (equation 13).

$$I(AH^+) = 100\ e^{-k_{12} n_B \bar{t}} \qquad (13)$$

n_B = molecules B/cm^3 in the gas phase

$$n_B = 9.8 \times 10^{18}\ (T)^{-1}\ P_B\ (\text{torr}) \qquad (14)$$

$$P(B)/P(H_2O) = [B]_{aq}\ /\beta \qquad (15)$$

$P(H_2O)$ is approximately P(tot)

$$n_B = 9.8 \times 10^{18}\ (T)^{-1}\ (\beta)^{-1}\ P(\text{tot})\ [B]_{aq} \qquad (16)$$

where the concentration n_B = molecules B per cm^3 relates to the gas phase. The rate constant k_{12} is for the gas phase proton transfer and is expected to be about 2×10^{-9} molecules^{-1}.cm^3.sec^{-1} for B = 4-MePy (35,36). The reactive average residence time of the ions in the TSP ion source is $\bar{t}$, which we assume to be constant at a given ion source pressure and temperature. The gas phase concentration n_B is also constant for each experiment with a given $[B]_{aq}$. The neutral B molecules in the gas phase are of much higher concentration than the ions AH^+ such that no depletion of B occurs due to ion molecule reactions (pseudo first order rate constant = kn). Equation (14) relating n_B to the partial pressure of B and the temperature of the ion source is based on the ideal gas law, and equation (16) follows from equation (15) which is based on the assumed complete vaporization of the aqueous B.

Obviously equation (13) can be identified with the

experimentally observed relationship (11). A plot of $\ln[I(AH^+)]$ vs $[B]_{aq}$ (and n_B) i.e. a replot of the data from Figure 2.7, is shown in Figure 2.8. The slope obtained assuming $k_{12} = 2 \times 10^{-9}$ molecules^{-1}.cm^3.sec^{-1} leads to $\bar{t} = 340$ μsec for a measured TSP ion source pressure 1 torr. However, since the pressure gauge is downstream from the ion source [see experimental section], the actual pressure may be somewhat higher, which would lead to a lower $\bar{t}$.

The BH^+ intensity in Figure 2.7 increases linearly with $[B]_{aq}$ for $[B]_{aq} < 10^{-3}$ M. At higher concentrations this linear response is lost, due to depletion of the reagent ions AH^+ by reaction (12). An additional source leading to nonlinearity is the formation of B_2H^+, at high [B]. This product should be formed by the well known (37) gas phase clustering reaction (17).

$$BH^+(g) + B(g) = B_2H^+(g) \qquad (17)$$

The assumption that relatively little protonated 4-MePy is produced by primary TSP ionisation is supported by the success of the kinetic treatment of the data in Figure 2.7 and 2.8. The presence of uncharged B in the gas phase is also clearly indicated by the observed concentration dependence of B_2H^+, Figure 2.7, which fits the expected shape for gas phase first order consecutive reaction (12) followed by (17). Since 4-MePy is very volatile (b.p. 145°C), its presence in the vapor phase at about 180°C is not at all surprising.

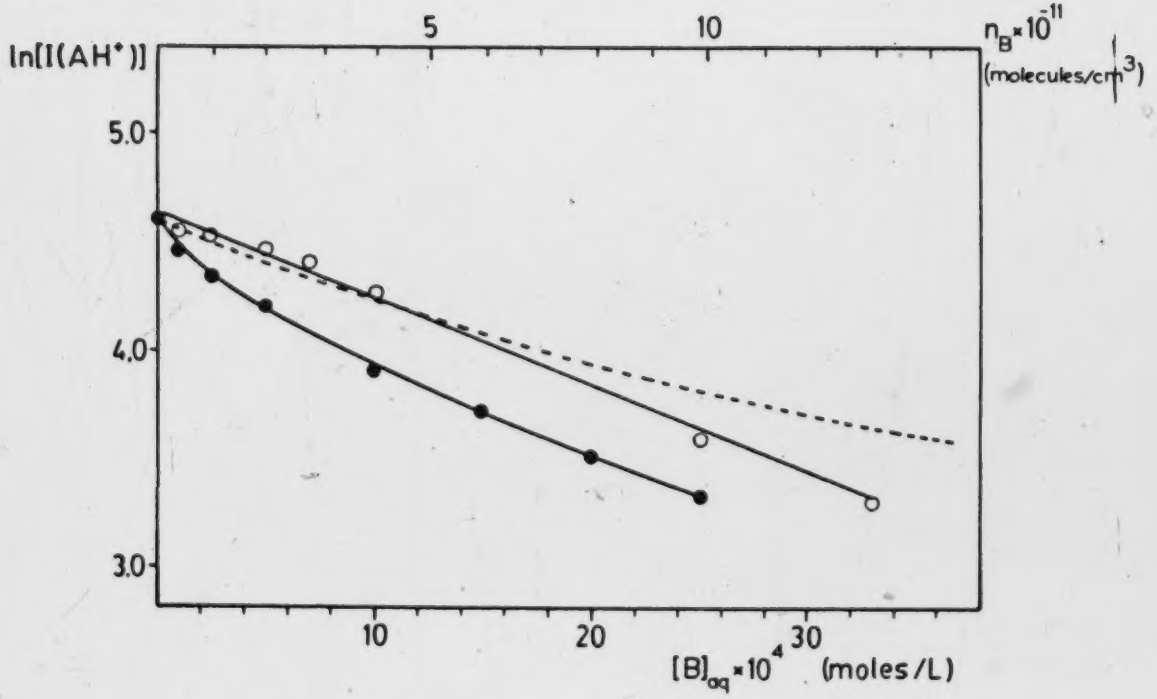

Figure 2.8 Plot of $\ln[I(AH^+)]$ versus $[B]_{aq}$; n_B is the concentration of B in the gas phase calculated from equation (16).
○ $I(AH^+)$ data from Figure 2.7, B = 4-MePy;
● $I(AH^+)$ data from Figure 2.9, B = 4-Me_2NPy.
Dashed line, calculated $I(AH^+)$ using rate constant $k_{12} = 2 \times 10^{-9}$ molecules^{-1}.cm^3.sec^{-1} and ion residence time distribution P(t) for HPMS ions, Figure 2.5.

The situation when significantly less volatile analytes are present in solution may be different.

The ion intensities-concentration dependence from a series of experiments involving the much stronger base 4-N,N dimethylaminopyridine = 4-Me_2NPy are shown in Figure 2.9. On the whole, there is considerable similarity between the appearance of this Figure and the corresponding results for 4-MePy shown in Figure 2.7. However, the rate of decrease of $I(AH^+)$ is slower for 4-MePy. The $\ln[I(AH^+)]$ plot for 4-Me_2NPy is shown in Figure 2.8. The slope obtained is about twice as large as that for 4-MePy. This result indicates that the proton transfer rate constant k_{12} for 4-Me_2NPy is twice as large as that for 4-MePy, assuming that the efficiency for vaporization (i.e. β) is the same in each case.

An exactly linear logarithmic plot (Figure 2.8) is not expected when a reaction time distribution is present. An exact evaluation of the expected product $I(AH^+)$ is possible if the time distribution curve P(t) is known. The evaluation is obtained with equation (18):

$$I(AH^+) = 100 \int_0^\infty P(t) e^{-kn_B t} dt \qquad (18)$$

Using the HPMS residence time distribution P(t) of Figure 2.5, $I(AH^+)$ were evaluated with equation (18) for each

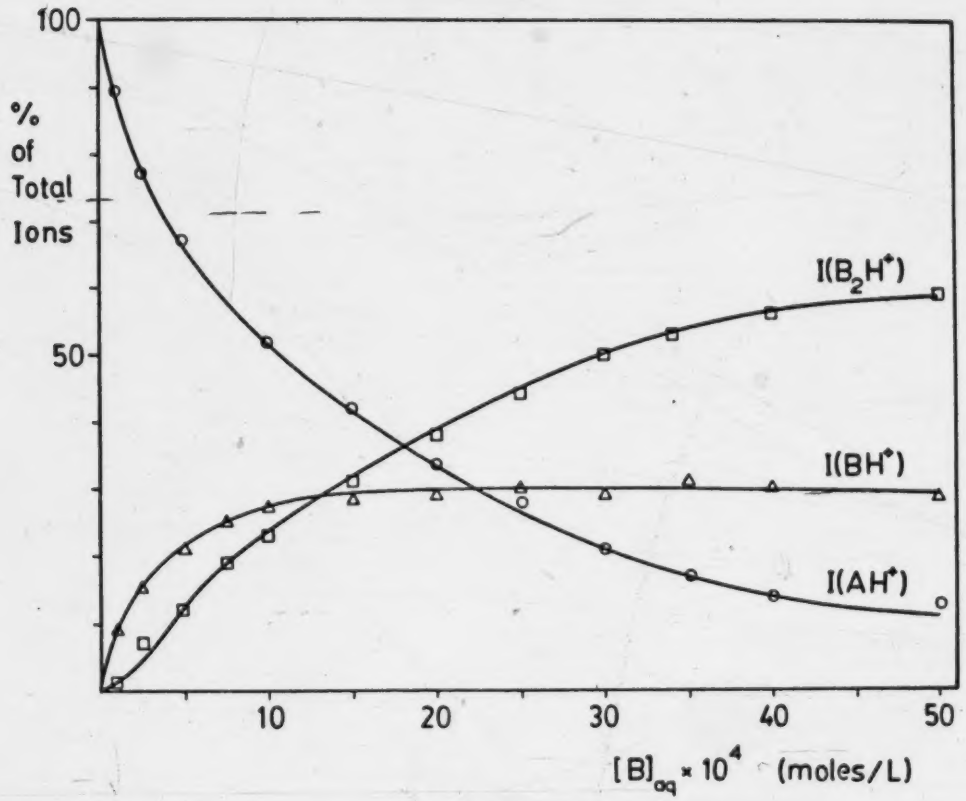

Figure 2.9 Same as Figure 2.7, but for B = 4-Me_2NPy.

n_B corresponding to a given $[B]_{aq}$, see equation (16), using the rate constant $k = 2 \times 10^{-9}$ molecules^{-1}.cm^3.sec^{-1}. A logarithmic plot of the calculated $I(AH^+)$ is shown in Figure 2.8. The plot has curvature, as expected. The similarity of the three plots indicates that the TSP residence time distribution may be similar to that of the HPMS.

The TSP mass spectra obtained with 0.1 M ammonium acetate and equimolar 10^{-4} M concentrations of each of the pyridines: Py, 4-MePy, 4-MeCOPy, 3-ClPy, 4-CNPy are shown in Figure 2.10a. The ammonium ion AH^+ intensities are very large while the various BH^+ ion intensities are quite small i.e. less than 5% of the AH^+ intensity, a result anticipated from Figures 2.7 and 2.9. The relative intensities of the ions BH^+ from bases B relative to that for PyH^+ from Py, all at 10^{-4} M, will be called the response for BH^+ = $r(BH^+)$. The $r(BH^+)$ for the pyridines are given in Table 2.1. Also given in Table 2.1 are $r(BH^+)$ for other bases studied. In some cases a group of 3-4 bases was used simultaneously in the solution, in others only a given pair. The $r(BH^+)$ were essentially independent of the presence of the other bases, see Table 2.1.

The observed independence of $r(BH^+)$ on the presence of other bases, at 10^{-4} M is consistent with the results and interpretation of Figures 2.7 and 2.9, where it was shown that when $[B]_{aq}$ is about 10^{-4} M, the corresponding gas phase concentration n_B is very low and therefore the

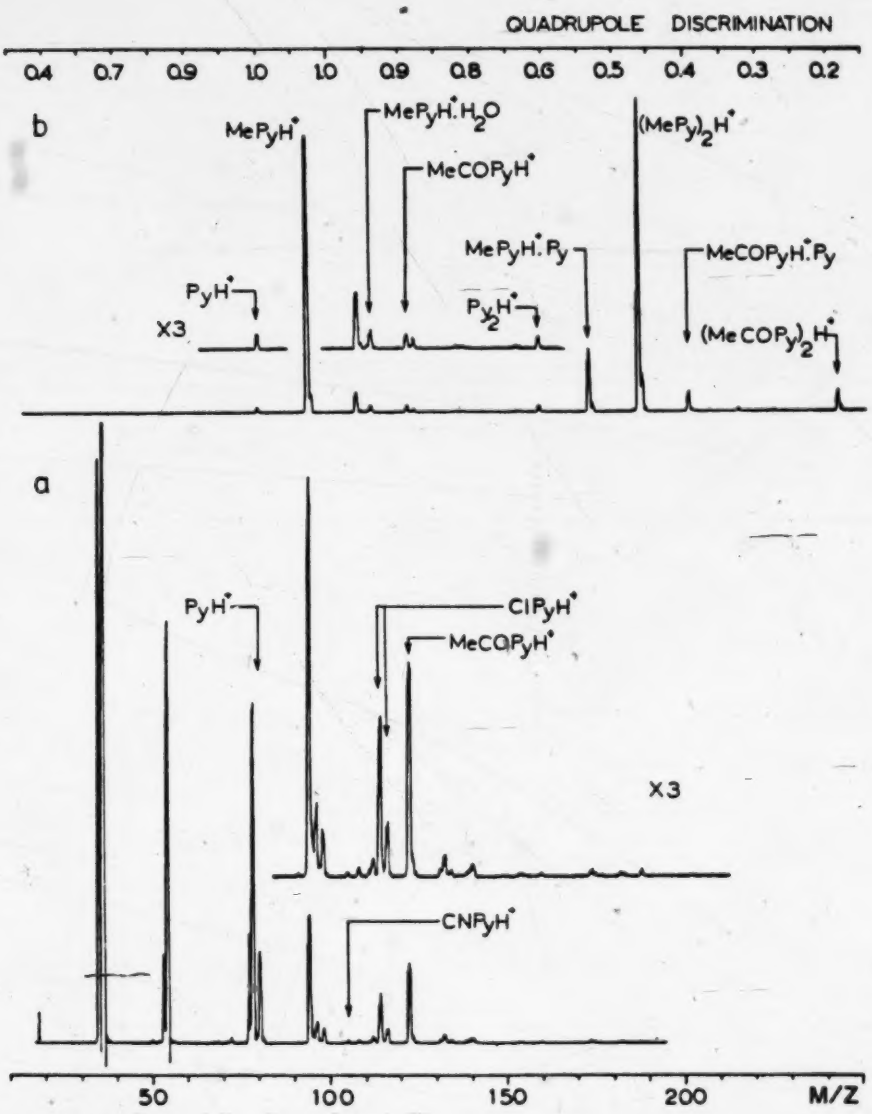

Figure 2.10 TSP mass spectra for mixture of pyridines in 0.1 M aqueous ammonium acetate: (a) each pyridine at 10^{-4} M concentration; (b) each pyridine at 10^{-2} M.

Table I. Relative Intensities of BH^+ Ions of Bases B in TSP Mass Spectra

analyte (B)[a]	pK_B[b]	PA(B)[c]	$r(BH^+)$[d] C	D	E	F	G	H
Proton Sponge	1.66	241.8		46	32			
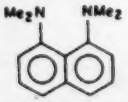								
4-(dimethylamino)pyridine	4.4	236.2		38				
4-methylpyridine	8.0	225.0	13	16				
1,8-diaminonaphthalene	9.39	223.8		11				
adenine	9.85	223.5				34	40	
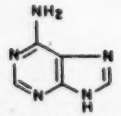								
m-phenylenediamine	9.1	222.4					10	10
pyridine	8.8	220.8	10	10	10	10	10	
4-acetylpyridine	10.5	217.4	8.6					
3-chloropyridine	11.2	214.8	5.5					
4-cyanopyridine	12.2	210.3	0.3					
pyrazine	13.4	209.0						<0.01

[a]The concentration of all analytes B was $[B]_{aq} = 10^{-4}$ M. [b]Basicity constant in aqueous solution 298 K. [c]Proton affinity in (kcal/mol). [d]Intensity of BH^+ ion relative to BH^+ for pyridine. Ion intensities corrected for mass-dependent discrimination of quadrupole. Sample sets D, E, F, and G in 75% 0.1 M aqueous ammonium acetate and 25% methanol and sets C and H in 0.1 M aqueous ammonium acetate.

kinetics of proton transfer from AH^+ to B are also slow(kinetic control). This leads to only insignificant depletion of the ammonium reagent ions AH^+ due to proton transfer to B. The depletion of BH^+ by consecutive reactions (17) and (19) is much slower still and this leads to linear response at low concentrations even in the presence of other bases.

$$B_1H^+ + B_2 = B_1 + B_2H^+ \qquad (19)$$
$$PA(B_2) > PA(B_1)$$

Examining the $r(BH^+)$ for various bases B with different proton affinities PA(B), see Table 2.1, one finds that bases with PA(B) > 214 kcal/mol have a response near 10. Below this value the response decreases rapidly with decrease of PA(B), becoming essentially zero from PA(B) =209 kcal/mol downwards. Somewhat surprisingly, the response for the very high proton affinity bases PA(B) >> 214 kcal/mol is quite high i.e. between 30 and 50. One may be interested to examine why the cut off point is approximately around PA(B) = 209 kcal/mol and not at 204 kcal/mol, the value corresponding to $PA(NH_3)$ and why there is a change in response of the high PA bases.

The proton transfer (12) from AH^+ to B is represented in equations (20) and (21) where the cluster ion $NH_4^+.OH_2$ is used as it is the major ion in the AH^+ group.

$$NH_4^+.OH_2 + B = NH_3 + BH^+ + OH_2 \qquad (20)$$

$$\Delta H_{20} = D(NH_4^+ - OH_2) + PA(NH_3) - PA(B)$$

$$\Delta H_{20} = 20 + 204 - PA(B)$$

$$NH_4^+.OH_2 + B \xrightarrow{a} (H_3NHB)^+ + OH_2 \qquad (21)$$

$$(H_3NHB)^+ \xrightarrow{b} BH^+ + NH_3$$

$$(H_3NHB)^+ \xrightarrow{c} B + NH_4^+$$

The direct route (20) can be followed only by compounds with PA(B) > 224 kcal/mol, i.e. the top three to five compounds in Table 2.1. Compounds B with lower PA, probably will follow route (21). Reaction (21a) is a ligand switching reaction. Data from limited kinetic studies for such reactions are available (33). These were performed at room temperature and involved small ligands (H_2O, NH_3 etc.). The rate constants were found to be close to the value of 10^{-9} molecules^{-1} cm^3 sec^{-1} when the reactions were exothermic. It is possible that at the present high temperature of about 180^{o}C these reactions might be slower and thus dependent on the nature of B. Although contrary to that expected for "conventional reactions", the phenomenon of negative temperature dependence has been previously observed and studied for a number of ion-molecule reactions (39,40). This expectation would hold even to a greater extent for the other AH^+($NH_4^+.NH_3$, $NH_4^+.CH_3COOH$) in which the bonding in

the clusteris stronger. A dependence of the rate constant k_{21} on the exothermicity of the reaction is therefore possible. The thermal dissociation of $BHNH_3^+$, the product of (21a), by reaction (21b) is probably fast at 450°K. This dissociation will take the desired route (21b) only when $PA(B) > PA(NH_3)$.

The above discussion suggests it is very likely that the rate constant k_{12} for the overall proton transfer from AH^+ to B is considerably below 10^{-9} for B if the PA(B) is only a few kcal/mol higher than $PA(NH_3)$ = 204 kcal/mol. Increases of k_{12} above 10^{-9} and up to the ADO collision limit (35) of approximately 5×10^{-9} molecules^{-1}.cm^3 sec^{-1} for large polarisable B can be expected to occur as PA(B) increases over the range 210 to 220 kcal/mol (Table 2.1). Thus, the changing $r(BH^+)$ observed in Table 2.1 probably largely reflects changes of the proton transfer rate constant k_{12}.

Another ion-molecule process contributing to the $r(BH^+)$ decline above the proton affinity of NH_3 is reaction (22).

$$BH^+ + NH_3 = B + NH_4^+ \qquad (22)$$

It can be shown that due to the high ratio of $P(NH_3)/P(B)$ which is approximately 1000, reaction (22) will be effectively deprotonating BH^+ from bases B whose proton affinity is only a few kcal/mol higher than that of NH_3.

Other factors that could be affecting $r(BH^+)$ are changing efficiency of vaporization of B from solution (i.e. β = 55.5) and direct primary TSP ionisation of BH^+ from solution for B with high aqueous basicities e.g. proton sponge, 4-Me_2NPy (Table 2.1). A variation of β for very nonvolatile B is a distinct possibility, however for the present set of compounds where the least volatile adenine and proton sponge show strong responses, variability of β need not be invoked. Primary TSP ion production of BH^+ for strong aqueous bases B cannot be excluded but direct evidence for this process in the presence of excess ammonium acetate is hard to obtain.

The TSP mass spectrum obtained with 0.1 M ammonium acetate and a mixture of pyridines each at 10^{-2} M is shown in Figure 2.10b. The high gas phase concentrations of n_B of the bases B resulting from the high $[B]_{aq}$ make the proton transfer reactions (12) from AH^+ to B and (19) from B_1H^+ to B_2 very fast so that the reactions approach thermodynamic equilibrium. The mass spectrum is dominated by the $MePyH^+$ and $(MePy)_2H^+$ ions. The next highest BH^+ is PyH^+. The observed ratio: $I(MePyH^+)/I(PyH^+)$ is about 40. The thermodynamically predicted ratio, based on evaluation of the proton transfer equilibrium constant K can be obtained as follows.

The enthalpy change for reaction (19) can be obtained from equation (23).

$$\Delta H_{19} = PA(B_1) - PA(B_2) \qquad (23)$$

This is related to the free energy change by

$$\Delta G_{19} = \Delta H_{19} - T\Delta S_{19} \qquad (24)$$

The equilibrium constant K_{19} can be obtained from the free energy change by use of equation (25), where K_{19} is given by equation (26).

$$-RT\ln K_{19} = \Delta G_{19} \qquad (25)$$

$$K_{19} = [B_1]/[B_2] \times [B_2H^+]/[B_1H^+] \qquad (26)$$

As entropy changes associated with protonation are generally small (22,24), ΔG_{19} can be approximately set equal to ΔH_{19}. Combining equations (23) and (25) one obtains

$$\ln K_{19} = [PA(B_2) - PA(B_1)]/RT \qquad (27)$$

If the efficiency of vaporization for B_1 and B_2 are assumed to be the same, and $[B_1]_{aq} = [B_2]_{aq}$ then combining equations (26) and (27) yields

$$\ln[B_2H^+]/[B_1H^+] = [PA(B_2) - PA(B_1)]/RT \qquad (28)$$

The expected ratio, obtained using equation (28) at 450°K from the gas phase basicity difference of 4-MePy and Py (22) is 132. However, in other measurements involving bases B_1 and B_2 at about 10^{-2} M aqueous concentrations and 0.1 M ammonium acetate, the TSP observed intensity ratios $I(B_2H^+)/I(B_1H^+)$, where B_2 is the base with the higher proton

affinity, were generally lower and at times considerably lower than the equilibrium ratios. For example, for B_1 and B_2 = p-anisidine and m-phenylenediamine, the observed ratio was about 132 while the thermodynamic one is 8,100. Similarly for aniline and pyridine the observed ratio is about 60, while the predicted equilibrium ratio is 283,700. Part of the above discrepancies are undoubtedly due to the wide ion residence time distribution in the TSP source. Ions BH^+ with very short residence times will not reach equilibrium, i.e. they will not be converted to B_2H^+ and their presence in the TSP mass spectrum will lead to low B_2H^+/B_1H^+ ratios. This error will be particularly large when the thermodynamically predicted ratio is large. Other instrumental sources of non-equilibrium B_1H^+ in the region immediately outside the TSP ion source region may also be present. However, even though the TSP ratios are lower than the thermodynamically predicted ones, their values clearly reflect the thermodynamically favoured direction.

(c) Application of ion cluster stability rules to TSPMS

It has been shown in the preceding sections that gas phase ion cluster equilibria are probably achieved with solvent, NH_3 and CH_3COOH molecules present from the vaporization of ammonium acetate and analyte molecules when these are present at above 10^{-3} M in the aqueous solution.

A very simple rule for the stability of hydrogen bonded adducts $(B_2HB_1)^+$ has emerged from studies of gas phase ion

cluster equilibria with HPMS and other apparatus. This rule will be illustrated with examples of relative ion intensities obtained from the TSP spectra presented in the previous sections.

It is found (41-46) that the stability of hydogen bonded adducts B_2H^+- B_1, where B_2 is the stronger base, increases with the gas phase acidity of the hydrogen donor B_2H^+ and the gas phase basicity of the hydrogen acceptor B_1. Since the gas phase acidity of B_2H^+ decreases with increasing basicity of the conjugate base B_2, the cluster stability of B_2H^+- B_1 increases with the proton affinity of B_1 and decreases with the proton affinity of B_2. The rule is best illustrated if one of the partners, say B_1 is kept constant and the other, B_2H^+, is changed. An example is given in Figure 2.11. The constant base B_1 is H_2O and the changing B_2H^+ species are oxonium and nitronium ions. The bond energy in B_2H^+- OH_2 is seen to increase with decreasing proton affinity of B_2 i.e. with increasing acidity of the conjugate acid B_2H^+.

An example of the application of this rule to the present TSP spectra is illustrated by comparing the $NH_4^+.OH_2$ intensity in the ammonium acetate spectrum (Figure 2.4) with the $MePyH^+.OH_2$ intensity in the spectrum of Figure 2.6b. In spite of the presence of a large $MePyH^+$ intensity in Figure 2.6b, the observed intensity of the hydrate $MePyH^+.OH_2$ is very small, while in the ammonium acetate spectrum the $NH_4^+.OH_2$ ion is dominant. The small relative intensity of

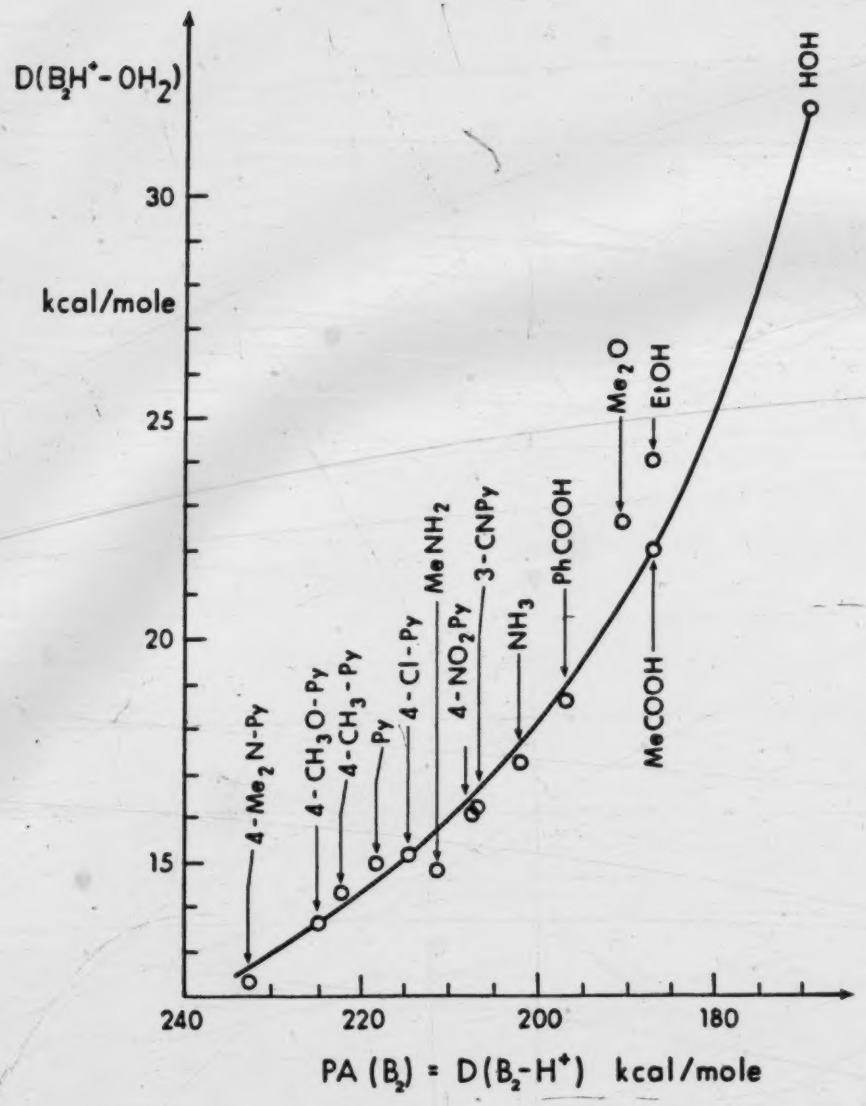

Figure 2.11 Stability of hydrogen bonded adducts $B_2H^+ - OH_2$. The bond dissociation energy $D(B_2H^+-OH_2)$ increases with decreasing proton affinity of B_2 i.e. with increasing acidity of the conjugate acid B_2H^+. The compounds B_2 are shown in the Figure. From Davidson 42.

the $MePyH^+.OH_2$ ion follows from the much weaker acidity of $MePyH^+$, PA(MePy) = 224, relative to the acidity of NH_4^+, $PA(NH_3)$ = 204 kcal/mol.

Illustrations of the rule that the stability of B_2H^+- B_1 increases with the gas phase basicity of B_1 are present in the TSP spectra Figures 2.4 and 2.6. Thus in Figure 2.4 the $NH_4^+.OH_2/NH_4^+.NH_3$ intensity ratio is only about 3 for a partial pressure difference OH_2 to NH_3 of about 555. This is due to the stronger base B_1 = NH_3, PA = 204 kcal/mol, forming a stronger cluster with NH_4^+ and thus partially offsetting the very large concentration ratio in favour of the weaker base $PA(H_2O)$ = 166 kcal/mol. Similarly, the observed ratio $NH_4^+.NH_3/NH_4^+.CH_3COOH$ is about 2 while the partial pressure ratio NH_3/CH_3COOH is about 1. If we examine the proton affinities, $PA(NH_3)$ =204, $PA(CH_3COOH)$ = 190 kcal/mol, we see that again the stronger base forms the more stable cluster.

In Figure 2.6b, one observes a very large $(MePy)_2H^+$ to $MePyH^+.OH_2$ ratio even though $P(MePy)/P(H_2O)$ is about 1/11,000. This illustrates the much higher stability of the $MePyH^+$- MePy relative to the $MePyH^+$- OH_2 adduct which follows from the much higher PA(MePy) = 225 relative to $PA(H_2O)$ = 166 kcal/mol.

Adduct ions B_2H^+- OH_2 and B_2H^+- CH_3OH observed in TSP spectra with aqueous/methanol mixtures will show relatively large intensities for the methanol adducts due to $PA(CH_3OH)$ = 181 kcal/mol being larger than $PA(H_2O)$ = 166 kcal/mol.

All proton affinities quoted in this section are from the Lias compilation (22).

CONCLUSIONS

1. The observed positive ion TSP mass spectrum of ammonium acetate is determined by the gas phase ion-molecule equilibria between NH_4^+ and OH_2, NH_3, CH_3COOH for 10^{-2} to 1 M ammonium acetate concentrations. The NH_3 and CH_3COOH molecules in the gas phase must result from the thermospray vaporization process. A good fraction of the ammonium acetate in solution is converted to gas phase NH_3 and CH_3COOH.

2. The TSP mass spectra of organic bases B from aqueous or aqueous/methanol solutions containing 0.1 M ammonium acetate can be explained on the basis of gas phase ion-molecule kinetics and equilibria. The primary TSP ions are clustered ammonium ions. Gaseous B molecules (bases) are protonated by proton transfer from the ammonium ions. At $[B]_{aq} < 5 \times 10^{-3}$ M the partial pressure of B is small and the formation of BH^+ is kinetically controlled. Linear response for BH^+ on $[B]_{aq}$ is observed. At increasing $[B]_{aq}$ from 5×10^{-3} to 10^{-2} M the intensity of BH^+ is increasingly determined by gas phase proton transfer thermodynamics. For a mixture of bases, the one with the highest proton affinity will dominate the TSP spectrum.

3. Gas phase ion-molecule reaction kinetics can at least semi-quantitatively be applied to the gas phase TSP

conditions. The average effective reaction time of the ions $\bar{t}$ is a few hundred microseconds.

4. The above conclusions are valid for volatile and moderately volatile analytes (see examples in Table 2.1). Their applicability to increasingly nonvolatile analytes remains to be tested.

Postscript

During the course of this investigation there was a growing realisation amongst many TSP practitioners that ion-molecule reactions play a significant role in the second stage TSP process. Vestal, in a paper describing the principles and applications of the TSP LC/MS interface (47), acknowledges that neutral compounds are apparently ionised by the same gas phase ion-molecule reactions that occur in ordinary CI sources, even though the primary "reagent ions" are produced by means of a different mechanism. Data consistent with this hypothesis was obtained by Bursey and co-workers (48) who conducted a limited study with reactions which were endothermic in solution but exothermic in the gas phase. The TSP spectra they obtained showed the expected gas phase products.

The negative ion TSP spectrum of 0.1 M ammonium acetate consists of CH_3COO^- and its dimer with CH_3COOH (9). If gas phase ion-molecule chemistry governs the second stage TSP process then the gas phase acidities of the analytes should determine the observed negative ion spectra. That is

CH_3COO^- will form A^- from HA by proton abstraction if CH_3COOH is a weaker gas phase acid than HA (CH_3COO^- stronger gas phase base than A^-). Conversely if CH_3COOH is a stronger gas phase acid than HA (CH_3COO^- weaker gas phase base than A^-) then adduct formation to give $[AHCH_3COO]^-$ is more likely (21). Parker and co-workers (49) recently showed this to be the case for several model analytes which were not appreciably ionised in the pH 7 0.1 M ammonium acetate solution used as mobile phase.

APPENDIX TO CHAPTER 2

Thermospray evaporation of inorganic ions.

Several inorganic cations could be detected by thermospray mass spectrometry. Aqueous solutions containing 10^{-3} M of the metal salt (nitrate or sulfate), were pumped to the interface, which was operated under normal conditions. For the alkali metals, lithium, sodium, potassium, rubidium and cesium the ion signals were due to clusters of the form $X^+(H_2O)_n$, where X^+ was the alkali ion in solution. The results obtained are presented, in bar graph form in the lower half of Figure 2.12. Intensities are shown normalized with respect to the largest cluster for each metal. The position of the maximum in the water cluster distribution decreases from n=3 for Li^+ to n=1 for Cs^+. This is in agreement with the decrease in cluster binding energies from Li^+ to Cs^+ (24). The degree of solvation expected under equilibrium conditions at this temperature may be may be predicted from the thermochemical data obtained by Kebarle et al (24). That is for the gas phase equilibrium:

$$X^+(H_2O)_{n-1} + H_2O = X^+(H_2O)_n$$

$$K_{n-1,n} = \frac{[X^+(H_2O)_n]}{[X^+(H_2O)_{n-1}] \times P_{H_2O}} = \frac{[n]}{[n-1]P_{H_2O}} \quad torr^{-1}$$

where $P(H_2O)$ is the pressure of water in torr.

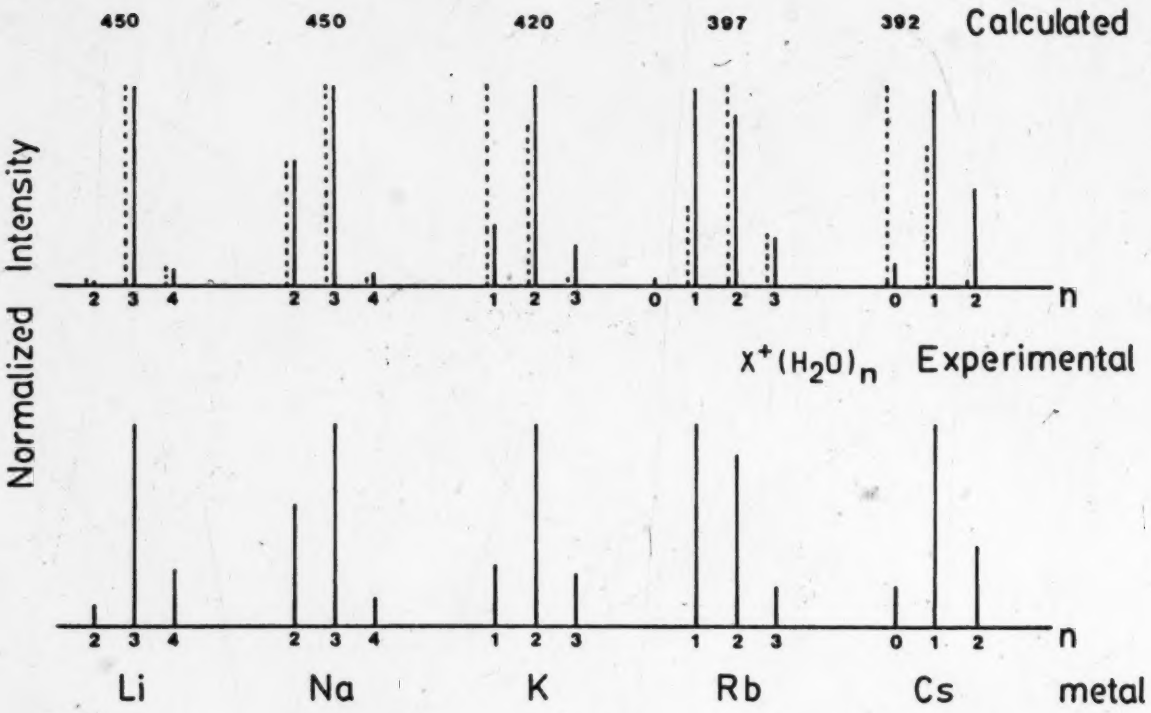

Figure 2.12 Cluster ions produced by ion evaporation from 10^{-3} M aqueous solutions of alkalie metal salts using a TSP source.

Lower trace: Experimental results, jet temperature 170°C.

Upper trace: ---- calculated equilibria using a temperature of 450°K

—— calculated equilibria using "best-fit" temperature

From standard thermochemical relationships

$$K_{n-1,n} = e^{-(\Delta H_{n-1,n} - T\Delta S_{n-1,n})/RT}$$

$\Delta H_{n-1,n}$ and $\Delta S_{n-1,n}$ are known and this allows $K_{n-1,n}$ to be calculated using the previouly estimated effective TSP temperature of 450°K . With values for $K_{n-1,n}$ the relative intensities of the clusters can be obtained from:

$[n_1]/[n_0] = K_{0,1} \times P(H_2O)$

$[n_2]/[n_1] = K_{1,2} \times P(H_2O)$ etc.

The calculated equilibrium intensities, assuming a TSP source pressure of 2 torr, are shown as dashed lines in the upper part of Figure 2.12. Considering that these equilibria are strongly temperature dependent, the agreement between observed and predicted results is surprisingly good. It also confirms that near equilibrium conditions are attained in the TSP source.

The only other singly charged anion detected was silver, and this was only as low intensity $Ag^+(H_2O)_n$ clusters. No doubly charged cations, or any other species were detected from solutions containing cobalt, nickel, barium or calcium. Thomson and Iribarne, in their original experiments with ion evaporation at atmospheric pressure (17), were also unable to obtain signals from divalent ions, either positive or negative. They attributed this failure to the much higher solvation energies expected for such species.

Relative ion evaporation efficiencies

Figure 2.13 shows the ions detected from a 10^{-4} M equimolar mixture of lithium, sodium, potassium, rubidium and cesium salts in water. The relative evaporation efficiencies for the different ions can be obtained by summing the intensities of the various ion hydrates, $X^+(H_2O)_n$, for each metal and expressing this as a function of the total ionization (TI). Tabulated below are the results obtained for duplicate experiments:

Metal	Sum of Ion Hydrates (%TI) Run: 1	2	Evaporation Relative to Na
Li	12	13	0.7
Na	18	20	1.0
K	17	22	1.1
Rb	22	19	1.1
Cs	30	28	1.5

The observed diffences in relative evaporation are small. At first glance this is a surprising result, considering these ions have large differences in hydration energies, ranging from -505 kJ/mol for Li^+ to -278 kJ/mol for Cs^+ at 298°K (50).

Thompson and Iribarne (17), also obtained relative evaporation rates for alkali ions. Normalized relative to Na^+ these were $Li^+:Na^+:K^+:Rb^+:Cs^+$ = 2.8:1.0:1.2:0.6:0.8. According to their treatment the evaporation rate constant

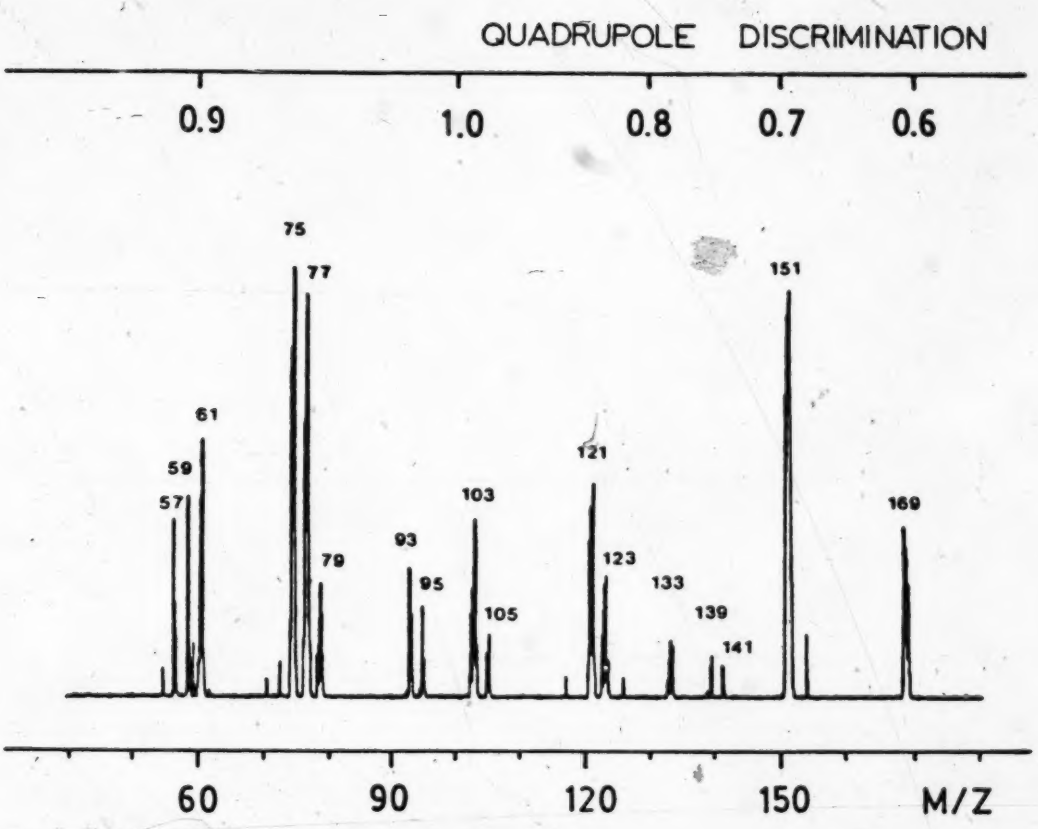

Figure 2.13 TSP mass spectrum obtained from an aqueous mixture of Lithium, Sodium, Potassium, Rubidium and Cesium salts all at 10^{-4} M. TSP conditions: flow rate 1 mL/min; temperatures: jet 175, vaporizer 246, source 300°C. Cluster ions are all $X^+(H_2O)_n$ where X^+ is the alkali ion.

X	n	m/z	X	n	m/z	X	n	m/z
K	1	57	Na	2	59	Cs	0	133
	2	75		3	77		1	151
	3	93		4	95		2	169
Li	3	61	Rb	1	103/105			
	4	79		2	121/123			
				3	139/141			

is equal to $Ae^{-(E*/kT)}$ where E* is the height of the Gibbs free energy barrier and depends on the solvation energy of the ion and the strength of the applied field. Assuming equal concentrations of ions at the surface of the charged drop, then the observed concentrations of ions 1 and 2 in the gas phase should be in the ratio $\exp(\Delta G_{s1} - \Delta G_{s2})/kT$ where ΔG_s is the free energy of solvation of the respective ion and is a function of the number of attached water molecules. Therefore the relative rates of ion evaporation should be strongly dependent on the cluster size. The evaporation of small clusters is more energetically favourable than the corresponding naked ion as the energy barrier is considerably smaller. If the standard free energy of hydration (ΔG_s) is plotted as a function of cluster size (n) for the various alkali metals, then ΔG_s progressively decreases with increasing n for each metal (Figure 11, reference 17). At values of $n > 6$ very similar values for ΔG_s are obtained. The similar evaporabilities obtained by Thomson and Iribarne were taken as an indication that the clusters which evaporate contain more than 6 or 7 water molecules. The present results, although obtained under different experimental conditions, also show similar evaporation efficiencies for Li^+, Na^+, K^+, Rb^+ and Cs^+ and tend to support this hypothesis. However, as the clusters ultimately observed reflect the conditions in the TSP source, rather than the original state of the evaporated ion, confirmation of this is hard to obtain.

REFERENCES

1. Arpino, P.J.; Guiochon, G.; Anal. Chem., **1979**, 51, 682A-701A.
2. Arpino, P.J.; Guiochon, G.; Krien, P.; Devany, G.; J. Chromatog., **1979**, 185, 529-547.
3. Snyder, L.R.; Kirkland, J.J; "Introduction to Modern Liquid Chromatography", 2nd. Edn., Wiley-Interscience, New York, 1979.
4. Vestal, M.L.; Science (Washington D.C), **1984**, 226, 275-281.
5. Arpino, P.J.; J. Chromatog., **1985**, 323, 3-11.
6. Bruins, A.P.; J. Chromatog., **1985**, 323, 99-111.
7. Karger, B.L.; Vouros, P.J.; J. Chromatog., **1985**, 323, 12-32.
8. Crowther, J.B.; Covey, T.R.; Silvestre, D.; Henion, J.D.; L.C. Mag., **1985**, 3, 240-254.
9. Vestal, M.L.; in "Ion Formation from Organic Solids", Benninghoven, A. (Ed.), Springer-Verlag, New York, 1983, pp. 246-263.
10. Blakley, C.R.; Vestal, M.L.; Anal. Chem., **1983**, 55, 750-754.
11. Vestal, M.L.; Anal. Chem., **1984**, 56, 2590-2592.
12. Covey, T.; Henion, J.; Anal. Chem., **1983**, 55, 2275-2280.
13. Voyksner, R.D.; Haney, C.A.; Anal. Chem., **1985**, 57, 991-996.

14. Vestal, M.L.; Fergusson, G.J.; Anal. Chem., 1985, 57, 2373-2378.

15. Katta, V.; Fergusson, G.J.; Vestal, M.L.; Proceedings of the 33 rd. Annual Conference on Mass Spectrometry and Allied Topics, San Diego, 1985, pp. 769-770.

16. Dodd, E.E.; J. Appl. Phys., 1953, 24, 73-80.

17. Thomson, B.A.; Iribarne, J.V.; J. Chem. Phys., 1979, 71, 4451-4463.

18. Thomsom, B.A.; Iribarne, J.V.; J. Chem. Phys., 1976, 64, 2287-2293.

19. Pilosof, D.; Kim, Y.H.; Dyckes, D.F.; Vestal, M.L.; Anal. Chem., 1984, 56, 1236-1240.

20. Liberato, D.J.; Fenselau, C.C.; Vestal, M.L.; Yergey, A.L.; Anal. Chem., 1983, 55, 1741-1744.

21. Harrison, A.G.; "Chemical Ionisation Mass Spectrometry", CRC Press, Boca Raton, Florida, 1983.

22. Lias, S.G.; Liebman, J.F.; Levin, R.D.; J. Phys. Chem. Ref. Data, 1984, 13, 695-808.

23. Keough, T.; DeStefano, A.J.; Org. Mass Spectrom., 1981, 16, 527-533.

24. Kebarle, P.; Ann. Rev. Phys. Chem., 1977, 28, 445-476.

25. Nikelly, J.G.; Am. Lab. (Fairfield Conn.), Oct 1982, 54-60.

26. Lawson, G.; Todd, J.F.J.; Chem. Britain, 1972, 8, 373-380.

27. Lau, Y.K.; Ph.D Thesis, Dept. of Chemistry, University of Alberta, Edmonton, Alberta, 1979, p.76.

28. Message, G.M.; "Practical Aspects of Gas Chromatography Mass Spectrometry", John Wiley, N.Y. 1984, pp. 204-205.

29. McLafferty, F.W.; "Interpretation of Mass Spectra", 3rd. Edn., University Science Books, Calf., 1980, Unknown 9.1, p.195.

30. Payzant, J.D.; Cunningham, A.J.; Kebarle, P.; Can. J. Chem., **1973**, 51, 3242-3249.

31. Lindinger, W.; Albritton, D.L.; J. Chem. Phys., **1975**, 62, 3520-3522.

32. McDaniel, E.W.; "Collisional Phenomena in Ionised Gases", John Wiley, N.Y. 1964, p.435.

33. Fehsenfeld, F.C.; Ferguson, E.E; J. Chem. Phys., **1973**, 59, 6272-6276

34. Lau, Y.K.; Ikuta, S.; Kebarle, P.; J. Am. Chem. Soc., **1982**, 104, 1462-1469.

35. Su, T.; Bowers, M.T.; in "Gas Phase Ion Chemistry", Bowers, M.T. (Ed.), Academic Press, N.Y. 1979, vol.1, p.81.

36. Bohme, D.K.; in "Interactions between Ions and Molecules", Ausloos, P. (Ed.), Plenum Press, N.Y. 1975, p.489

37. Yamdagni, R.; Kebarle, P.; J. Am. Chem. Soc., **1973**, 95, 3504-3510

38. Aue, D.H.; Bowers, M.T.; in "Gas Phase Ion Chemistry", Bowers, M.T. (Ed.), Academic Press, N.Y. 1972, vol.2 p.9.

39. Sen Sharma, D.K.; Kebarle, P.; J. Am. Chem. Soc., **1982**, 104, 19-24, and references therein.

40. Caldwell, G.; Magnera, T.F.; Kebarle, P.; J. Am. Chem. Soc., 1984, 106, 959-966, and references therein.

41. Yamdagni, R.; Kebarle, P.; J. Am. Chem. Soc.,1971, 93, 7139-7143

42. Davidson, W.R.; Sunner, J.; Kebarle, P.; J. Am. Chem. Soc., 1979, 101, 1675-1680

43. Meot-Ner (Mautner), M.J.; J. Am. Chem. Soc., 1984, 106, 1257-1264

44. Larson, J.W.; McMahon, T.B.; J. Am. Chem. Soc., 1983, 105, 2944-2950

45. Larson, J.W.; McMahon, T.B.; J. Am. Chem. Soc., 1984, 106, 517-521

46. Larson, J.W.; McMahon, T,B.; J. Am. Chem. Soc., 1984, 104, 6255-6261

47. Garteiz, D.A.; Vestal, M.L.; LC Mag., 1985, 3, 334-346.

48. Bursey, M.M.; Parker, C.E.; Smith, R.W.; Gaskell, S.J.; Anal. Chem., 1985, 57, 2597-2599.

49. Parker, C.E.; Smith, R.W.; Gaskell, S.J.; Bursey, M.M; Anal. Chem., 1986, 58, 1661-1664.

50. Berry, R S.; Rice, S.A.; Ross, J.; "Physical Chemistry" John Wiley and Sons, 1980, N.Y. p. 992.

CHAPTER 3

THERMOSPRAY PULSED ELECTRON IONISATION EXPERIMENTS

INTRODUCTION

Background

Non-polar as well as a large number of moderately polar molecules cannot be ionised by direct thermospray (TSP) ionisation (1-4). In order for these compounds to be analysed the TSP interface must be fitted with an external filament. Electron ionisation (EI) is then used to generate reagent ions from the vaporized mobile phase (1). This "abnormal" mode is refered to as "filament-on" thermospray, and the analyte is ionised by the same ion-molecule reactions that occur in conventional chemical ionisation (CI) sources (5). For aqueous solvents the reagent ions consist of an equilibrium set of proton hydrates $H_3O^+(H_2O)_n$. Due to the low proton affinity (PA) of H_2O (166.5 kcal/mol.) analytes with PA less than NH_3 (204.0 kcal/mol.) but greater than H_2O are generally protonated under these conditions, whereas they would not be under normal TSP conditions. Also in many cases more structural information is obtained by filament-on TSP due to the occurance of a more exothermic protonation reaction (2).

In the preceeding chapter it was shown that volatile and moderately volatile analytes are ionized by a two-step process analogous to conventional CI. That is, gas phase

NH_4^+ cluster ions, formed by direct ion evaporation, protonate gas phase sample molecules generated by TSP vaporization. To gain a better understanding of this process it would be useful to know the gas phase concentration of the neutral analyte.

In order to determine this information our existing TSP source was modified so that ions could be generated by pulsed high energy electrons. By pulsing the electron beam the protonation of a neutral analyte (B) can be followed as a function of time after the initial ionisation. Kinetic data can then be extracted from the observed time decay and used to obtain an estimate for the gas phase concentration of B.

EXPERIMENTAL

Modifications to existing TSP apparatus

The existing thermospray apparatus was modified for operation with a high energy pulsed electron beam. This required the following changes.

Source modifications: A diagram of the modified source is shown in Figure 3.1. On the right side is the joint to the pump out line, while on the left hand side the limited expansion volume copper tube is shown screwed into the source block. The LC vaporizer is not shown. Also for clarity the central heater assembly, which is mounted directly opposite the ion exit cone, has been omitted. The upper drawing gives the sectional view looking from the

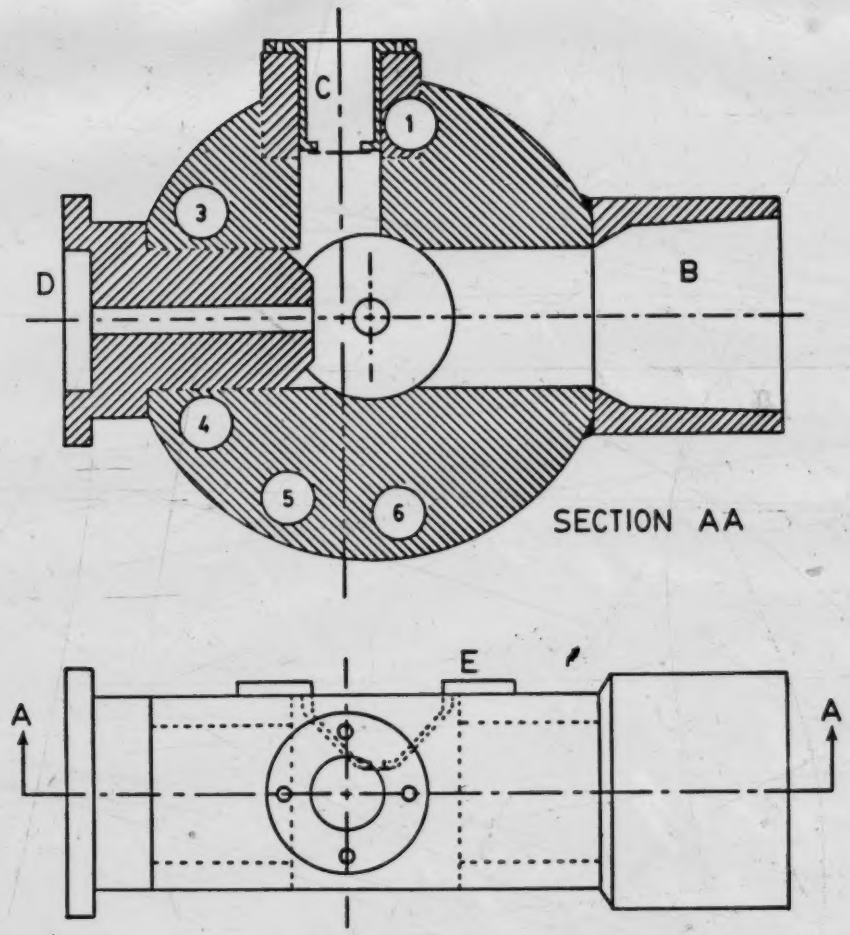

Figure 3.1. Top and cross-sectional views of thermospray source modified for pulsed-EI operation.

B: Joint to pump out-line.
C: Electron beam entrance slit flange.
D: Limited expansion copper tube.
E: Ion exit cone.
Holes 1,3,4,5,and 6 are for the source cartridge heaters.

support tower side of the source. The ion exit orifice is in the centre of the source. A stainless steel insert, tapped with 4 holes, was mounted on the top of the source block to provide a flat surface on which to seal the electron entrance slit flange. This required the sacrifice of cartridge heater #2 which was mounted symmetrically opposite #5. A 0.7 in. i.d. hole was then drilled through the insert into the central volume of the source to take the entrance slit assembly as shown. This hole was drilled as close to the copper expansion tube as the existing design allowed. That is, as far "upstream" as possible from the ion exit hole. The electron entrance slit was constructed by spot welding, under magnification, two small lengths of stainless steel razor blade across the machined slot in the end of the "top hat section" flange. In this way an aperature of 35 μm x 1 mm was obtained. This was then inserted into the hole in the source and sealed by a gasket constructed from 0.015 in. o.d. gold wire. The distance from the electron entrance slit to the ion exit slit was calculated to be about 4 mm.

Mounting and alignment of electron gun: A high energy electron gun assembly (Figure 3.2), described by Lau (6), was mounted on the top flange of the vacuum chamber so that it was vertically above the electron entrance slit. The gun operating voltages were obtained from a simple potential divider circuit. The heater supply for the thorium irridium filament was floated at -2 kV. Typical

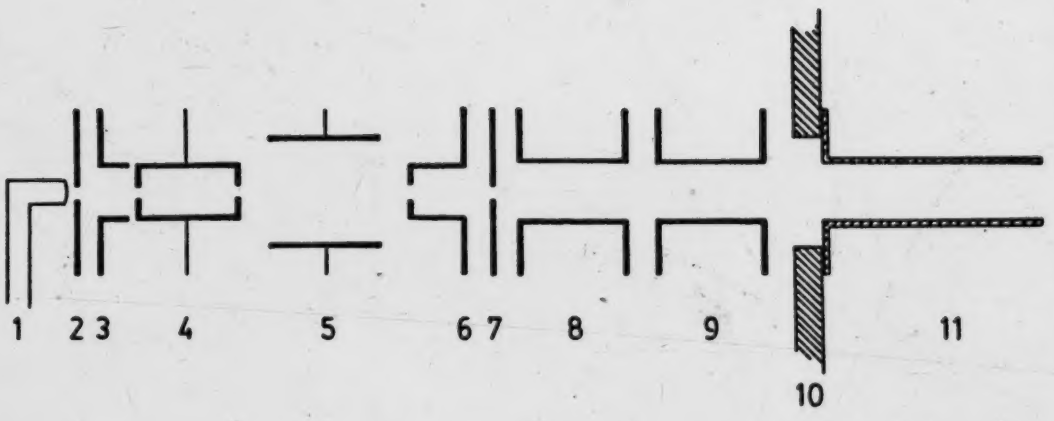

Figure 3.2. Schematic diagram of high energy electron gun.

1. Filament.
2. Drawout plate.
3. Extractor.
4. Lens #1.
5. Focus (Lens #2).
6. Lens #3.
7. Extractor.
8. Y deflection 1/2 plates.
9. X deflection 1/2 plates (shown rotated 90° from true position).
10. Vacuum flange.
11. Shielding cylinder.

operating voltages are given in Table 3.1. In order to direct the electron beam through the entrance slit and into the source it is normal practice to locate, in the wall of the source, an electron trap electrode opposite the entrance slit. Due to the position of the source heaters it was not possible to mount such an electrode in this case. To circumvent this problem the following procedure was adopted to initially obtain maximum electron transmission into the source. The vaporizer was removed from the TSP source and replaced by a threaded Vespel SP-1 resin spacer with a 1/16 in. i.d. hole drilled in the centre. A small trap electrode was constructed by spot welding a small stainless steel disk to a length of 1/16 in. o.d. stainless steel rod. The trap electrode was then positioned opposite the electron beam entrance slit by pushing the rod through the hole in the insulating spacer. Electrical connection to the rod was made from one of the spare feedthroughs on the TSP flange by means of a length of copper wire. A Keithley 610B electrometer was used to measure the trap current. With the system under vacuum the electron beam deflection voltages were manipulated to achieve a maximum trap current of 0.3 μA (see Table 3.1).

TABLE 3.1

Typical Operating Voltages for Electron Gun used for thermospray pulsed-EI studies

	Electrode[a]	Voltage (volts)
1.	Filament	-2000[b]
2.	Drawout	-1950
3.	Extractor	-1880
4.	Lens #1	-50[b]
5.	Lens #2 (Focus)	-1805
6.	Lens #3	-50[b]
7.	Deflection half-plates	
	X_1	-59
	X_2	-50[b]
8.	Deflection half-plates	
	Y_1	-39
	Y_2	-50[b]
	TSP ion source	+5

Typical control meter readings under continuous electron bombardment were:

Emission current: 1 mA

Case current (electrons hitting TSP source): 44 μA

[a] Numbers refer to Figure 3.2.

[b] These voltages were fixed, other voltages were variable.

For routine pulsed-EI thermospray operation it was found that these settings only had to be altered very slightly to obtain maximum ion intensities.

Pulsing of the electron beam: A schematic diagram showing the electrical circuitry employed for pulsed-EI thermospray operation is shown in Figure 3.3. Pulsing of the electron gun was accomplished by varing the potential of the drawout electrode at regulated intervals. A complete discription of this process is given by Lau (6). Briefly, if this electrode is held at about 40 volts more negative than the filament then no electrons are gated into the electron gun. A floating pulse generator, triggered by a master pulse generator, is used to switch the drawout potential to about 60 volts more positive than the filament for a preset length of time (pulse width). Electrons are now accelerated through the gun and pass into the TSP source. The frequency of the electron beam on/off cycle (pulse repitition rate) was typically 0.8 to 2 ms, whilst the pulse width was varied from 10 to 100 μsec. The triggering pulse from the master pulse generator also initiates the sweep of a multichannel analyser which was used to record the ion intensity time dependence of a selected ion after the initial ionising electron pulse.

Detection system: The existing channeltron electron multiplier (CEM # 4830), which could be used in either an analog or pulse counting mode, was retained for this study. Such multipliers are designed for high gain, and to give

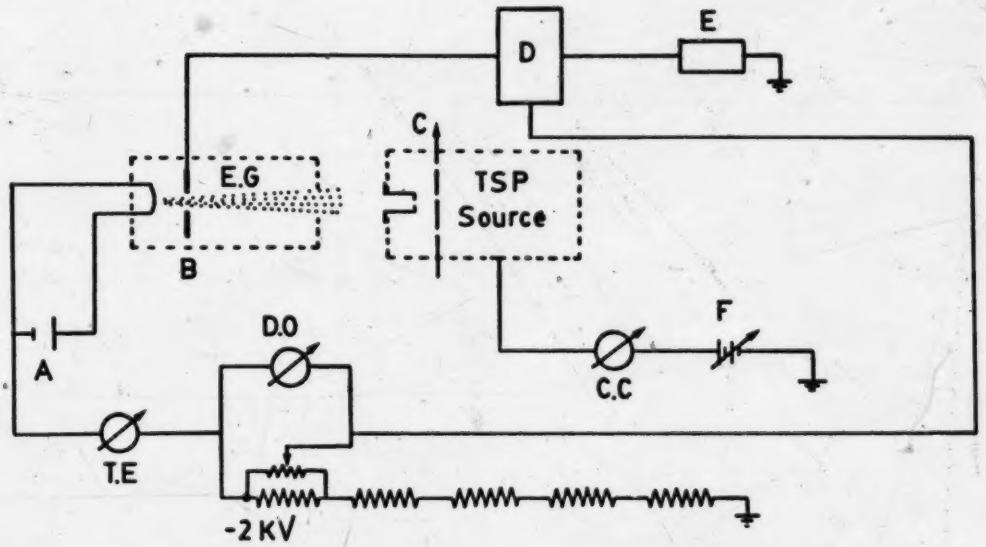

Figure 3.3. Schematic diagram showing electrical circuitry employed for pulsed-EI TSP operation. Only the filament and drawout plate are shown for the electron gun, voltages for the other lenses were obtained from the same potential divider.

A: Isolated filament supply.
B: Drawout plate.
C: Direction of flow through source.
D: Floating pulse amplifier.
E: Master pulse generator.
E.G: Electron Gun.
F: TSP source voltage.
T.E: Total emission.
D.O: Drawout voltage.
C.C: Case current.

more uniform pulse amplitudes (7). This allows the use of standard discriminator techniques to eliminate spurious noise events originating either elsewhere in the CEM, or from soft x-rays or neutrals hitting the conversion dynode (7). Also in the pulse counting mode a change in the absolute magnitude of the pulses is not significant, provided they remain above the discriminator level. Consequently factors affecting the amplification efficiency, such as ion mass or velocity are not important when pulse counting is employed.

The high speed picoammeter, which had been used to measure the analog output from the CEM, was replaced by a pulse counting system. Experimental details of the application of this detection technique to pulsed high pressure mass spectrometry (HPMS) are given by Lau (6). In this study the instrumentation used consisted of a four stage amplifier (EG&G # AN201/N), a discriminator (EG&G # T101/N) and a ratemeter (Ortec # 441). Output pulses from the CEM are amplified, but only those above the preset threshold level are counted by the ratemeter. To measure the CEM output, as a function of time after the electron pulse, the signal from the ratemeter was connected to a multichannel analyser (Nuclear Data # 2200). Conventional ion intensity vs m/z spectra were obtained by performing a frequency to voltage conversion and feeding the DC signal into the Y input of the X-Y recorder (Hewlett Packard # 7004B).

Typical operating conditions

The TSP source was operated under the same conditions as those previously used. That is: vaporizer temperature 240°C; source temperature 300°C; jet temperature 170°C and source potential +5 volts. Typical pulsed-EI TSP operating pressures were about 4×10^{-5} torr in main chamber, 3×10^{-6} torr at the back of the quadrupole chamber and 1 torr in the exit line.

Measurement of time dependence and treatment of data

The time dependence of selected ions, that is, the recording of ion intensity as a function of elapsed time after the electron pulse, were obtained as follows. The dwell time of the multichannel analyser was set to 10 μsec. per channel and 256 channels were utilised. In the first 10 μsec. after the electron pulse the number of ions arriving at the detector were accumulated in channel 1. The number of ions that arrived from 10 to 20 μsec. were accumulated in channel 2, and so on for 256 channels. The change in ion intensity is recorded in this way for 2.56 msec. In the pulsed-EI thermospray mode the signal decay is much faster than is typically observed in pulsed HPMS measurements (see results and discussion) and the ion intensity decays by about a factor of 10^3 in less than 1 msec. Consequently, to repeat the process, the electron gun was pulsed again after only 0.8 msec. The total collection time per ion was tyically 2 minutes.

The operation of the pulsed-EI instrumentation was tested under "static conditions", that is at ambient temperature and without any liquid flow into the TSP source. Instead water vapour was introduced into the source through the pump out line. A pressure of about 1 torr H_2O was maintained in the source. After the pulse of 2keV electrons, rapid reactions in the reagent gas produce an equilibrium set of proton hydrates $H_3O^+(H_2O)_n$. These ions, due to their low gas phase basicity, rapidly ionise the analyte B by proton transfer providing $PA(B) > PA(H_2O)$. The time dependence of the reagent ions involved in ion molecule reaction (1)

$$H_3O^+(H_2O)_n + NH_3 = NH_4^+(H_2O)_m + (n-m+1)H_2O \qquad (1)$$

is shown in Figure 3.4 for n = 3,4 and 5. The variables plotted are natural logarithm of accumulated counts per channel against time elapsed after the electron pulse. The rate of loss of these ions, given by the slope of the lines, is determined by the rate of reactive loss plus diffusive loss to the walls. The analyte, in this case NH_3, was present in residual traces in the ion source. The time dependence of the ions involved in the ion-molecule equilibria (2) and (3) are shown in Figure 3.5.

$$NH_4^+(H_2O)_2 + H_2O \rightleftharpoons NH_4^+(H_2O)_3 \qquad (2)$$

$$NH_4^+(H_2O)_3 + H_2O \rightleftharpoons NH_4^+(H_2O)_4 \qquad (3)$$

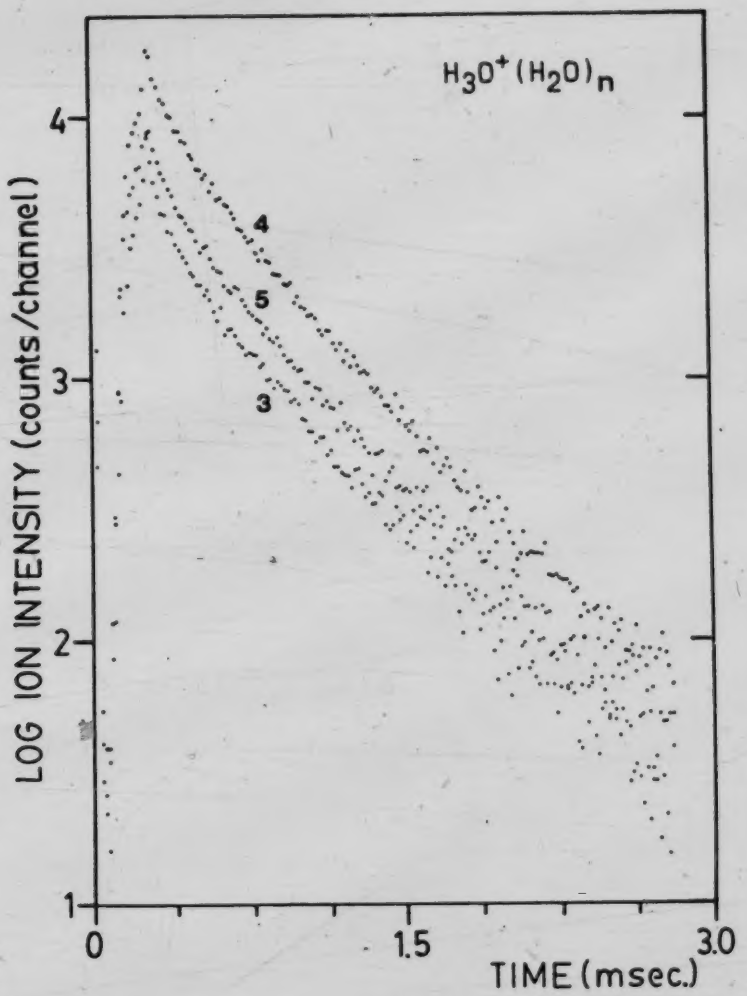

Figure 3.4. Time dependence for $H_3O^+(H_2O)_n$ ion intensities, where n=3,4,5 under "static" operation. Gaseous mixture in the TSP source: 1 torr H_2O, trace concentration of NH_3. Source temperature 300°K. Pulse width: 100 μsec., repetition rate: 2 ms.

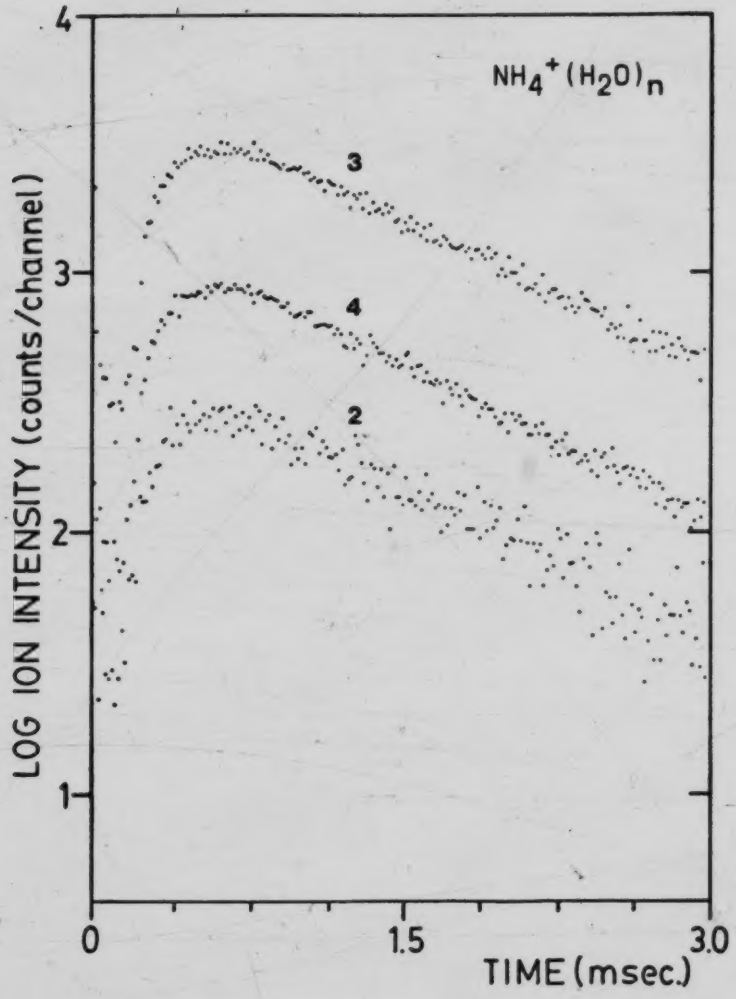

Figure 3.5. Time dependence for $NH_4^+(H_2O)_n$ ion intensities, where n=2,3,4 under "static" operation. Same conditions as those given for Figure 3.4.

In equations (2) and (3) the concentration of water is constant, therefore the invariance of the relative ion intensities with time in Figure 3.5 is indicative of equilibrium having been obtained. It is assumed that the relative intensities of the ions in Figure 3.5 represent the relative intensities of the ions in the ion source (8). After a time of about 1 ms. the rate of loss of these product ions is determined primarily by the rate of diffusion to the walls.

The gas phase intensity of a given reagent ion involved in equation (1), say $H_3O^+(H_2O)_4 = AH^+$, will obey first order kinetics, i.e. equation (4).

$$\ln[AH^+]_t - \ln[AH^+]_{t=0} = k_1[NH_3]t \qquad (4)$$

where k_1 is rate constant for proton transfer and $[NH_3]$ is the number of molecules of NH_3/cm^3 in the gas phase. Since $[NH_3]$ is many orders of magnitude higher than $[AH^+]$, the concentration of the former can be considered constant. The rate of reaction (1) is therefore dependant on the pseudo first order rate constant ν_1 where $\nu_1 = k_1[NH_3]\ sec^{-1}$. Plotting $\ln[AH^+]$ against t gives a slope of ν_1. Hence a value for ν_1 can be obtained directly from the slope of the reactant ion decay in Figure 3.4. Providing k_1 is known, or a reasonable estimate can be made, one can obtain the gas phase concentration of the neutral base, in this case ammonia. To obtain this value in

torr, the appropriate values can be substituted into equation (5).

$$P(B)_{torr} = (1.03 \times 10^{-19} \times T \times \nu_1)/(k_1) \qquad (5)$$

where T is the ion source temperature. Thus by obtaining the time dependence of specific ions during pulsed-EI thermospray operation this method, via equation (5), allows the concentration of the neutrals produced by the TSP vaporization process to be estimated.

RESULTS AND DISCUSSION

Time dependence of ions at normal flow rate

Initially the kinetics of proton transfer to volatile and moderately volatile analytes was investigated as there was good evidence that these were present in the gas phase as predominantly neutral species after TSP vaporization (see Chapter 2). The results obtained from a 10^{-2} M aqueous solution of pyridine (Py) are shown in Figure 3.6. In this experiment the protonation reaction (6) is being followed as a function of time after an initial 20 μsec. pulse of ionizing electrons.

$$H_3O^+(H_2O)_n + Py = PyH^+ + (n+1)H_2O \qquad (6)$$

It is evident from Figure 3.6 that reactant ions, $H_3O^+(H_2O)_n$, and the product ion, PyH^+, all have very similar intensity vs time profiles. Furthermore the decay is very fast, the half-life ($t_{1/2}$) being only about 8 μsec. If sufficient time was available for this reaction to occur then the reactant ions would decay at a rate similar to that observed under "static conditions" as illustrated in Figure 3.4. The decay of PyH^+ would be slower and be determined mainly by the rate of diffusional loss to the walls as seen in Figure 3.5.

Assuming pseudo first order kinetics and complete vaporization of the analyte the expected half-life, for a system not limited by time, can be calculated from equation

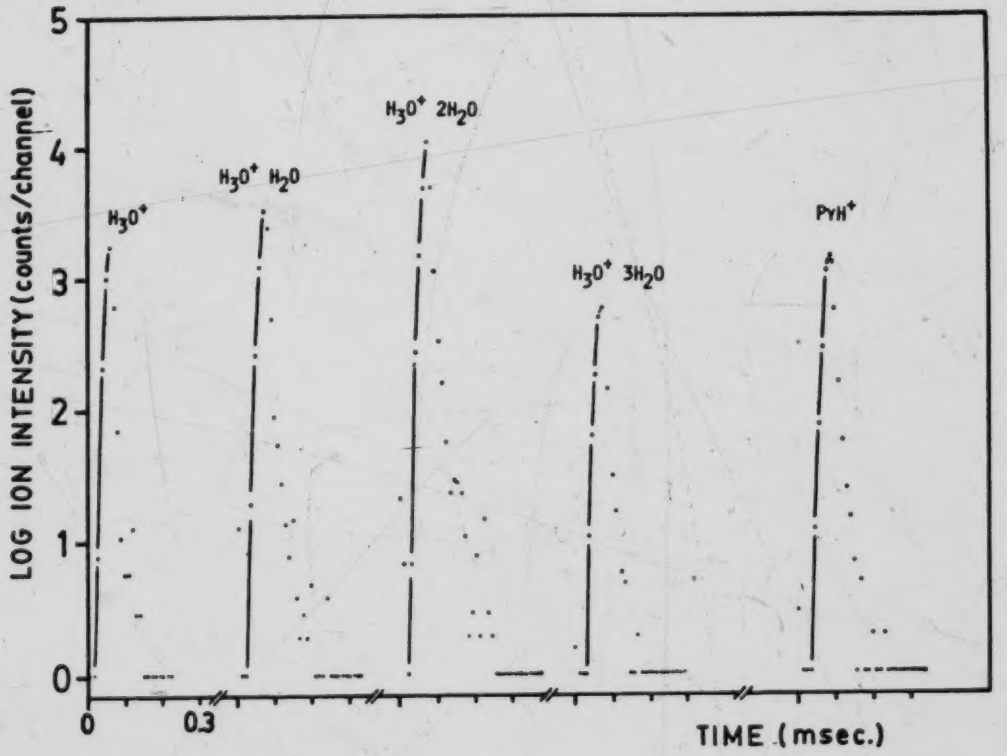

Figure 3.6. Time dependence for $H_3O^+(H_2O)_n$ and PyH^+ ion intensities generated from pulsed-EI ionization of TSP flow. Analyte: 10^{-2} M aqueous pyridine (Py). Flow rate: 1 mL/min, source pressure: about 1 torr, pulse width: 20 μsec., repetition rate: 0.8 ms.

(7), where n = number of Py molecules/cm^3 in the gas phase.

$$t_{1/2} = (0.69)/(k_6 n) \qquad (7)$$

$$n = 9.8 \times 10^{18} (T)^{-1} P(Py) \quad torr$$

Assuming the actual pressure in the TSP source is about twice the reading on the downstream pressure gauge, then the total pressure will be about 2 torr. The partial pressure of analyte, P(Py), is therefore equal to $2/5550 = 3.6 \times 10^{-4}$ torr, assuming the molar ratio Py/H_2O is preserved in the gas phase. The rate constant k_6 is assumed to be close to the collision limit of 2×10^{-9} molecules $^{-1}$ cm^3 sec^{-1}. If a TSP temperature of 450°K is taken then equation (7) can be evaluated to give $t_{1/2}$ = 44 μsec. This suggests that under pulsed EI-thermospray conditions the reaction time is severely limited. This is possibly due to a combination of the placing of the electron entrance slit and the fast flow through the source. If this is the case then the limiting factor will be the time it takes a "slug of ions" generated by the pulsed electron beam to reach the hole in the ion exit cone.

Tabulated below are the results from an experiment where the time dependence of the $H_3O^+(H_2O)_2$ cluster ion was studied as a function of the duration of the electron pulse (pulse width). Distilled water was pumped to the TSP source which was operated under normal conditions of flow and temperature.

Pulse width (μsec.)	Width of time profile at 1/10 height (μsec.)
20	45
40	60
80	100
100	120

The actual time profiles, in this case plotted using a linear intensity scale, are shown in Figure 3.7. In each case the start of the electron pulse is indicated by an arrow. Data points were taken at 10 μsec intervals. It can be seen that the width of the observed time decays parallel the increase in pulse width from 20 to 100 μsec. That is peak width (1/10 height) = pulse width + 20 μsec. These results are consistant with the time decay being determined by the time taken for a "slug of ions" to pass across the source exit hole.

In each case the time delay between the centre of the electron pulse and the corresponding maximum in the ion decay profile in Figure 3.7 is about 70 μsec. This delay is a combination of the time taken for the ions to move from the point of creation to the ion exit hole, that is the reaction time for proton transfer if an analyte B was present, plus the time of flight from the TSP source to the quadrupole detector. After the ions leave the source they are accelerated towards the skimmer electrode (see Figure 2.11, Chapter 2) by a potential of -30 volts. Once inside they travel at constant velocity, with an energy of 30 eV,

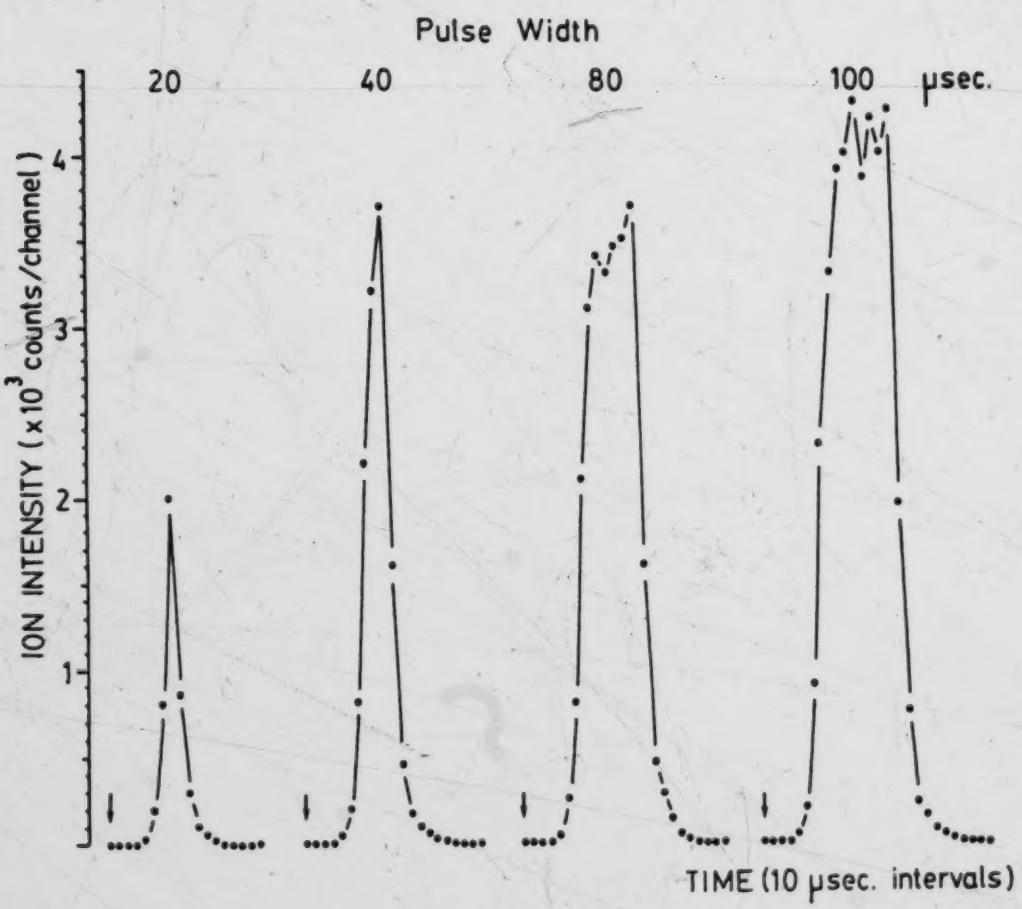

Figure 3.7. Time dependence for $H_3O^+(H_2O)_2$ cluster ion intensity as a function of increasing electron beam pulse width. Arrows indicate start of electron pulse in each case. Data points are at 10 μsec. intervals. Other conditions same as those given for Figure 3.6.

until they reach the auxillary ion source. When the TSP source is in operation the plates in this source are held at the same potential as the quadrupole and detector, i.e. at ground. Consequently as the ions enter the auxillary source they are retarded and attain an energy of 5 eV which corresponds to the potential difference between the TSP source and ground. The time of flight, over a distance d(cm), for an ion with energy E(eV) and mass M(amu) can be obtained from equation (8).

$$t = 0.714\ d\ (M/E)^{1/2} \quad \mu sec. \qquad (8)$$

Using this expression flight times were estimated for the following distances:

d_1, from ion source to the front of the skimmer, = 1.2 cm.

$t_1 = 0.32(M)^{1/2}$

d_2, length of skimmer electrode, = 4 cm.

$t_2 = 0.52(M)^{1/2}$

d_3, distance through auxillary ion source, = 0.8 cm.

$t_3 = 0.26(M)^{1/2}$

d_4, length of quadrupole rods, = 14 cm.

$t_3 = 4.5(M)^{1/2}$

Note t_1 was obtained assuming that on acceleration from the ion source to the skimmer electrode the ions reach on average only one half of there terminal energy (6).

An estimate for the total flight time (t_T) can be obtained from $t_1+t_2+t_3+t_4 = 5.6(M)^{1/2}$ μsec. In this case

M=55 and t_T is approximately 42 μsec. Hence the reaction time under pulsed-EI thermospray conditions is approximately (70-42) μsec., or 28 μsec. As the pulsed electron beam enters the TSP source approximately 4 mm "upstream" from the ion exit hole this yields an extimate for the flow velocity through the source of $0.4/(28 \times 10^{-6}) = 1.4 \times 10^4$ cm/sec.

An order of magnitude calculation for the flow velocity through the TSP source may be made as follows. Assuming a density of 1, the mass flow into the vaporizer is 1 gm/min., which is equivalent to 0.06 moles/min. for H_2O. Assuming complete vaporization, the volume of gas generated at a source pressure of 2 torr and temperature of 250°C, calculated using the ideal gas equation, is 16.3 litres/sec. (1.6×10^4 cm^3/sec.). Assuming the flow exiting the limited expansion volume region (see Figure 2.2 chapter 2) has an effective area of 0.5 cm^2, this flow translates into a linear velocity of about 3×10^4 cm/sec. This is in good agreement with the experimentally derived value noted above.

The distance from the tip of the capillary to the exit hole in the TSP source is 3 cm. Using a flow velocity of 1.4×10^4 cm/sec an upper limit of $3.0/(1.4 \times 10^4)$ secs. or 214 μsec. can be calculated for the normal "filament off" average TSP reaction time. However, as direct thermospray ions are probably formed slightly "downstream" of the capillary exit, then the actual average reaction time will be somewhat less. This is in good agreement with the value of 340 μsec. obtained from kinetic treatment of TSP data given in chapter 2, as that time was

uncertain by at least a factor of 2.

Time dependence of ions as a fuction of TSP flow rate

The time dependence of PyH^+ as a function of the liquid flow rate into the TSP source is shown in Figure 3.8. As the flow rate was decreased the exit valve on the pump out line was adjusted to maintain a constant source pressure of about 1 torr. Also the TSP vaporizer temperature was reduced to maintain a constant jet temperature of approximately 180°C in each case. The results obtained confirm that the observed time decay is strongly dependent on the flow velocity through the source. At flow rates near 1 mL/min the slope is very steep and the decay essentially parallels the pulse width. Whereas at low flow rates, that is less than 40 μL/min., the decay is primarily determined by the rate of diffusional loss to the walls.

At a flow rate of 40 μL/min. $t_{1/2}$ for the decay of $H_3O^+(H_2O)_2$ for a pyridine concentration of 10^{-2} M was about 32 μsec. (see Figure 3.9). This is considerably closer to the calculated value of 44 μsec. and indicates that, to a large extent, ion/molecule kinetics are now determining the observed decay rates. The gas phase concentration of pyridine present from TSP vaporization was calculated as follows:

From Figure 3.9 the slope of the time decay for $H_3O^+(H_2O)_2$, which is due to reactive plus diffusive loss, gave a value of 21400 sec^{-1} for ν_6. Using the slope of the time decay for PyH^+ an estimate of 10900 sec^{-1} was obtained

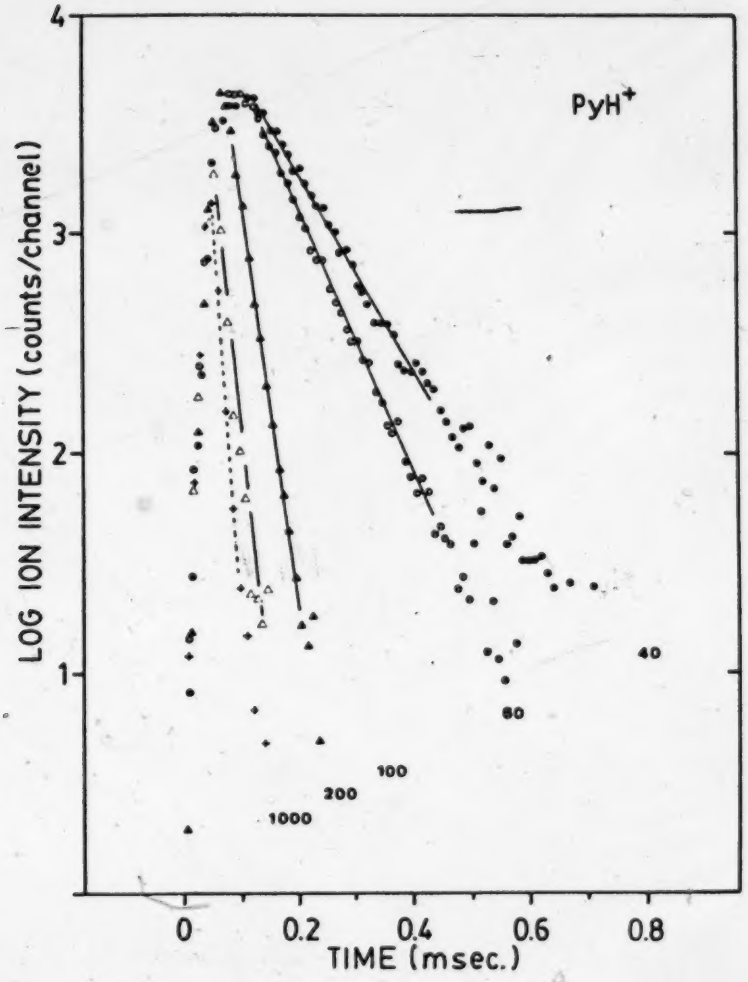

Figure 3.8. Time dependence of PyH^+ generated from pulsed-EI ionisation of TSP flow as a function of liquid flow rate. Flow rates in uL/min are indicated. Analyte: 10^{-2} M pyridine (Py), source pressure: about 1 torr, jet temperature: about 170°C, pulse width: 20 μsec., repetition rate: 0.8 ms.

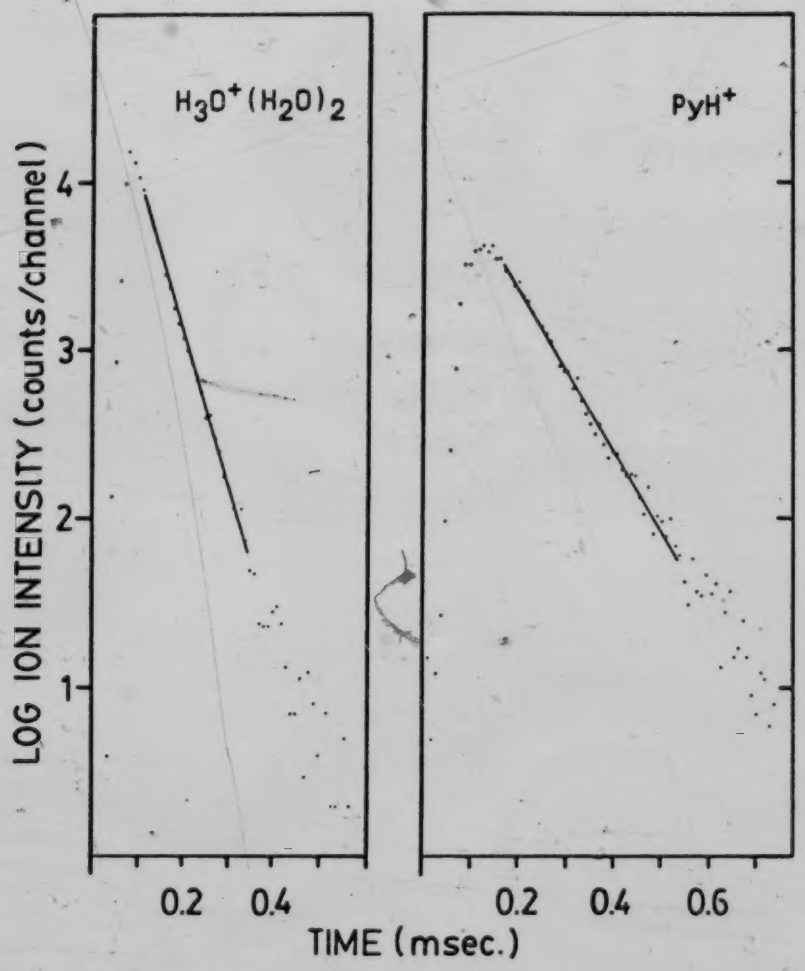

Figure 3.9. Time dependence of $H_3O^+(H_2O)_2$ and PyH^+ generated from pulsed-EI ionization of TSP vapor under conditions of reduced flow. Analyte: 10^{-2} M pyridine (Py), flow rate: 40 μL/min. Other conditions same as those given in Figure 3.8.

for the rate of diffusive loss.

Thus $\nu_{reactive} = 21400 - 10900 = 10500\ sec^{-1}$.

Substituting this value into equation (5) and assuming a value of 2×10^{-9} molecules^{-1} cm^3 sec^{-1} for k_6 one obtains a value for P(Py) of 2.5×10^{-4} torr at the TSP temperature of 450^{o}K.

This is in good agreement with the expected partial pressure of 3.6×10^{-4} torr calculated previously. But considering that pyridine is very volatile this is hardly an unexpected result. Unfortunately, when this experiment was repeated at the same flow rate with a less volatile analyte, 10^{-2} M proton sponge in acidified water, the TSP source was so severely contaminated with carbonised material that no reliable kinetic data could be obtained. However, the results obtained with pyridine do illustrate that the experimental method is sound. Furthermore, with a redesigned TSP source in which the electron beam is placed considerably further away from the ion exit hole, there is no obvious reason why kinetic data could not be obtained at normal flow rates with lower analyte concentrations.

CONCLUSIONS

At flow rates of 1 mL/min. the flow through the TSP source is very fast, being approximately 1.4×10^4 cm/sec. With an electron beam placed only 4 mm "upstream" from the ion exit hole this limits the reaction time under pulsed-EI conditions to about 28 μsec.

Under these conditions the time dependence plots for both reactant and product ions are practically identical. In each case the time decay profile parallels that of the electon beam pulse and consequently no kinetic data on ion molecule reactions can be obtained.

Using a value of 28 μsec. for the reaction time under pulsed-EI conditions it is possible to estimate an upper limit of 214 μsec. for the normal "filament-off" average TSP reaction time. This is in good agreement with the value of a few hundred microseconds obtained from the kinetic treatment of TSP data given in chapter 2.

Kinetic data for the gas phase protonation of pyridine by $H_3O^+(H_2O)_2$ was obtained by reducing the liquid flow rate to about 40 μL/min. The results obtained were consistent with TSP vaporization of the pyridine as neutral molecules and the molar ratio H_2O/Py in solution being maintained in the gas phase. However this approach was not successful with less volatile analytes.

These initial studies demonstrate that the pulsed-EI technique has considerable potential for the determination of neutral analyte concentrations in the gas phase after

TSP vaporization. Unfortunately, the location of the electron beam with respect to the ion exit hole was determined by the design of our existing TSP source and vacuum housing and was far from ideally positioned. With a TSP system specifically designed for pulsed-EI operation it should be possible to obtain reliable kinetic information at flow rates of 1 mL/min.

REFERENCES

1. Garteiz, D.A.; Vestal, M.L.; L.C Mag. **1985**, 3, 334-346.
2. Voyksner, R.D.; Bursey, J.T.; Presented at the 33rd Annual Conference on Mass Spectrometry and Allied Topics; San Diego, 1985, pp.95-96.
3. Chapman, J.R.; J. Chromatog. **1985**, 323, 153-161.
4. Covey, T.R.; Lee, E.D.; Bruins, A.P.; Henion, J.D.; Anal. Chem. **1986**, 1451A-1461A.
5. Harrison, A.G.; "Chemical Ionization Mass Spectrometry", CRC Press, Boca Raton, FL., 1983.
6. Lau, Y.K.; Ph.D Thesis, Dept. Chemistry, University of Alberta, Edmonton, Alberta, 1979.
7. Kurz, E.A.; Am. Lab. (Fairfield Conn.) March 1979.
8. Kebarle, P.; Ann. Rev. Phy. Chem. **1977**, 28, 445-476.

CHAPTER 4

CHARACTERIZATION OF RADIATION INDUCED DAMAGE TO POLYADENYLIC ACID USING HIGH PERFORMANCE LIQUID CHROMATOGRAPHY TANDEM MASS SPECTROMETRY

INTRODUCTION

Radiation damage to living cells

The deleterious effect of ionising radiation on living cells arises as a consequence of free radical damage to critical biomolecules such as DNA (1). Due to the relatively high proportion of molecular water in cells, 60-70% of cell damage has been attributed to hydroxyl radical-induced events (2). When water absorbs ionising radiation it decomposes according to the overall equation:

$$H_2O \xrightarrow{\sim\sim} \cdot OH,\ \cdot H,\ e^-_{aq},\ H_3O^+,\ H_2,\ H_2O_2.$$

Both radical ($\cdot OH$, $\cdot H$, e^-_{aq}) and molecular products (H_2, H_2O_2) are formed within a local region of high concentration commonly refered to as a spur (3). The steady state yields after 10^{-8} seconds at neutral pH are as follows (4):

1. A version of this chapter has been accepted for publication: Alexander, A.J.; Fuciarelli,A.F.; Kebarle, P.; and Raleigh, J.A.; Anal. Chem. 1987.

Species:	e^-_{aq}	·H	·OH	H_3O^+	H_2	H_2O_2
G value[1]	2.7	0.55	2.7	2.7	0.45	0.7

1. G = molecules produced per 100 eV (5).

The relative importance of hydroxyl radical-induced events have largely been deduced from studies that have used either dimethyl sulfoxide to scavenge hydroxyl radicals (·OH converted to less reactive CH_3·) or nitrous oxide to increase the yield of hydroxyl radicals (5,6). Nitrous oxide converts aqueous electrons to hydroxyl radicals, $N_2O + e^-_{aq} + H_2O = {\cdot}OH + OH^- + N_2$, thereby maximizing their yield from water radiolysis (G = 5.4). In general, the interaction of the strongly oxidizing ·OH radical with nucleic acid constituents results in the formation of secondary radicals through either an addition process at sites of unsaturation, or by a hydrogen abstraction reaction (6). Such reactions can ultimately lead to strand breaks (double and single), crosslinks (DNA-DNA) and molecular modifications to the bases and sugar moieties (1). Free radical damage of this kind has been implicated in mutagenesis, carcinogenesis and proliferative cell death (7). Therefore, characterisation of specific molecular products in irradiated aqueous solutions of nucleic acids may lead to an important advancement in understanding the consequences of molecular modifications at the cellular level. However, detection of such damage is complicated for two reasons; specific product formation is very low and

radiation-induced damage is relatively non-specific. To overcome these complications, the analytical methodology must ideally posses high sensitivity and universal detection.

Detection of molecular damage

The detection of molecular damage in irradiated solutions containing nucleic acids is a challenging analytical problem. Immunochemical assays for specific radiation-induced molecular products have been developed (8) and used in radiation chemical studies (9,10). Such assays have the ability to measure damage in situ with high sensitivity and good specificity. Recent studies have demonstrated that capillary column gas chromatography - mass spectrometry (GC-MS) combined with micro-derivatisation can be utilised to identify a wide variety of products resulting from radiation-induced damage to DNA with very high sensitivity (11-15). The successful coupling of high performance liquid chromatography and mass spectrometry (HPLC-MS) has provided an alternative route of analysis for polar and thermolabile compounds which has potential for radiation chemical studies. Recent studies have shown the utility of HPLC-MS for the analysis of nucleosides present in urine (16) and for the detection of modified nucleosides in enzymatic digests of tRNA (17). However, most HPLC-MS interfaces, including direct liquid introduction [DLI] (18,19), thermospray (20), ion evaporation (21) and

nebulisation into an atmospheric pressure chemical ionisation [APCI] source (22-24) all produce abundant pseudo-molecular ions, but few fragment ions. Although this is beneficial in terms of overall sensitivity, only limited structural information is obtained.

Tandem mass specrometry

Tandem mass spectrometry [MS/MS] (25,26), is a means of overcoming this inherent lack of specificity whilst also maintaining good sensitivity. With MS/MS, structurally significant daughter ions are produced by collisionally-induced dissociation [CID] of the respective parent ion. In this way additional structural data is obtained and the MS/MS separation stage enables co-eluting compounds to be distinguished and identified. MS/MS instruments having triple quadrupole geometry (triple-Q) have an in-line arrangement of 2 independent mass analysing quadrupoles (Q_1 and Q_3) with an enclosed rf only (total ion) mode quadrupole collision cell (Q_2) inserted between them. If only one detector is used then this is mounted after Q_3. In normal operation the first quadrupole (Q_1) is set to transmit only a selected parent ion, which maybe collisionally dissociated with argon in Q_2. The ionic products of decomposition (daughter ions) are then mass analysed by the third quadrupole (Q_3). If conventional mass spectra are required these may be obtained by operating Q_2 without collision gas and Q_3 in the rf only (total ion) mode and

mass scanning with Q_1. Other more sophisticated scanning modes are also available (27).

Covey and co-workers (28) have recently demonstrated the advantage gained when a heated nebuliser APCI interface is used in combination with a triple-Q MS for the analysis of drugs in crude equine urine. In this present study a triple-Q instrument using the same type of interface has been used to identify molecular products resulting from radiation damage to a model nucleic acid, polyadenylic acid (Poly A), after enzymatic hydrolysis of the polymer to the mononucleoside level.

EXPERIMENTAL

Reagents

Authentic samples of R- and S-8,5′-cycloadenosine were obtained from the radiolysis of adenosine-5′-monophosphate (5′-AMP) and 8-hydroxyadenosine was synthesized as described previously (29). Alkaline phosphatase, nuclease P1 (NP1), adenine, adenosine, 2′-AMP, 3′-AMP, 5′-AMP, 2′,3′-O-isopropylidine-adenosine and polyadenylic acid (Poly A) were obtained from the Sigma Chemical Company (St. Louis, Missouri) and used without further purification. The compound, 9-α-ribofuranosyladenine-5′-monophosphate (α-AMP) was a kind gift of Dr. M.J. Robins (Chemistry Department, University of Alberta). Alkaline phosphatase was used to hydrolyse α-AMP to the corresponding nucleoside. Other chemical were chromatographic or reagent grade and were

obtained from local suppliers.

Irradiation

Irradiations were performed in a Gammacell 220 ^{60}Co-δ radiation source (Atomic Energy of Canada Ltd.) at a dose rate of 57.4 Gy/min. as measured by Ficke dosimetry (30). The total dose was 1000 Gy (1 Gy = 100 Rad = Joule/kg). Solutions of poly A containing 694 µg/mL were made up in distilled water (pH 7.0) which had been purified and deionized before use by passage through a Barnstead three module NANOpure water purification system (supplied by Fisher Chemical Co.). The 2.0 mL samples of poly A were bubbled with nitrous oxide for 15 minutes prior to and throughout the time of irradiation. Nitrous oxide converts aqueous electrons to hydroxyl radicals [$N_2O + e^-_{aq} + H_2O = \cdot OH + OH^- + N_2$] (5) thereby maximizing the yield of hydroxyl radicals from radiolysis of water. In the presence of nitrous oxide the yield of hydroxyl radicals from water radiolysis, expressed in terms of the G value (molecules produced per 100 eV) is 5.4 (5). The nitrous oxide was scrubbed free of oxygen by passage through a 0.1 M sodium dithionite trap and free of acidic impurities by passage through a 0.1 M sodium carbonate trap.

Hydrolysis of Irradiated Poly A

The irradiated poly A was hydolysed with nuclease P1 as previously described (10). Briefly, 0.25 mL of a solution

of nuclease P1 containing 7.5 units/mL enzyme in a buffer of 30 mM sodium acetate (pH 5.3) and 2 mM $ZnSO_4$ were added to 0.5 mL of poly A solution. This mixture was incubated for 18 hours at 37 ^{o}C.

The mixture of mononucleotide products was further hydrolysed to the corresponding nucleosides with alkaline phosphatase. In a typical experiment 0.25 mL of a solution of alkaline phosphatase (25 units/mL of alkaline phosphatase in 0.1 M sodium carbonate/bicarbonate buffer at pH 9.6 containing 0.1 M magnesium chloride) was added to the NP1 digest of the irradiated poly A and the mixture was incubated at 37^{o}C for 18 hours.

Chromatography

A Waters model 6000A liquid chromatograph pump, a Rheodyne model 7125 injection valve with a 100 µL sample loop, and a Waters model 440 fixed wavelength UV detector (254 nm) were used for the HPLC separation. The HPLC chromatogram was recorded on a chart recorder (Yokogawa, Tokyo, Japan). A reversed-phase Supelco LC-18-S (4.6 mm x 250 mm) analytical column was used with an eluent of 10 % methanol in 0.02 M ammonium formate buffered to pH 4 with formic acid. Prior to use the mobile phase was filtered through a Nylon-66 0.45 µm membrane filter (MFS Micro filtration System supplied by Rainin Insrument Co.) and degassed with helium. The exit of the UV detector was connected to a heated nebuliser LC/MS interface (Sciex,

Thornhill, Ont.).

Mass Spectrometry

HPLC-MS and HPLC-MS/MS spectra were obtained using a TAGA 6000E triple quadrupole mass spectrometer (Sciex, Thornhill, Ont.) utilising an atmospheric pressure chemical ionisation [APCI] source. The HPLC effluent was introduced directly into the APCI source via the heated nebuliser at flow rates between 0.8 and 1.0 mL/min. Nitogen was used as the nebulisation gas.

Description of interface

The Sciex nebuliser consists of 3 stainless steel tubes fitted inside each other as shown in Figure 4.1. The HPLC effluent is introduced through the central inner microbore tube which terminates in a 100 μm i.d. stainless steel capillary. It is converted into a fine mist by a high velocity jet of nitrogen which is introduced through the second coaxial capillary. This gas, together with a second make-up flow introduced through the outermost coaxial tube, are used to carry the droplets through a heated quartz tube. The combination of gas flow and heat rapidly vaporizes the droplets. Typically, for largely aqueous mobile phases, an external heater temperature of between 480 and 500^{o}C results in a nebulised vapor temperature of about 150^{o}C. The heated gas plus entrained solvent and analyte molecules flows from the quartz tube into the

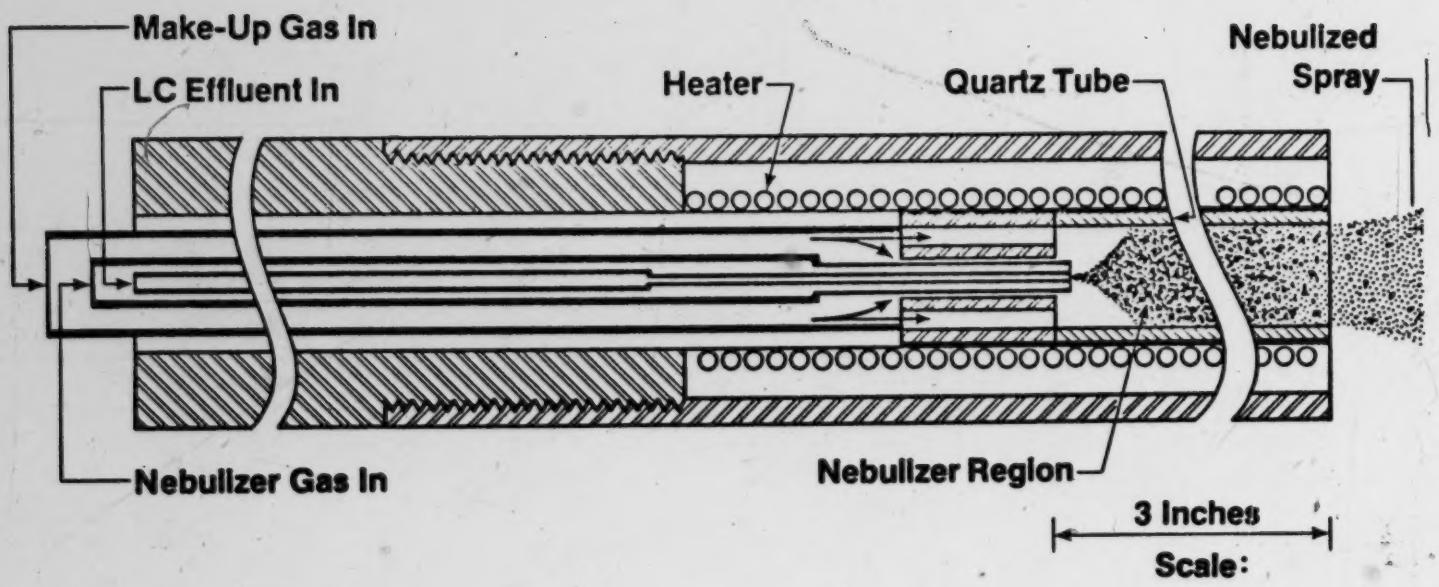

Figure 4.1 Schematic diagram showing internal construction of the Sciex HPLC/MS nebulizer.

reaction regions of the APCI source (Figure 4.2).

Here the analyte is ionised by ion-molecule reactions which are initiated by a corona discharge obtained from a needle held at high potential. These ions are accelerated towards the interface plate and pass through a flow of dry nitrogen before they are sampled into the mass spectrometer by a 100 μm atmosphere-to-high vacuum orifice.

The dry nitogen (interface gas) serves two purposes. Firstly it prevents any solvent, buffer or neutral analyte from entering the mass analyser region and thus prevents any contamination of the quadrupole rods, lenses, or vacuum system. Secondly it strips clustered solvent molecules from the ions as they are accelerated towards the sampling orifice. Lack of declustering would result in a severe loss of sensitivity as the analyte ion intensity (MH^+) would be "smeared out" over a large number of $MH^+(H_2O)_n$ cluster ions. After the ions have passed through the sampling orifice residual clustering can be minimised by accelerating the ions in the free jet expansion by means of a "cluster-buster" electrode mounted on the inside of the vacuum separation plate (note: for clarity this has been omitted from Figure 4.2).

The mobile phase which is being continuously vaporized into the source is removed by an air pump connected to the plenum chamber.

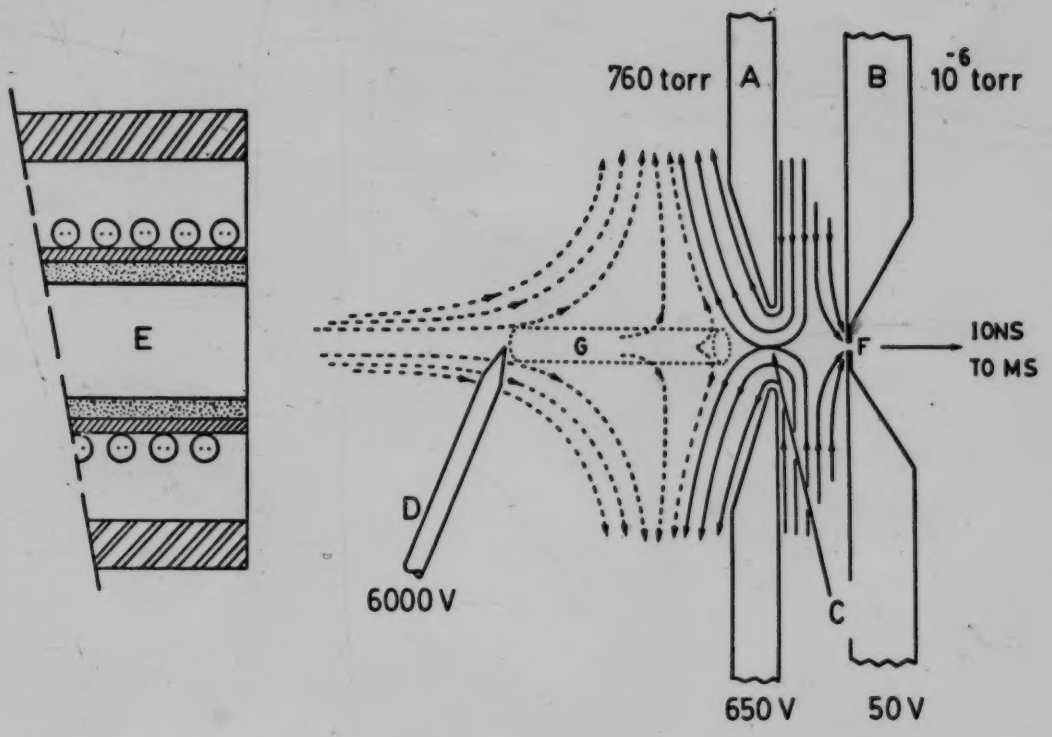

Figure 4.2 Schematic diagram showing Sciex APCI interface.

A: Interface plate, B: Atmosphere to vacuum separation plate,

C: Interface plate aperture,

D: Corona discharge needle,

E: Front of HPLC/MS nebulizer,

F: 100 μm orifice,

G: Ion-molecule reaction volume,

——→ : Interface gas flow (High purity N_2),

----→ : Carrier gas flow (Industrial N_2).

Sample ionisation

The primary ionisation, that is electron impact of corona electrons, generates reagent ions from the solvent vapor. In the positive ion mode, and for largely aqueous mobile phases, these consist of an equilibrium set of proton hydrates $H_3O^+(H_2O)_n$ (25, chapter 18). However, if a volatile buffer such as ammonium formate is present, the reagent ions are predominantly NH_4^+ clusters with water, methanol and ammonia molecules. A spectrum of the residual reagent ions, that is after the clusters have been reduced in size by passage through the interface gas and "cluster buster" region, is shown in Figure 4.3. Presumably, as in thermospray vaporization, the ammonium formate is converted to gas phase NH_3 and HCOOH (see Chapter 2). $NH_4^+(H_2O)_n$ is then produced by proton transfer from $H_3O^+(H_2O)_n$ as $PA(NH_3)$:204 kcal/mol > $PA(H_2O)$: 166.5 kcal/mol. Chemical ionisation of the analyte occurs by either proton transfer from NH_4^+ (equation 1), or by transfer of a proton water cluster as indicated in equation 2.

$$NH_4^+ + M = MH^+ + NH_3 \quad (1)$$

$$NH_4^+(H_2O)_n + M = MH^+(H_2O)_m + NH_3 + (n-m)H_2O \quad (2)$$

The value of m will depend on the proton affinity and hydrophilicity of the analyte M. Chemical ionisation is very efficient at atmospheric pressure due to the high collision rate (31). Also the moderating influence of the

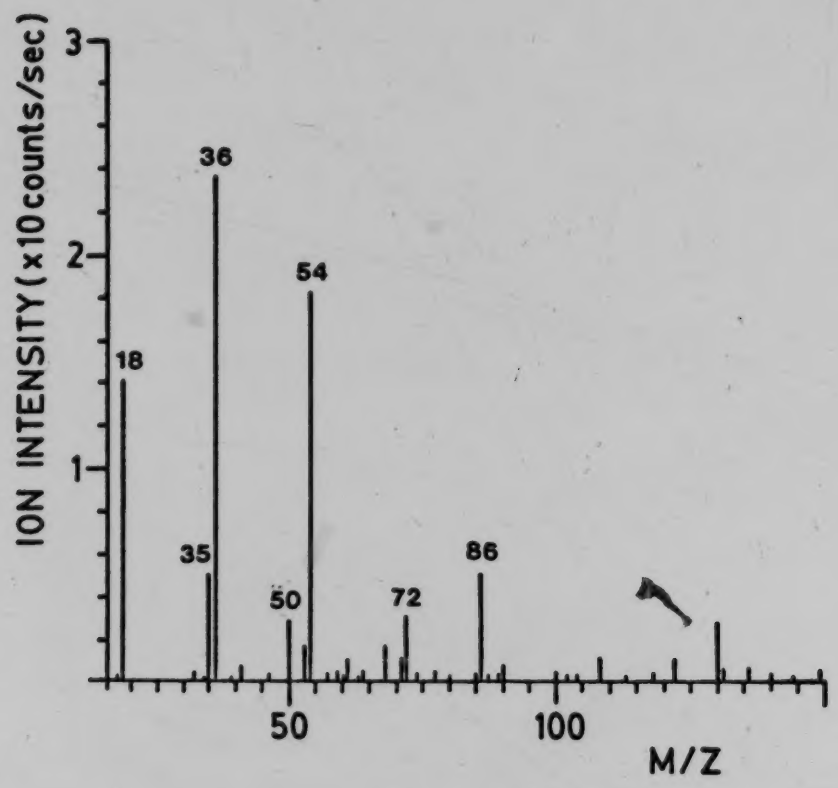

Figure 4.3 HPLC-APCI spectrum of residual reagent ions (NH_4^+X) generated from an eluent of 10% methanol in 0.02 M ammonium formate buffered to pH 4 with formic acid.
Note:. the cluster size distribution is not the same as that originally present in the APCI source.

m/z	Nature of X	m/z	Nature of X
35	NH_3	54	$(H_2O)_2$
36	H_2O	72	$(H_2O)_3$
50	CH_3OH	86	$(H_2O)_2\ CH_3OH$

solvent clusters upon the exothermicity of protonation (see Chapter 2), and the rapid thermalisation of the ions at high gas pressures reduces the degree of fragmentation during ionisation.

Operation of the interface

Detailed instructions for the operation of the LC/MS nebuliser are available from Sciex (32). What follows is a brief discussion of the relevant parameters and their optimisation for operation with largely aqueous solvents containing ammonium formate. For convenience some gas flow rates will be given in standard cubic feet per hour (SCFH), the conversion to SI units is 10 SCFH = 4.7 L/min.

1. The interface plate and plenum chamber were preheated for about 1 hour prior to turning on the liquid flow or the air pump. This was achieved by turning on the make-up flow (4 SCFH) and nebuliser gas (30 psi) and heating the nebuliser to about 400^{o}C. At this stage the gate valve to the orifice was open and the interface gas flow set to 500 mL/min.

2. Prior to turning on the HPLC flow, the following operations are carried out.

(a) Nebuliser gas pressure increased to about 80 psi.

(b) Make-up flow increased to between 6 and 8 SCFH.

(c) Interface gas flow increased to 1 L/min.

(d) Power supplies to quadrupoles and discharge needle switched on. Set Q.1 single ion monitoring for suitable solvent cluster ions (m/z 36, m/z 54 see Figure 4.3) and Q.3 in total ion mode.

(e) Air pump switched on and flow into plenum chamber adjusted to about 2.5 L/min.

3. Set HPLC flow rate to 0.8 ml/min. and switch on pump. Observe interface plate and ion signals on display terminal. If ion signals drop drastically and condensed vapor is present on the interface plate then unvaporized droplets are penetrating the interface gas. Shut off HPLC pump, ion signals should recover, and wait for interface plate to heat up further before repeating procedure.

Optimisation

Prepare about 200 mLs of 10^{-5} M adenosine in the mobile phase to be used for chromatography, disconnect column and injection valve and connect HPLC pump directly to nebuliser via an in line filter. Set flow rate to 0.8 ml/min. and pump solution continuously through the interface. Single ion monitor m/z 268 (MH^+) and m/z 136 $(BH+H)^+$ with Q.1, set Q.3 to total ion mode. After optimisation one should obtain about 10^5 counts/sec for the parent and about 2×10^6 counts/sec for the fragment ion. The following parameters can be varied:

1. Heater temperature: Generally this has little effect

in the range 470 - 530°C for adenosine which is relatively volatile. However for less volatile samples this may have to be altered prior to the chromatographic separation.

2. Position of interface probe with respect to sampling orifice: Generally the x and y motion of the inlet fitting is not critical to sensitivity.

2. Air pump setting: Although the absolute ion intensity is relatively insensitive to this parameter it does have a marked influence on signal stability.

3. Nebulizer pressure and make-up gas flow: The former requires at least 60 psi to achieve efficient nebulisation; however, above that it has only a marginal effect on ion intensity. Conversely, the make-up flow has a strong influence on both stability and ion intensities.

4. Position of discharge needle: The ion intensities are not strongly dependent on the needle position unless it is laterally displaced from the centre line of the probe.

5. Interface gas flow: Generally this has little effect provided flow is initially high enough to prevent droplets from penetrating the interface.

Typical optimised settings for the detection of adenosine type nucleosides:

heater temperature:	about 530 °C.
make-up flow:	6 SCFH.
nebulisation pressure:	85 psi.
interface flow:	1 L/min.

Air flow into plenum chamber: 2.5 L/min.

LC flow rate: 0.8 mL/min.

needle position: aligned with centre,

and positioned about 2 cm from end of nebuliser.

Mass calibration and tuning of quadrupoles

Mass calibration together with optimisation of peak shape and transmission was carried out on constant signals obtained from a 50:50 water methanol solution containing 10 ppm each of Adenosine (MH^+=268), and Riboflavin (MH^+=377) and 20 ppm of Tetracycline (MH^+=445). Q_1 and Q_3 were tuned (using RE1, DM1 and RE3, DM3 respectively) to give a constant peak width at half-height of 0.6 amu across the mass range 80 to 377 amu. The parameters used are listed below, for explanation of their significance please refer to TAGA 6000E operation manuals.

MTL	0.015,	STEP	1.0,	PE	0.5,	C	10,	TH	500
DI	2.0,	IN	650,	OR	60.0,	CB	35.0,	RO	30.0
IQ	0.0,	DM1	0.40,	DM3	0.15,	RE1	135,	RE3	135
R1	28.0,	R2	-20.0,	R3	AUTO,	FP	60.0,	MU	-3400

Operation of triple quadrupole MS

Conventional positive ion mass spectra, starting from m/z 80, were obtained with quadrupole 1 in the mass filter mode and quadrupole 3 in the total ion mode. Daughter ion spectra were generated under standard conditions using argon as the collision gas. (Effective target thickness: about 300

x 10^{12} atoms.cm^{-2}, collision energy: 50 eV). An FP value of 30 volts was found to be optimum for detection of daughter ions. In general, the reproducibility of major daughter ions was found to be good. However, significant variations in intensity were often observed for low intensity daughter ions, particularly when the parent ion intensity was also low (< 5 x 10^4 counts/sec.).

The sensitivity loss under MS/MS conditions, that is the combination of transmission losses due to having gas in the collision cell and operating Q_3 in the mass resolving mode, was estimated in the following way. Conventional and MS/MS spectra were recorded for 1 nmole injections of adenosine (MH^+=268) whilst other scan independent instrumental parameters were held constant. The parent ion intensity obtained, $I(MH^+)$, was approximately 10^5 counts/sec. Daughter and residual parent ion intensities in the MS/MS spectrum of MH^+ were summed to give the total ion yield, $I(D_T^+)$. For this nucleoside the transmission in the MS/MS mode, $I(D_T^+)/I(MH^+)$, was typically 15 %.

In many of the CID spectra presented (Figures 4.4c,d; 4.8; 4.10a,b; and 4.11-14) ions corresponding in mass to M^+ are present. These ions are observed both in the presence and absence of collision gas under MS/MS conditions, i.e. with Q_1 focussed on MH^+ and Q_3 mass resolving. Since in the absence of a collision gas only MH^+ and its most abundant metastable ion are generally observed, M^+ must be an instrumental artifact caused by the peak shape of MH^+.

RESULTS AND DISCUSSION

APCI and CID mass spectrum of adenosine

The APCI spectrum of adenosine (1), the mononucleoside

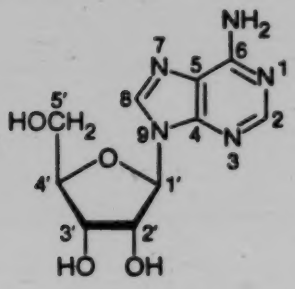

(1)

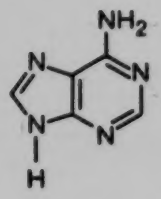

(2)

moiety of polyadenylic acid (Figure 4.4a), reveals that in addition to the protonated molecular ion MH^+ at m/z 268 , cleavage of the $C_{1'}$ - N_9 glycosylic bond in MH^+ accompanied by transfer of a hydrogen atom (33) leads to an intense ion at m/z 136 which will be designated $(BH+H)^+$, since it probably corresponds to the protonated base adenine (2). Cleavage of the same bond, without H transfer and with the charge localized on the sugar fragment leads to (S^+), m/z =133, as only a very minor ion. This is typical of chemical ionisation (CI) spectra of nucleosides in general (16,33,34), and can be rationalized on the basis that the proton and thus the positive charge in MH^+ will stay with the higher proton affinity base. In contrast to previously published ammonia CI spectra (33), the ions $(B+30)^+$ and $(B+44)^+$ corresponding to base plus portions of the sugar were not observed. Probably this is a consequence of the

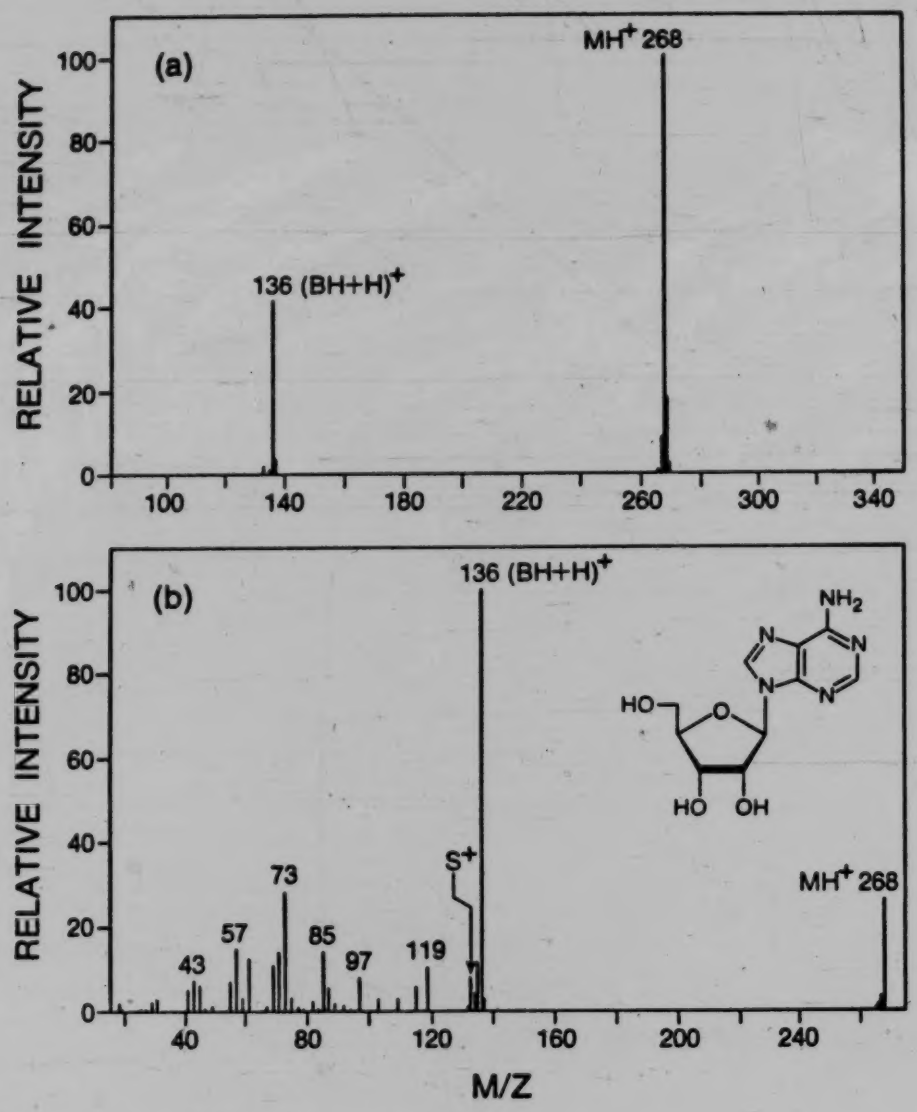

Figure 4.4a APCI spectrum of adenosine (about 10^{-7} moles) after background subtraction. MH^+ is protonated adenosine, $(BH+H)^+$ is probably protonated adenine.

Figure 4.4b CID spectrum of the MH^+, m/z 268 ion of adenosine.

much milder i.e. less exothermic proton transfer leading to MH^+ in APCI where the reagent ions are NH_4^+ clusters. The CID spectrum of the MH^+ m/z 268 ion from adenosine, see Figure 4.4b, contains $(BH+H)^+$ m/z 136 as the major fragment and a number of less abundant fragments all of mass lower than m/z 136. The fragments divide into two groups; those derived from the base and those from the sugar S.

In order to assign the ions originating from the base moiety a CID spectrum of the $(BH+H)^+$ m/z 136 ion was obtained (see Figure 4.4c lower trace). CID of this fragment was found to yield a number of low intensity ions, which have been tentatively assigned to successive losses of NH_3 and HCN (m/z 119, 109, 92, 65), sequential loss of HCN (m/z 109,82,55) and loss of H_2NCN from m/z 109 (m/z 67). These same daughter ions are present in the CID spectrum of the MH^+ m/z 136 ion from an authentic sample of adenine (2). This spectrum, also normalized to the intensity of MH^+, is shown in the upper part of Figure 4.4c. Except for minor variations in intensity the spectra are identical. It is of interest to note that in the electron impact (EI) mass spectrum of adenine the same neutral losses occur in the fragmentation of $M^{+\cdot}$ (35). The base derived fragments in the CID spectrum of protonated adenosine (Figure 4.4b) are therefore m/z 119, 109, 92, 82, 67, 65 and 55. These fragments are of lesser intensity than the sugar derived ions. Other diagnostically useful ions, $(B+30)^+$ and $(B+44)^+$ (33), were either not observed (m/z 164) or were

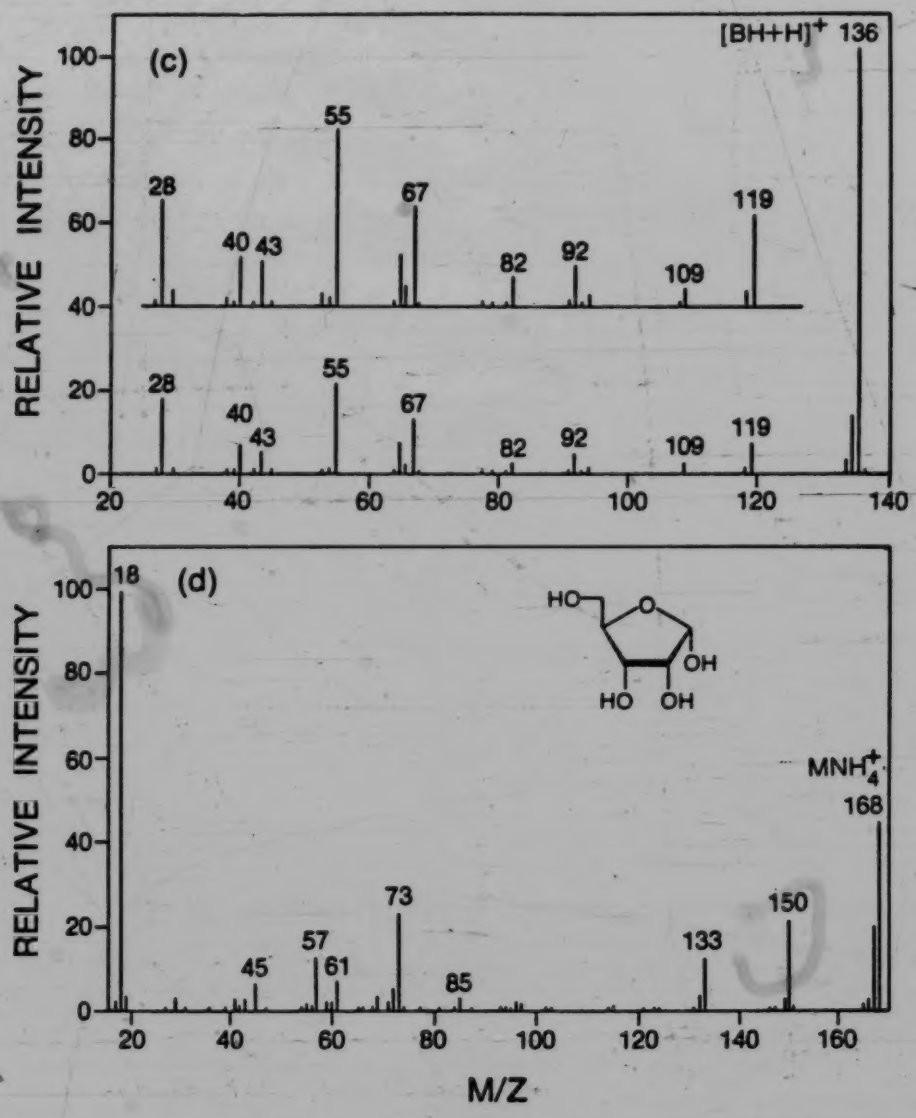

Figure 4.4c CID spectrum of the $(BH+H)^+$, m/z 136 ion of adenosine. Upper spectrum shows the CID of MH^+, m/z 136 from an authentic sample of adenine (structure 2).

Figure 4.4d CID spectrum of the MNH_4^+ adduct ion from D-ribose.

present only at very low intensity (m/z 178) in Figure 4.4b. One might have expected that with CID, which presumably involves energetic collisions, these ions would be more prominent.

Due to the low intensity of S^+ in the APCI spectrum of adenosine a CID spectrum could not be obtained. In order to trace the fragments arising from the sugar moiety D-ribose NH_4^+ m/z 168 was collisionally dissociated. Protonated D-ribose does not form in APCI due to the low proton affinity of the sugar (< 207 kcal/mol.). The CID spectrum, Figure 4.4d, contained fragments with nominal masses corresponding to $C_4H_5O_2^+$ (m/z 85), $C_3H_5O_2^+$ (m/z 73), $C_2H_5O_2^+$ (m/z 61) and $C_3H_5O^+$ (m/z 57). Also observed are m/z 150 which is likely to be the $[NH_4^+-H_2O]^+$ ion and m/z 133 which corresponds to loss of NH_3 from m/z 150. Some of these ions, m/z 61,73 and 85 have been previously observed in the methane CI spectra of underivatised sugars (36).

If we now reexamine Figure 4.4b, the CID spectrum of the MH^+ ion from adenosine, it is apparent that m/z 57, 73 and 85 are fragments of the sugar moiety. Also present are low intensity ions at m/z 115 and 97. These must also be sugar derived fragments as they do not occur in the CID spectrum of $(BH+H)^+$ shown in Figure 4.4c. It is possible that these ions are due to sequential loss of water from S^+.

APCI and CID mass spectra of radiolysis products

Irradiation of a nitrous oxide saturated aqueous solution of poly A, at neutral pH, yields a series of products resulting primarily from hydroxyl radical attack on the polymer (10). Enzymatic hydrolysis of the irradiated poly A yields a complex mixture of mononucleosides which can be separated by HPLC (Figure 4.5). Chromatography of the enzyme hydrolysate from unirradiated solutions of poly A (data not shown) reveals only the presence of adenosine - the unchanged subunit of poly A. The chromatogram shown in Figure 4.5 was obtained with approximately 130 nmoles of irradiated and hydrolysed material injected into the column. Peaks corresponding to the presence of 8-hydroxyadenosine (peak 18), adenine (peak 6) and R- and S-8,5'-cycloadenosine (peaks 4 and 13) had been previously identified by co-chromatography with authentic samples (10,37). The known products of radiolysis, quantified in earlier work on the basis of calibration curves using authentic samples (10), are present in the range of 0.66 - 2.8 nmoles. Reconstructed ion chromatograms for these radiation induced compounds (Figure 4.6) and mass spectral date (Table 4.1) obtained in the present work were consistent with the above peak assignments and confirmed that no other co-eluting compounds were present. Due to the high concentration of adenosine, which represented approximately 92% of the total amount of material injected into the column, the ion signals for m/z 136 and m/z 268 were saturated at about 3×10^6 counts/sec.

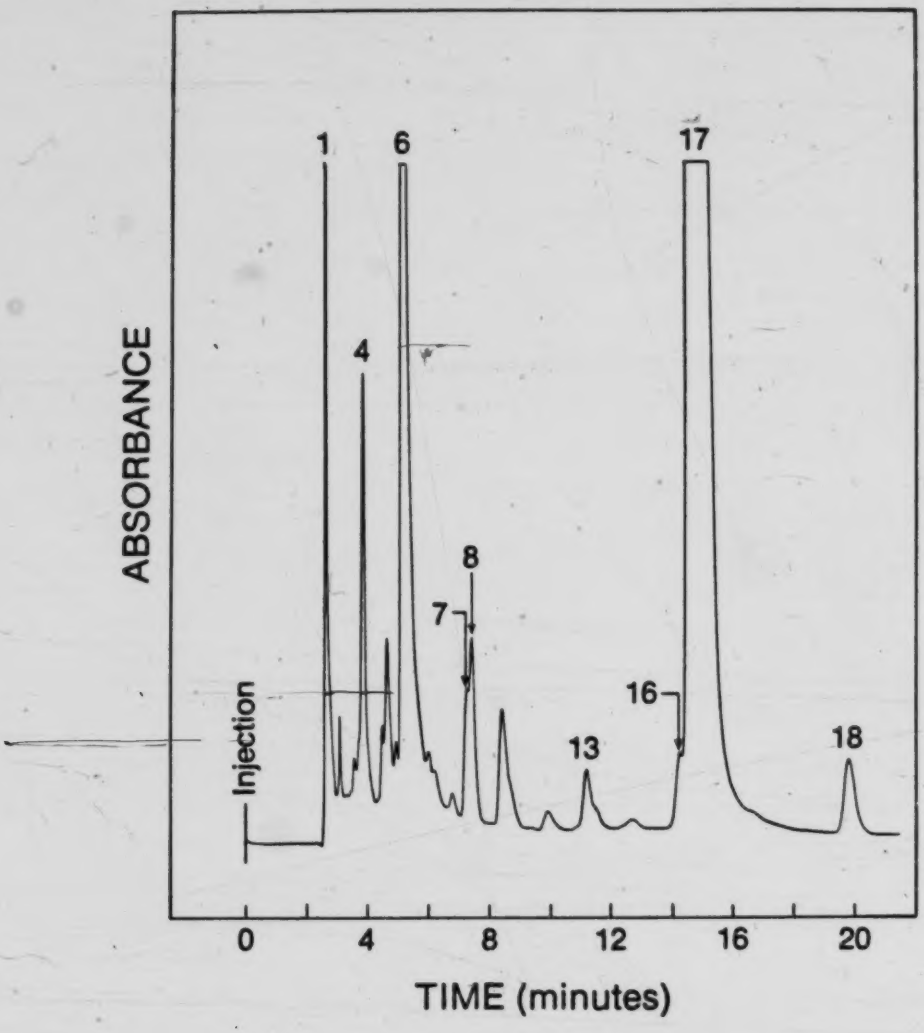

Figure 4.5 HPLC of a nitrous oxide-saturated, enzyme hydrolysed, solution of poly A irradiated to 1000 Gy at neutral pH. Numbered peaks correspond to compounds for which mass spectra were obtained.

Peak 1: 4-amino-5-formamido-6-(ribosyl)aminopyrimidine,
Peak 4: R-8,5'-cycloadenosine, Peak 6: adenine,
Peak 7: 8-hydroxyadenine, Peak 8: α-adenosine,
Peak 13: S-8,5'-cycloadenosine, Peak 16: unconfirmed,
Peak 17: adenosine, Peak 18: 8-hydroxyadenosine.
Unlabelled peaks represent unidentified components.

TABLE 4.1

APCI MASS SPECTRA OF RADIOLYSIS PRODUCTS FROM POLYADENYLIC ACID IRRADIATED IN N_2O-SATURATED AQUEOUS SOLUTION AT NEUTRAL pH

Peak#	Compound	MH^+	$(BH+H)^+$	$(S)^+$	Other Ions
1	FAPY nucleoside[a]	286(22)	154(100)	133(1)	196(23),178(19)
4,13	R & S-8,5'-cycloadenosine	266(100)	-	-	164(7)
6	Adenine	136(100)	-	-	-
7	8-OH adenine	152(100)	-	-	-
8	α-Adenosine[b]	268(100)	136(76)	-	-
16	?	250(100)	136(70)	-	232(10),97(7)
17	Adenosine	268(100)[c]	136(100)[c]	133(2)	-
18	8-OH adenosine	284(52)	152(100)	133(1)	-

Relative intensities (%) are given in parenthesis.

a 4-amino-5-formylamino-6-(ribosyl)aminopyrimidine

b 9-α-ribofuranosyladenine

c detector saturated due to high concentration.

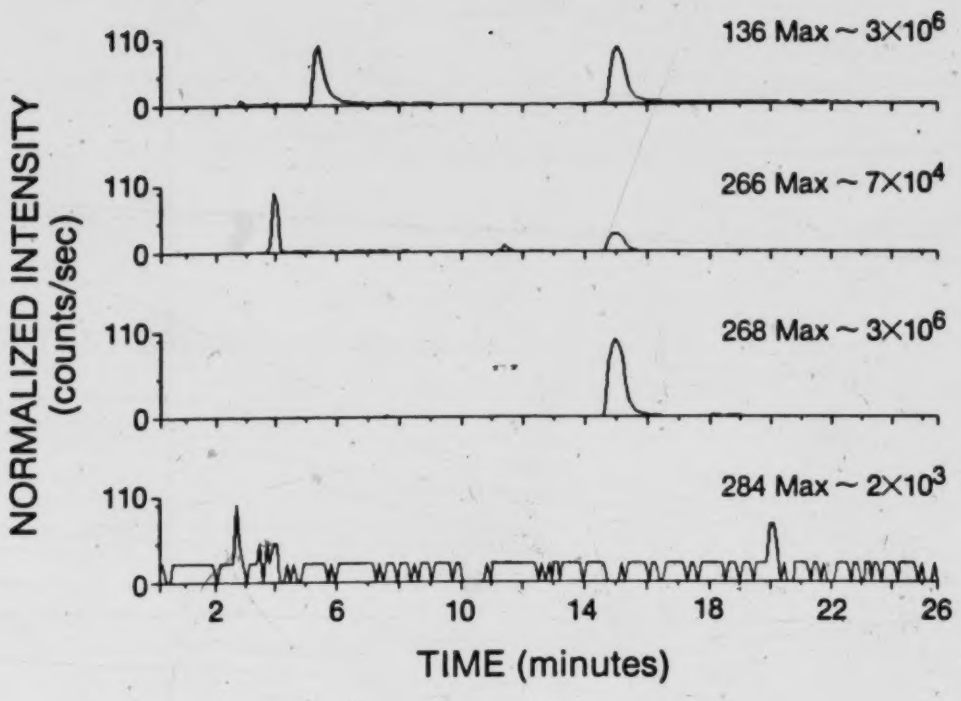

Figure 4.6 Reconstructed ion chromatograms for peaks corresponding to:
adenine (MH^+,m/z 136),
R- and S-8,5'-cycloadenosine (MH^+, m/z 266),
adenosine (MH^+,m/z 268)
and 8-hydroxyadenosine (MH^+,m/z 284).

The other compounds, except for 8-hydroxyadenosine, were also detected with good sensitivity. Based on the relative amount of 8-hydroxyadenosine present the MH^+ ion count for this nucleoside was considerably lower than that expected (see later discussion).

Radiation-induced formation of 8-hydroxyadenosine has been observed in irradiated solutions of purine mononucleosides (tides) (10,29), poly A (10,37) and DNA (8,37). In the present study, the CID spectrum of MH^+ obtained from peak 18 in the UV chromatogram (Figure 4.5) was identical to that obtained from authentic samples of 8-hydroxyadenosine (Figure 4.7). The fragmentation pattern is similar to that of adenosine in that the major ion is the protonated base $(BH+H)^+$ at m/z 152. Low intensity ions can be accounted for by assumed sucessive loss of NH_3 and HCN (m/z 135, 125, 108, 81), and sequential loss of HCN (m/z 125, 98, 71) from $(BH+H)^+$.

Radiation-induced formation of 8,5'-cycloadenosine (see structure in scheme X) has been observed in irradiated, deoxygenated solutions of purine mononucleosides (tides) (29,38) poly A (9,10,37) and DNA (9,14). The major ions in the MH^+ CID spectrum of S-8,5'-cycloadenosine (peak 13, Figure 4.5), obtained from an irradiated solution of poly A, were identical to those obtained using an authentic sample (Figure 4.8). The CID spectrum of the protonated R epimer obtained from peak 4 was essentially the same as that of the S epimer except for the absence of ions at m/z 207 and 82

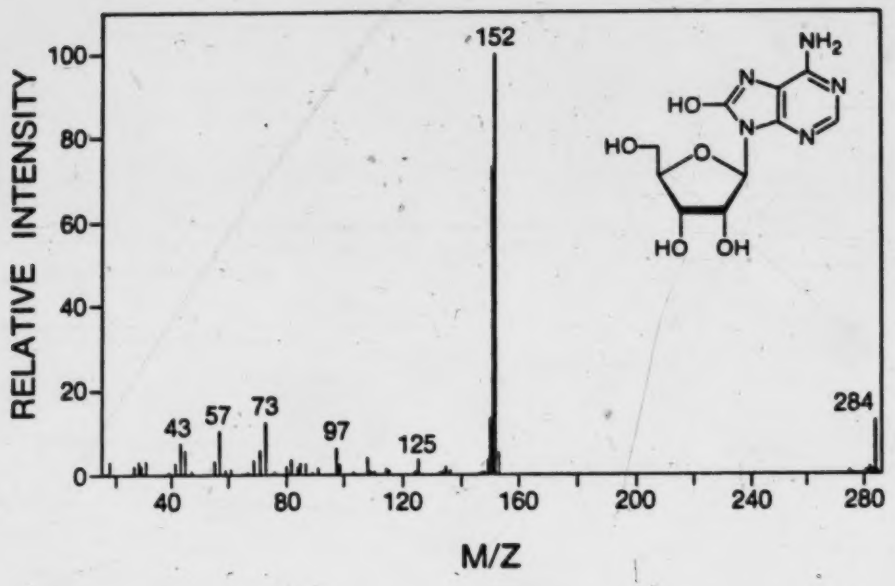

Figure 4.7 CID spectrum corresponding to peak 18, identified as 8-hydroxyadenosine (MH^+, m/z 284).

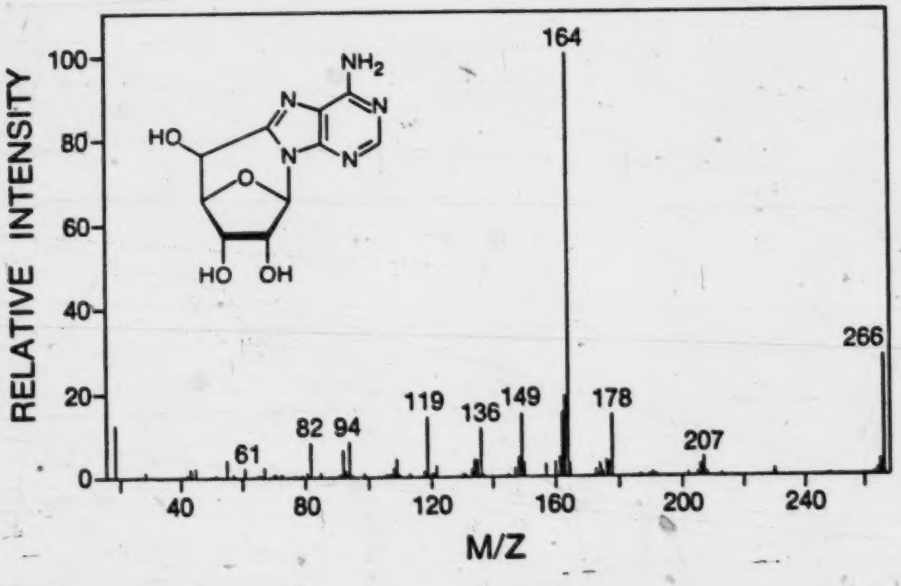

Figure 4.8 CID spectrum corresponding to peak 13, identified as S-8,5'-cycloadenosine.

(data not shown). The relatively high intensity of the MH^+ ion in the CID spectrum reveals that the intramolecular cyclisation between the C_8-C_5' carbon atoms leads to greater stability of MH^+. The possible fragmentation patterns leading to characteristic daughter ions are illustrated in schemes X and Y.

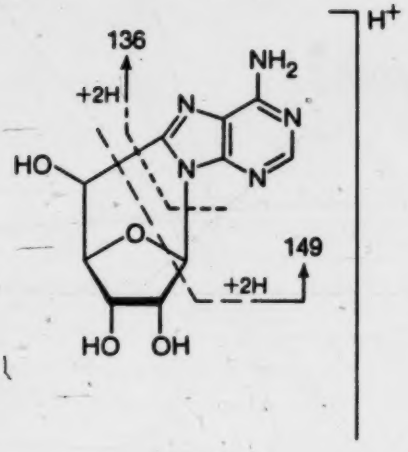

Scheme X

MH^+ 266

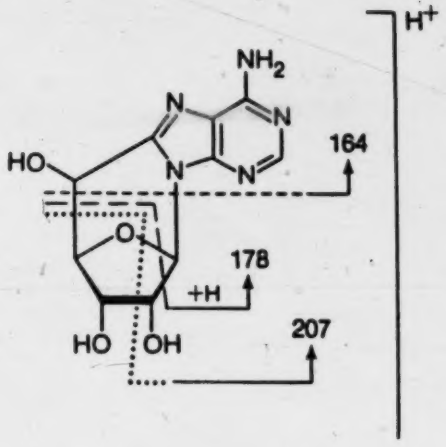

Scheme Y

Similar bond cleavages have been proposed to account for the major ions in the EI mass spectrum of S-8,5'-cycloadenosine-$(Me_3Si)_4$ (14). Minor ions at m/z 248 and 230 can be accounted for by sequential loss of H_2O from m/z 266.

The search for unidentified radiolysis products was initiated by examining the reconstructed total ion chromatogram. This was obtained by summing the total ion intensity for each of the scans, about 300 in total,

obtained during the HPLC separation. Where a local maximum was apparent at the retention time of interest, an APCI spectrum was plotted by averaging the number of scans associated with the ion peak and subtracting an average background spectrum. The background spectrum was obtained by averaging a combination of scans taken just before and after elution of the HPLC peak. A number of extraneous ions, that is ions which did not maximize at the correct retention time, were often present after background subtraction. The reasons for this are not clearly understood. However, these ions were generally of low intensity and did not complicate the interpretation of the APCI spectrum. The APCI mass spectra of peaks 1,7,8 and 16, obtained in this way, are given in Table 4.1. Reconstructed ion chromatograms were also plotted for the ions shown in Table 4.1. In each case the ion maximum obtained coincided with the assigned peak in the HPLC chromatogram. Such reconstructed ion chromatograms are shown in Figure 4.9 for the suspected parent ions m/z 152, 250, 268 and 286. Background corrected spectra were also obtained at retention times of other prominent peaks in the HPLC chromatogram. However, instead of showing distinct parent or fragment ions, these APCI spectra generally contained a large number of low intensity ions. This made it very difficult to establish which were the authentic ions originating from the HPLC peak. Even when reconstructed ion chromatograms for the more prominent ions in these spectra were obtained

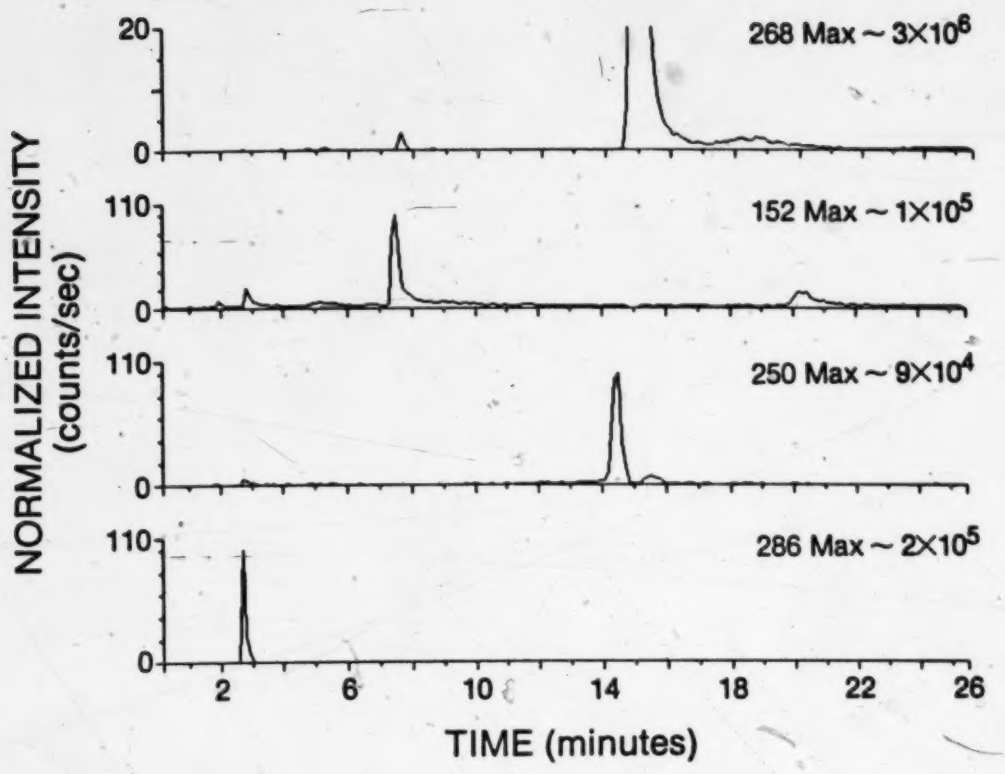

Figure 4.9 Reconstructed ion chromatograms for peaks corresponding to:
4-amino-5-formylamino-6-(ribosyl)aminopyridine(MH^+,m/z 286),
8-hydroxyadenine (MH^+,m/z 152),
α-adenosine (MH^+,m/z 268),
? (MH^+,m/z 250)
and adenosine (MH^+, m/z 268).

molecular maxima at the correct retention time could not be found.

The CID spectrum of the m/z 286 ion whose maximum coincides with peak 1, shown in Figure 4.10a, was assigned to 4-amino-5-formylamino-6-(ribosyl)aminopyrimidine. Formation of this product has been observed in irradiated solutions of mononucleosides (1) and DNA (11,13). The intense ion at m/z 154 corresponds to $(BH+H)^+$; loss of NH_3 and CO from this ion accounts for the ions at 137 and 126 respectively. The CID spectrum of $(BH+H)^+$, shown in Figure 4.10b, was identical, except for minor intensity changes, to the CID spectrum of MH^+ derived from an authentic sample of 4,6-diamino-5-formamidopyrimidine. This spectrum, normalized to the intensity of $(BH+H)^+$, is shown for comparison in the upper part of Figure 4.10b. Cleavage of the glyosylic bond without H transfer and with the charge remaining with the sugar moiety leads to the characteristic ion at m/z 133. Loss of $2H_2O$ from this ion accounts for the ion at m/z 97. The ion at m/z 196 fits the $(B+44)^+$ fragmentation route previosly observed in CI mass spectra of nucleosides (33).

The CID spectrum of the m/z 152 ion whose maximum coincides with peak 7, shown in lower part of Figure 4.11, was assigned to 8-hydroxyadenine. This base has been previously observed in irradiated solutions of DNA (11,13). Low intensity ions that can be accounted for by successive loss of NH_3 and HCN (m/z 135, 125, 108, 81), and seqential loss of HCN (m/z 125, 98 and 71) are present.

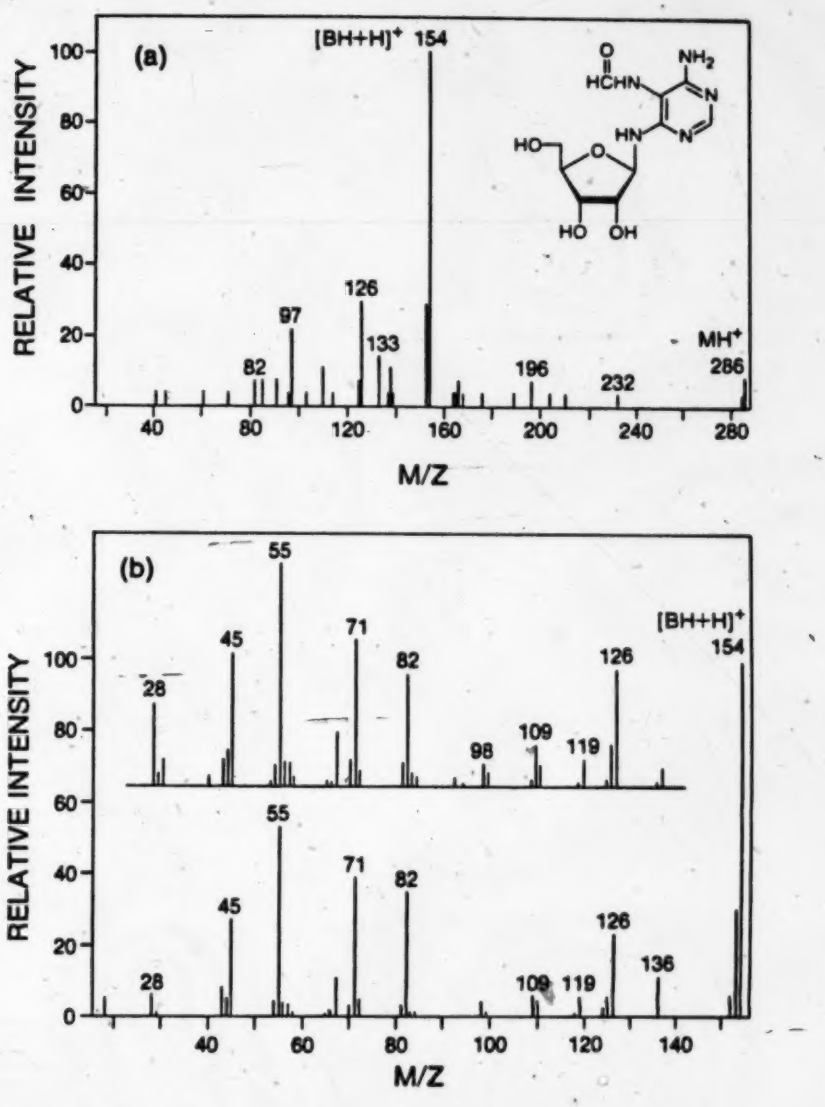

Figure 4.10a CID spectrum corresponding to peak 1, identified as 4-amino-5-formylamino-6-(ribosyl)amino pyrimidine (MH^+,m/z 286).

Figure 4.10b CID spectrum of $(BH+H)^+$ corresponding to peak 1. Upper spectrum shows CID of MH^+,m/z 154 from an authentic sample of 4,6-diamino-5-formamidopyrimidine.

These fragments parallel those produced by CID of protonated adenine, with the expected addition of 16 mass units. A good match was also obtained between this spectrum and a CID spectrum of $(BH+H)^+$ derived from an authentic sample of 8-hydroxyadenosine. For comparison this spectrum, normalized to the intensity of $(BH+H)^+$, is shown in the upper part of Figure 4.11.

The CID spectrum of the m/z 268 ion whose maximum coincides with peak 8, shown in Figure 4.12, was assigned to 9-α-ribofuranosyladenine (α-adenosine). The intense ion at m/z 136 $(BH+H)^+$, together with fragments at m/z 119, 109, 82 and 55, suggest the presence of the unmodified adenine base. In addition the low abundance ion at m/z 133 indicates that the sugar moiety is unaltered. Other ribose derived fragments are also present, although the intensity of these ions is somewhat different to that observed for the β-epimer. Authentic material for this compound was available and, except for minor intensity changes, had an identical daughter ion spectrum and retention time (data not shown).

The reconstructed ion chromatogram for m/z 250 (Figure 4.9) reveals the presence of an intense ion maximum at a retention time of 14.5 minutes which coincides with peak 16 in the UV chromatogram. In addition to MH^+ at m/z 250 the APCI spectrum contained a prominant ion at m/z 136 which corresponds in mass to the adenine moiety $(BH+H)^+$. The CID spectrum of m/z 250 (Figure 4.13) revealed, in addition

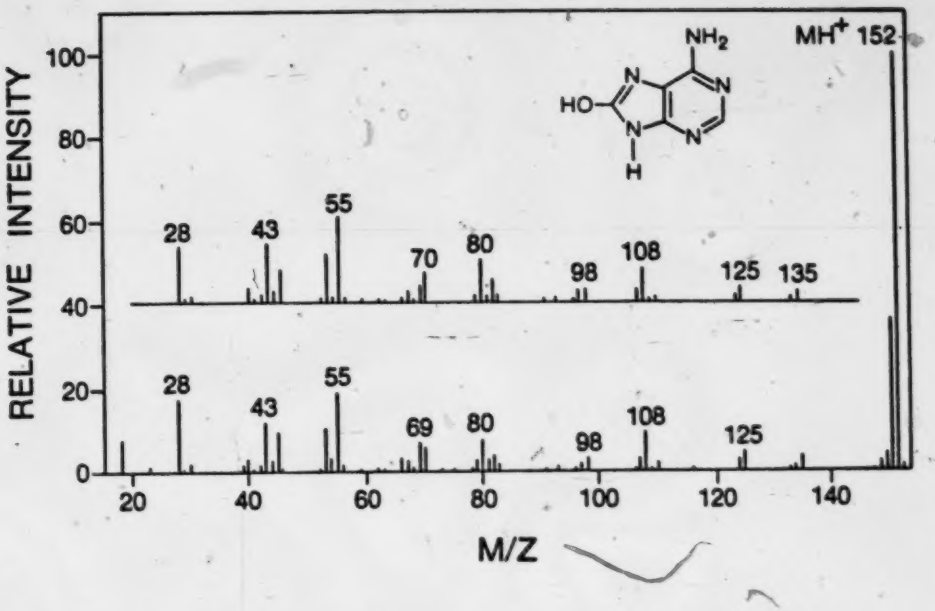

Figure 4.11 CID spectrum corresponding to peak 7, identified as 8-hydroxyadenine (MH^+,m/z 152). Upper spectrum shows CID of $(BH+H)^+$,m/z 152 from an authentic sample of 8-hydroxyadenosine.

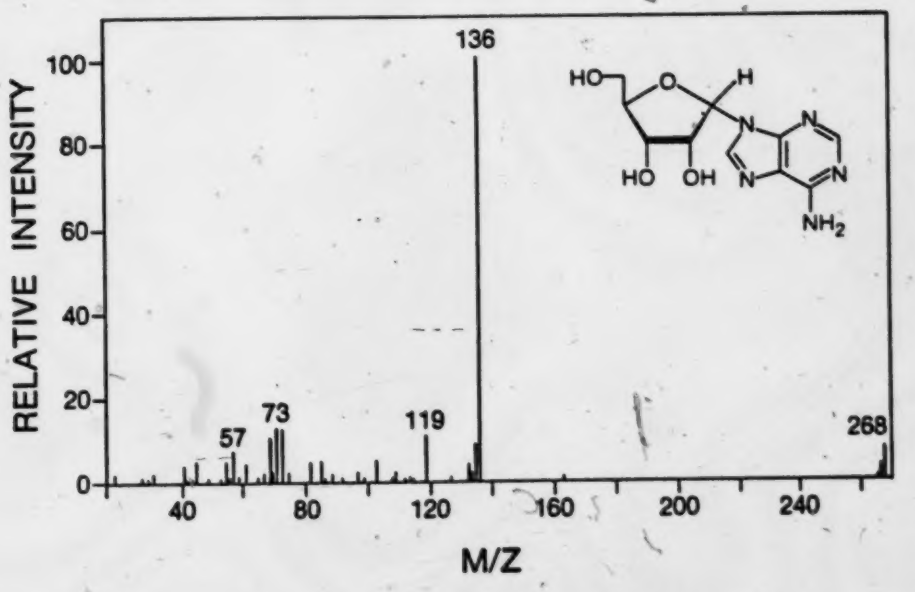

Figure 4.12 CID spectrum corresponding to peak 8, identified as α-adenosine (MH^+,m/z 268).

to the intense ion at m/z 136, fragments at m/z 119, 109, 92 and 82 which further support the argument that the adenine base is intact. Moreover, the lack of the characteristic ribose fragment at m/z 133 and the presence of ions at m/z 115 (modified S)$^+$, m/z 97 (modified S - H_2O)$^+$ are consistant with the possibility that radical attack, resulting in elimination of H_2O, has occured on the sugar. The intensity of the m/z 115 ion would be expected to be low and is similar to that observed for S^+ in the CID spectrum of protonated adenosine (Figure 4.4b). Other sugar derived fragments are also present at m/z 85 and m/z 73 which possibly originate from (S - H_2O)$^+$ for ribose nucleosides rather than (S)$^+$. It is possible that the fragment m/z 69 arises from elimination of H_2CO involving the $C_{5'}$ carbon to yield the ion $C_4H_5O^+$. The prominent ion at m/z 148 must incorporate adenine together with one of the sugar carbon atoms. It is conceivable that the $C_{1'}$ carbon atom has become incorporated into a linked pyrazine-pyrimidine type ion via a ring expansion process. The evidence points to a radiolysis product in which the adenine base is intact, whilst the sugar moiety is damaged in a way consistent with dehydration of the 2′ or 3′ position. While there are radiolytic precedents for such a process (39,40), positive identification of this compound appearing as peak 16 awaits further investigation. In addition to peak 16 there is an isomeric product eluting about 1 minute later and present at approximately 10% of its ion intensity. In irradiated

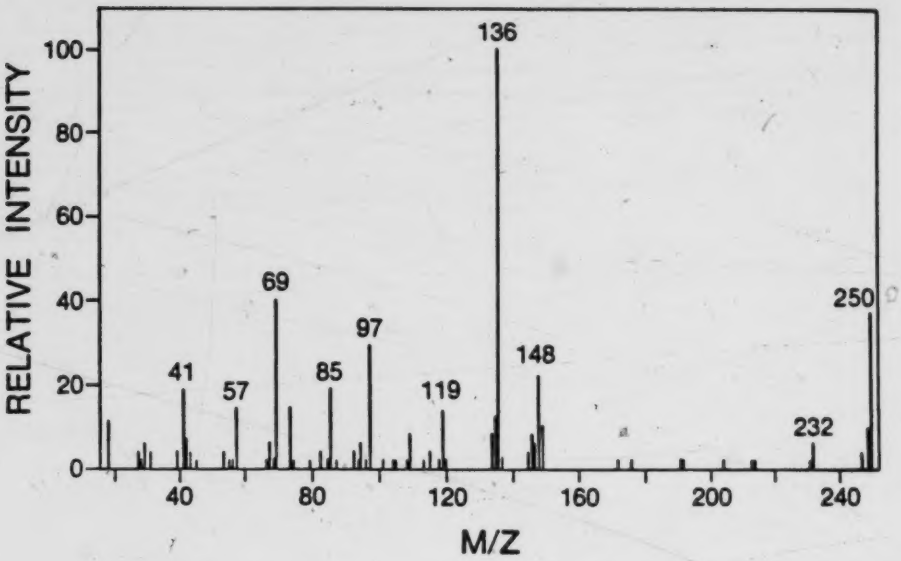

Figure 4.13 CID spectrum corresponding to peak 16.

MH^+ = m/z 250.

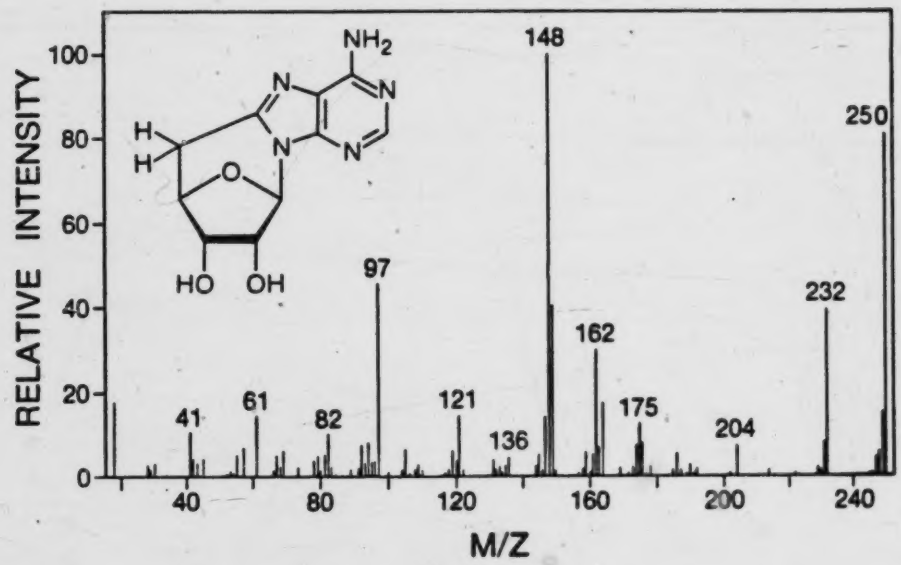

Figure 4.14 CID spectrum of MH^+,m/z 250, corresponding to a major product from the irradiation of S-8,5'-cycloadenosine-5'-monophosphate under reducing conditions. CID spectrum was obtained after hydrolysis to the mononucleoside level and HPLC separation. Identified as 5'-deoxy-8,5'-cycloadenosine, structure (3).

samples of 3′-AMP and poly A, UV detection of this peak is masked by the high concentration of adenosine present. A possible candidate for this product is 5′-deoxy-8,5-cyclo adenosine (3) which also exhibits a MH^+ ion at m/z 250.

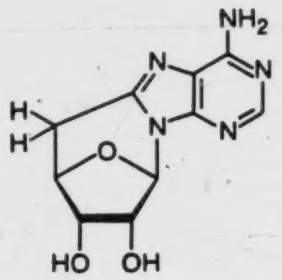

(3)

In order to explore this possibility an authentic sample of S-8,5′-cycloadenosine-5′-monophosphate was irradiated under reducing conditions and hydrolysed to the mononucleoside level. Reducing conditions are achieved by converting hydroxyl radicals to aqueous electrons by irradiation in the presence of sodium formate. This results in a 2-fold increase in the yield of aqueous electrons from water radiolysis. A major product, with a retention time of 15.5 minutes, gave a protonated ion at m/z 250. The CID spectrum of this ion is shown in Figure 4.14. The most intense daughter ion is m/z 148 which results from $C_{4'}$-$C_{5'}$ and $C_{1'}$-N_9 bond cleavage analogous to that observed for S-8,5′-cycloadenosine (Figure 4.8), whereas m/z 136 is only present at low intensity. Ions at m/z 162 and 149 also

result from analogous bond cleavages to those shown for S-8,5′-cyclcadenosine. Facile loss of H_2O could account for the relatively intense ion at m/z 232 and loss of HCN from m/z 148 for the ion at m/z 121. These ions together with the intense ion at m/z 97 do not appear to have +16 amu counterparts in the daughter ion spectrum of S-8,5′-cycloadenosine. The major fragments are, however, consistant with structure (3).

It is clear from the difference in retention time and CID spectra, together with the fact that m/z 136 is not observed in the APCI spectrum of 5′-deoxy-8,5′-cyclo adenosine that peak 16 is not this product. A sample of poly A, irradiated under nitrous oxide and hydrolysed, was spiked with an enzyme hydrolysate which had been obtained from S-8,5′-cycloadenosine -5′-monophosphate irradiated under reducing conditions. The reconstructed ion chromatogram for m/z 250 revealed that 5′-deoxy-8,5′-cyclo adenosine coeluted with the unknown peak at 15.5 minutes. However, the inability to obtain a CID spectrum of m/z 250 for the corresponding peak in irradiated poly A, due to the low quantity of product present, makes it impossible to confirm the presence of this product.

Detection of damage at low radiation doses

Radiation doses exceeding 10-20 Gy cannot be tolerated by mammalien cells (41). It is therefore of interest to ascertain whether HPLC-MS, based on nebulization into an APCI source, is sensitive enough for the purpose of studying radiation damage at low doses (<10 Gy). A sample of poly A was irradiated under exactly the same conditions as previously employed but to a dose of 10 Gy rather than 1000 Gy. Under these conditions 20 pmoles (5 ng) of R-8,5'-cyclo adenosine and 14 pmoles (4 ng) of 8-hydroxyadenosine were calculated to be present on the basis of the calibrated UV absorbance at 254 nm (10). The mass spectrometer was used in the single ion monitoring (SIM) mode, using only Q_1 to select the ions of interest.

Considering first the cyclonucleoside product, for which most of the ionization is concentrated in MH^+, one finds that the LC peak due to 5 ng leads to an MH^+ signal/noise ratio of about 3 (see Figure 4.15). Thus 5ng may be considered as the detection limit for this type of product. Nucleoside products which do not yield intense MH^+ ions generally have an intense $(BH+H)^+$ fragment. This is the case for 8-hydroxyadenosine for which 4 ng led to a signal/noise ratio of about 2 at m/z 152. The detection limits are therefore approximately the same for both compounds. These results indicate that this system is not sufficiently sensitive to monitor radiation damage at biologically significant levels. A number of products

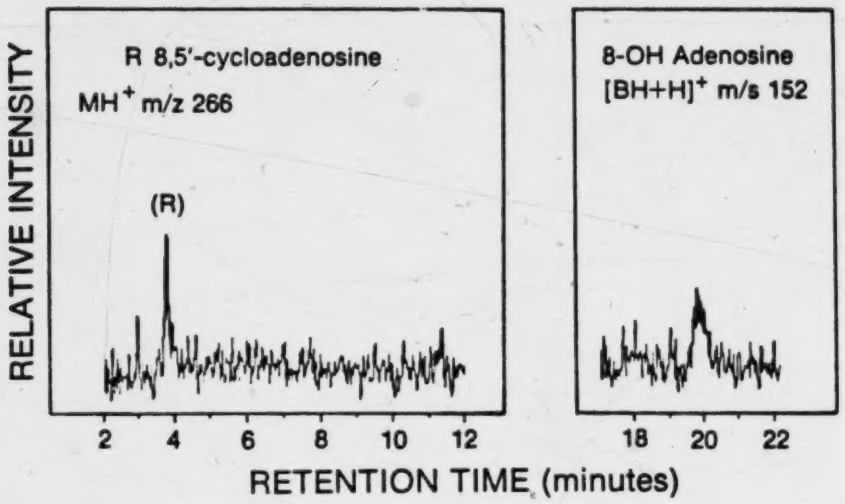

Figure 4.15 APCI ion chromatograms obtained for m/z 266 and m/z 152 from a sample of Poly A irradiated to a dose of 10 Gy, that is 100 times less than used to obtain the chromatogram shown in Figure 4.5.

Other conditions were the same as previously employed. Q_1 was used in the selected ion monitoring mode, Q_3 was in Rf only mode.

resulting from DNA irradiated at doses ranging from 0.1 to 10 Gy have been detected by GC-MS/SIM (13,15). Some of these products could be detected at doses as low as 0.1 Gy, but others required a minimum radiation dose of 10 Gy. However, this technique is limited to products that can be sucessfully derivatized.

Yield of MH^+ under HPLC/APCI conditions

As previously noted the APCI response, that is the efficiency of protonation, for 8-hydroxyadenosine was relatively poor (Figure 4.6). Both the proton affinity and the relative volatility of an analyte would be expected to strongly influence the yield of MH^+ when solutions are directly nebulised into an APCI source. Adenosine has a high proton affinity [> 226.6 kcal/mol.] (33) and is detected with good sensitivity, comparable to that obtained from other nitrogen containing bases using APCI (42). Although the site of protonation on nucleosides is not known, the presence of a hydroxyl group on the purine ring is unlikely to reduce the proton affinity significantly (43). However, additional hydroxyl groups, particulary when located on the purine ring, might limit volatility due to more extensive hydrogen bonding. For example, both inosine and guanosine are considerably less volatile than adenosine and ribose nucleosides are less volatile than their 2'-deoxy counterparts (35).

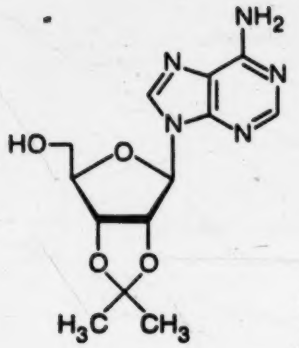

(4)

Direct comparison of adenosine with 2',3'-O-isopropylidine adenosine (4) and 8-hydroxyadenosine, using the intensities of MH^+ and $(BH+H)^+$ from 1 nmole injections, revealed that the intensities of these ions were a factor of about 5 times greater for the 2',3'-O-isopropylidine and about 35 times less for the 8-hydroxy derivatives than that for adenosine. The absolute intensity for adenosine (MH^+) was about 10^5 counts/sec. The total ionisation was essentially constant for each injection indicating that no depletion of the reagent ions had occurred. These trends in overall sensitivity suggest that the presence of a hydroxyl group on the heterocyclic ring, rather than the sugar, affects the efficiency of vaporization to a greater extent. It is possible that other prominent peaks not identified in the UV chromatogram (Figure 4.5) are due to radiation-induced products that are less volatile than 8-hydroxyadenosine.

CONCLUSIONS

MS/MS spectra have been used to identify a number of radiolysis products resulting from hydroxyl radical attack on a model nucleic acid. These assignments could not have been made on the basis of the primary APCI spectra alone.

The base containing fragment ion $(BH+H)^+$ is present in APCI spectra of nucleosides but no further ions derived from the base moiety are observed. Consequently it would be impossible to distinguish between say a substituted or ring opened base product if these happen to have the same nominal mass. By comparison the CID spectrum of $(BH+H)^+$ is rich in structural information and can be used to identify the base, modified by hydroxyl radical attack, as has been illustrated for 8-hydroxyadenine (peak 7) and 4-amino-5-formylamino-6-(ribosyl)aminopyridine (peak 1).

The sugar fragment S^+ is either not formed, or is of such low intensity (< 1%) in APCI that it cannot be reliably used for diagnostic purposes. In the CID spectrum of MH^+ the intensity of this fragment is also low; however, it is consistently present. Furthermore, other important diagnostic sugar fragments, at higher yield, are also present. For the limited number of nucleosides studied it is apparent that the mass and relative intensity of these ions, together with fragments originating from the base moiety provide a useful MS/MS "fingerprint".

The greater specifity obtained with MS/MS is often offset by a corresponding loss in sensitivity due to higher

transmission losses. This is to a large extent dependent on the design of the quadrupoles and coupling lenses. However it is also mass dependent. In this study about a 10 fold loss in sensitivity was incurred for operation in the MS/MS mode. CID spectra for a number of low yield products were not obtained, either for this reason, or because the corresponding parent ions in the primary APCI spectra could not be detected.

This study demonstrates that HPLC-MS/MS, based on direct nebulisation into an APCI source, has considerable potential for product identification in studies of the molecular radiobiology of nucleic acids.

REFERENCES

1. Huttermann, J.; Kohnlein, W.; Teoule, R.; (Eds.) "Effects of Ionizing Radiation on DNA", Springer-Verlag, Berlin, 1978.
2. Roots, R.; Okada, S.; Int. J. Radiat. Biol., 1972, 21, 329-342.
3. Mozumder, A.; Magee, J.L.; Radiat. Res. 1966, 28, 203-214.
4. Scholes, G.; Br. J. Radiol., 1983, 56, 221-231.
5. Spinks, J.W.T.; Woods, R.J.; "An Introduction to Radiation Chemistry", Wiley, N.Y. 1976.
6. Chapman, J.D.; Reuvers, A.P.; Borsa, J.; Greenstock, C.L.; Radiat. Res., 1973, 56, 291-306.
7. Cerutti, P.A.; Science (Washington DC), 1985, 227, 375-381.
8. West, G.J.; West, I.W.L.; Ward, J.F,; Int. J. Radiat. Biol., 1982, 42, 481-490.
9. Fuciarelli, A.F.; Miller, G.G.; Raleigh, J.A.; Radiat. Res., 1985, 104, 272-283.
10. Fuciarelli, A.F.; Shum, F.Y.; Raleigh, J.A.; Radiat. Res., 1987, 110, 35-44.
11. Dizdaroglu, M.; Anal. Biochem., 1985, 144, 593-603.
12. Dizdaroglu, M.; Biochemistry, 1985, 24, 4476-4481.
13. Dizdaroglu, M.; J. Chromatogr., 1986, 367, 357-366.
14. Dizdaroglu, M.; Biochem. J. 1986, 238, 247-254.

15. Dizdaroglu, M.; Bertold, D.S.; Anal. Biochem., 1986, 156, 182-188.

16. Esmans, E.L.; Geboes, P.; Luytens, Y.; Alderweireldt, F.C.; Biomed. Mass Spectrom., 1985, 12, 241-245.

17. Edmonds, C.G.; Vestal, M.L.; McCloskey, J.A. Nucleic Acids Res., 1985, 13, 8197-8206.

18. Dedieu, M.; Juin, C,; Arpino, P.J. Guiochon, G.; Anal. Chem., 1982, 54, 2372-2375.

19. Lee, E.D.; Henion, J.D.; J. Chromatogr. Sci., 1985, 23, 253-264.

20. Garteiz, D.A.; Vestal, M.L.; LC Mag., 1985, 3, 334-346.

21. Iribarne, J.R.; Dziedzic, P.J.; Thomson, B.A.; Int. J. Mass Spectrom. Ion Phys., 1983, 50, 331-347.

22. Henion, J.D.; Thomson, B.A.; Dawson, P.H.; Anal. Chem., 1982, 54, 451-456.

23. Kambara, H.; Anal. Chem., 1982, 54, 143-146.

24. Crowther, J.B.; Cover, T.R.; Silvestre, D.; Henion, J.D.; LC Mag., 1985, 3, 240-254.

25. McLafferty, F.W.; (Ed.) "Tandem Mass Spectrometry", Wiley, N.Y. 1983.

26. Johnson, J.V.; Yost, R.A.; Anal. Chem. 1985, 57, 758A-768A.

27. McDowall, M.A.; Merren, T.O.; Smith, D.C.; Swain, D.; Am. Lab. (Fairfield Conn.), March 1987, 74-88.

28. Covey, T.R.; Lee, E.D.; Henion, J.D.; Anal. Chem., 1986, 2453-2460.

29. Raleigh, J.A.; Fuciarelli, A.F.; Radiat. Res., 1985, 102, 165-175.

30. Fricke, H.; Hart, E.J.; in "Radiation Dosimetry", 2nd. Edition, Vol. 2; Attix, F.H.; Roesch, W.C.; (Eds.), Academic Press, N.Y. 1966, pp.167-239.

31. Harrison, A.G.; "Chemical Ionization Mass Spectrometry", CRC Press, Boca Raton, FL., 1983.

32. Sciex, 55 Glen Cameron Road, #202 Thornhill, Ontario, Canada, L3T 1P2.

33. Wilson, M.S.; McCloskey, J.A.; J. Am. Chem. Soc., 1975, 97, 3436-3444.

34. Esmans, E.L.; Luyten, Y.; Alderweireldt, F.C.; Biomed. Mass Spectrom., 1983, 10, 347-351.

35. McCloskey, J.A.; in "Basic Princilples in Nucleic Acid Chemistry", Vol. 1; Ts'o, P.O.P.; (Ed.), Academic Press, N.Y. 1974, pp. 209-309.

36. Hogg, A.M.; Nagabhushan, T.L.; Tetrahedron Lett., 1972, 47, 4827-4830.

37. Fuciarelli, A.F.; Shum, F.Y.; Raleigh, J.A.; Biochem. Biophys. Res. Commun., 1986, 134, 883-887.

38. Raleigh, J.A.; Kremers, W.; Whitehouse, R.; Radiat. Res., 1976, 65, 414-422.

39. Burchill, C.E.; Perron, K.M.; Can. J. Chem. 1971, 49, 2382-2389.

40. Samuni, A,; Neta, P.; J. Phy. Chem., 1973, 77, 2425-2429.

41. Elkind, M.M; in "Radiation Biology in Cancer Research", Meyn, R.E.; Withers, H.R.; (Eds), Raven Press, N.Y. 1980, pp. 71-93.

42. Sunner, J.; Kebarle, P.; Int. J. Mass Spectrom. Ion Proc. submitted.

43. Taft, R.W.; Progr. Phys. Org. Chem., 1983, 14, 247-350.

CONCLUDING SUMMARY

Fast Atom Bombardment-MS Study

Saddle-field discharge guns are used extensively in fast atom bombardment mass spectrometry (FABMS) as the source of bombarding particles. In the work described in Chapter 1 it was shown that a range of monoatomic and polyatomic vapors can be used to produce a discharge in a saddle-field gun. This permitted atom/ion beams generated from mercury and polyatomic vapors to be evaluated relative to argon and xenon for the production of "molecular" ions from an analyte dissolved in a liquid matrix. Within the mass range of analytes used in this study the "molecular" ion yields obtained with mercury vapor were equal but not appreciably superior to that obtained with xenon.

Heavy polyatomic particles (MW>200) cannot be produced efficiently by simply using organic vapors in a saddle field gun as had been previously assumed (1). Two types of diffusion pump oils, DC 705 and Santovac-5, were found to produce only intense H_2^+, $C_2H_2^+$, and CO^+ ions and presumably the corresponding molecules comprise the neutral component of the beam. It appears unlikely that any other organic vapor would be significantly more successful, nor is it likely that high mass ions could be produced in any type of gun utilizing a plasma discharge. Thus if the value of using high mass polyatomic particles in FABMS is to be

determined, another type of gun, for instance one using electron impact followed by acceleration will have to be employed.

The beam generated from a saddle-field source contains both fast atoms and ions. The degree of neutralization is dependent on the operating conditions and design of the front cathode. At a constant discharge current the neutral component of the beam decreases with increasing applied voltage. In the MS9 FAB source used, only the neutral component of the luminous beam appeared to hit the surface of the probe, with the ionic component being deflected. With the FAB gun operating on xenon gas, at a constant discharge current of 1 mA, the "molecular" ion yield (MH^+) for beta-cyclodextrin was found to increase with increasing anode potential with no maximum up to a 15 kV limit. This suggests that in the generation of MH^+ ions the increasing kinetic energy of the bombarding atom more than compensates for the decreasing neutral atom flux. Thus it would appear that a more successful route to obtaining greater "molecular" ion yields by FAB would be to re-design the gun insulation so that accelerating voltages >15 kV can be routinely employed, rather than to increase the mass of the bombarding species.

The energy of the great majority of the ions in the beam correspond to between 81% and 84% of the anode potential irrespective of the vapor being used and not multiples of this value as originally reported by Ligon (2).

The particle beams generated from both Santovac-5 and DC 705 show an appreciable neutral component. In neither case can resonant charge transfer be a significant process leading to neutralization, whereas some form of electron capture is a more likely mechanism. There is, therefore, reason to believe that this might also be the predominant process for the monoatomic species which show similar degrees of neutralization.

The reproducibility of many of the measurements in this study was poor. In part this is due to the nature of the sputtering experiment itself; however, our experience has shown that variations within the saddle-field discharge are significant particularly if the gun has been voltage or current cycled during a series of experiments.

If a study comparing the secondary ion yields obtained with different bombarding particles is to have any value it is important that the comparison be made under controlled conditions. The total particle flux of the beam, the ion/neutral ratio, the particle energies and the trajectories of the ions and neutral species in the ion source field must all be known. Also, a distinction must be made between instantaneous ion current measured for "molecular" and other diagnostic ions and the total integrated flux of all secondary ions produced. Our experience shows that this is very difficult to accomplish.

Thermospray-MS Study

The thermospray interface and ionization method for liquid chromatography/mass spectrometry (TSP-MS) has become an important analytical technique for the determination of involatile or thermally labile compounds (3). This interface, when used with a mobile phase containing ammonium acetate, requires no external method of ionization and unlike other interfaces, permits 100% flow of eluent from conventional HPLC columns into the mass spectrometer source.

In Chapter 2 it was shown that gas phase ion-molecule reactions have a strong influence on the relative ion intensities in TSP mass spectra. The relative intensities of the positive ions in the TSP spectra of 0.1 M ammonium acetate solution follow a pattern that can be predicted on the basis of gas phase ion-molecule equilibria. That is, NH_4^+ ions preferentially form clusters with gas phase NH_3 and CH_3COOH molecules, rather than with gas phase H_2O. When volatile or moderately volatile analytes B are present in the ammonium acetate solution, the BH^+ ions are formed by gas phase protonation of gaseous B by the ammonium reagent ions. At $[B]_{aq} < 10^{-3}$ M , this gas phase protonation is slow (kinetic control) and the BH^+ signals are linear with concentration of B. However at $[B]_{aq} > 10^{-3}$ M the protonation becomes progressively faster, proton transfer equilibria conditions are approached, and the BH^+ response is nonlinear. Under these conditions the base with the highest proton affinity, in a mixture of bases, will dominate the TSP mass spectrum.

During the course of this investigation there was a growing realization amongst many TSP practitioners that ion-molecule reactions play a significant role in the second stage of the TSP process. Vestal, in a paper describing the principles and applications of the TSP LC/MS interface (4), acknowledges that neutral compounds are apparently ionized by the same gas phase ion-molecule reactions that occur in ordinary Chemical Ionisation sources, even though the primary "reagent ions" (NH_4^+ clusters) are produced by means of a different mechanism (direct ion evaporation). Data consistent with this hypothesis was obtained by Bursey and co-workers (5) who conducted a limited study with reactions that were endothermic in solution but exothermic in the gas phase. Recently, Parker and co-workers (6) studied the negative ion TSP spectra of several model analytes which were not appreciably ionized under the HPLC conditions used. They found that the negative ions formed, either by CH_3COO^- attachment or by proton abstraction, followed those predicted on the basis of gas phase acidities. These results, together with our own (7), firmly establish that, for moderately volatile analytes, ion-molecule reactions in the second stage determine the observed ion intensities in the TSP mass spectrum.

Several inorganic cations could also be detected by thermospray mass spectrometry. For the alkali metals, lithium, sodium, potassium, rubidium and cesium, cluster ions of the form $X^+(H_2O)_n$ were observed, where X^+ was the alkali ion in aqueous solution. These clusters presumably also arise from

direct ion evaporation. The relative distribution of water clusters for a given ion were close to the predicted gas phase equilibrium values, confirming that near equilibrium conditions are attained in the TSP source. Thus the observed cluster sizes reflect the conditions within the later stage of the TSP process, rather than the original state of the evaporated ion.

Pulsed-EI Thermospray-MS Study

In order to gain a better understanding of the TSP process, particularly for less volatile species, it would be beneficial to know the gas phase concentration of neutral analyte produced by TSP vaporization. In theory this can be achieved by generating reagent ions by pulsed high energy electrons, rather than by direct TSP ionisation, and following the protonation of the neutral analyte (B) as a function of time after the initial ionization. The results of such experiments are discussed in Chapter 3. It is perhaps best said at the onset that the results obtained were disappointing. The potential of the method was never fully realized due to the fact that the location of the electron beam was determined by the design of the existing TSP source and vacuum housing and did not allow for the very fast flow through the TSP source. Nevertheless, some useful data were obtained.

With an electron beam placed only 4 mm "upstream" from the ion exit hole the flow through the TSP source limits the

reaction time available under pulsed conditions to about 28 μsec. There is, therefore, insufficient time for ion-molecule reactions to significantly influence the time decay of the reactant ions. Thus meaningful kinetic data could not be obtained. Instead the time profile parallels the pulse width, that is the width of the ion decay (1/10 height) = pulse width + 20 μsec. However, a reaction time of 28 μsec. under these conditions can be used to estimate an upper limit for the normal "filament off" average TSP reaction time. The value obtained, 214 μsec., was in good agreement with the value of a few hundred microseconds obtained from the kinetic treatment of the TSP data given in Chapter 2.

By reducing the liquid flow rate to about 40 μL/min. it was possible to obtain kinetic information on the gas phase protonation of pyridine. Although, this approach was not successful with less volatile analytes the results did demonstrate that such a technique could be used to determine the gas phase concentrations of neutral analytes produced by TSP vaporization. A natural extension of this work would be to design and build a pulsed electron ionization-TSP source in which the position of the electron beam could be varied over the distance from the vaporizer capillary to the ion exit orifice. With such a system it should be possible to obtain kinetic information at flow rates of 1 ml/min.

Combined HPLC-Tandem/MS Study

The analysis of molecular products resulting from radiation damage to nucleic acids is an important area of cancer research (8). Capillary gas chromatography-mass spectrometry (GC-MS) has already made significant analytical contributions in this area (9,13). High performance liquid chromatography-tandem mass spectrometry (HPLC-MS/MS) has the potential to directly separate and analyse complex mixtures. However, few applications to "real-life" analytical problems have been reported. In the present study, HPLC-MS/MS, based on direct nebulization into an atmospheric pressure chemical ionization (APCI) source, was used to identify a number of products resulting from the radiolysis of aqueous poly-adenylic acid (after hydrolysis of the polymer to the mononucleoside level). These assignments, presented in Chapter 4, could not have been made on the basis of the primary APCI spectra alone. However, about a 10-fold loss in sensitivity was incurred for operation in the MS/MS mode. Collision induced dissociation (CID) spectra for a number of low yield products were not obtained, either for this reason, or because the corresponding parent ions could not be detected in the primary APCI spectra.

For the limited number of nucleosides studied the daughter ions arising from the base and sugar moieties provided a useful "MS/MS fingerprint". However, due to the small number of authentic, structurally related, nucleosides available it was not always possible to fully exploit the

power of the this technique. Also, the lack of standards hindered the possible confirmation of structural assignments by comparison of HPLC retention times.

Detection limits of about 5 ng were established for two typical radiolysis products using selected ion monitoring of MH^+ and $(BH+H)^+$ with only Q_1 mass analysing. These yields were obtained with a radiation dose of 10 Gy. Living systems require doses on the order of 100 times less to avoid excessive cell death (14). Consequently this system is not sufficiently sensitive to monitor radiation damage at biologically significant levels.

This study demonstrates that HPLC-MS/MS, based on direct nebulization into an APCI source, is well suited for the identification of products arising from the radiolysis of adenine based nucleosides. However, little is known about the efficiency of direct nebulization for compounds of low volatility. It is suspected that the absence of primary APCI parent ions for many prominent peaks in the UV chromatogram of irradiated and hydrolysed polyadenylic acid may be due to their low volatility. This "volatility problem" might limit the extension of this technique to the study of irradiated deoxyribonucleic acid (DNA), or similar more complex systems. Guanosine, for example, is known to be considerably less volatile than adenosine (15). In this respect further work on the relative responses of different biologically important nucleosides under HPLC-APCI conditions would be particularly useful.

REFERENCES

1. Wong, S.S.; Stoll, R.; Rollgen, F.W.; Z. Naturforsch Tiel A, 1982, 37, 718-719.
2. Ligon Jr.,W.V.; Int. J. Mass Spectrom. Ion Phy., 1982, 41, 205-208.
3. Covey, T.R.; Lee, E.D.; Bruins, A.P.; Henion, J.D.; Anal. Chem., 1986, 58, 1451A-1461A.
4. Garteiz, D.A.; Vestal, M.L.; LC Mag. 1985, 3, 334-346.
5. Bursey, M.M.; Parker, C.E.; Smith, R.W.; Gaskell, S.J.; Anal. Chem., 1985, 57, 2597-2599.
6. Parker, C.E.; Smith, R.W.; Gaskell, S.J.; Bursey, M.M.; Anal. Chem., 1986, 58, 1661-1664.
7. Alexander, A.J.; Kebarle, P.; Anal. Chem., 1986, 58, 471-478.
8. Hutterman, J.; Kohnlein, W.; Teoule, R.; (Eds.), "Effects of Ionizing Radiation on DNA", Springer Verlag, Berlin, 1978.
9. Dizdaroglu, M.; Anal. Biochem., 1985, 144, 593-603.
10. Dizdaroglu, M.; Biochemistry, 1985, 24, 4476-4481.
11. Dizdaroglu, M.; J. Chromatog., 1986, 367, 357-366.
12. Dizdaroglu, M.; Biochem. J., 1986, 238, 247-254.
13. Dizdaroglu, M.; Bergtold, D.S.; Anal. Biochem., 1986, 156, 182-188.

14. Elkind, M.M.; in "Radiation Biology in Cancer Research", Meyn, R.E.; Withers, H.R.; (Eds), Raven Press, N.Y. 1980, pp. 71-93.

15. McCloskey, J.A.; in "Basic Principles in Nucleic Acid Chemistry", Vol. 1, Ts'o, P.O.P.; (Ed), Academic Press, N.Y. 1974, pp.209-309.